CHEMICAL DOPING OF LIQUID EXFOLIATED 2D-MATERIALS

Farnia Rashvand

Thesis for the degree of

Doctor Rerum Naturalium

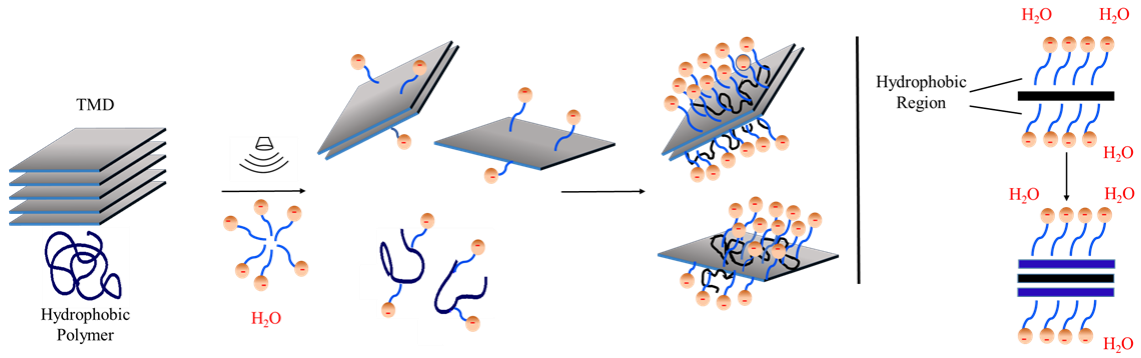

Department of Chemistry

Ruprecht Karl University of Heidelberg

DISSERTATION

CHEMICAL DOPING OF LIQUID EXFOLIATED 2D-MATERIALS

A thesis submitted to the

COMBINED FACULTY OF

NATURAL SCIENCES AND MATHEMATICS

HEIDELBERG UNIVERSITY, GERMANY

A thesis submitted for the degree of

DOCTOR RERUM NATURALIUM (Dr. rer. nat.)

presented by

Farnia Rashvand

Submitted at 30.09.2021

1. Examiner: Dr. Claudia Backes

2. Examiner: Prof. Dr. Petra Tegeder

Date of oral exam:

12.11.2021

“Creativity is contagious, pass it on.”

- Albert Einstein

Acknowledgements

This scientific work and my personal development would not have come true without the guidance, support, and accompaniment of many people.

First of all, I thank my supervisor, Dr. Claudia Backes, who has given me the opportunity of working in her outstanding (PhysChem2D) group and provided me with her awesome support and guidance throughout my time as a PhD candidate. I learned from her how to achieve your goals by being passionate, and thinking out of the box. Also, I want heartily to thank her for giving me opportunities for training, collaboration and attending different conferences. Dear Claudia, thank you for your almost unconditional and supportive guidance and mentorship.

I would like to thank Prof. Jana Zaumseil for all support, guidance, group meeting discussion and scientific comments over the last four years as well as giving me the opportunity of collaborating with her outstanding group. I have learned a great deal from her and discussions with her have always proved valuable.

I'm not less grateful to all members and alumni of the Physical Chemistry of Layered Nanomaterials (PhysChem2D) group as well as the nanomaterials for optoelectronics (NMOE) group. That was a great pleasure of mine to spend mostly my time with you in the labs and offices. A very special thanks to Thomas Higgins, Beata M. Szydłowska, Sebastian Grieger, Maximilian Krings, Kathrin Knirsch, Kevin Synnatschke and Steffen Ott to lift me up throughout my tough time as a PhD student as well as enjoyable scientific discussion and comments. I had a wonderful time with you guys in the office and labs. Thanks for all the exciting moments that you provided me and made me to be happy from depth of my heart.

I would like to thank all students that I had the opportunity to supervise: Sara, Phillip, Caroline, Ezgi, Julian, Zhaojung. We made a wonderful team together and supervising you gave me the chance of improving my ability of teaching.

I would like to express special thanks to my husband, Mohammad, for his constant support. You are the one always lift me up and believe in my abilities and encourage me.

Last, but definitely not the least, I would like to express my deepest gratitude to my mom (Farahnaz), my dad (Ahmad) and my brother (Nemo) for their continuous love and support. Without your love, guidance, and never-ending support, this accomplishment would not have been possible.

Abstract

Nanomaterials play an important role in the flourishing field of nanoscience. Size reduction of materials results in a broad range of outstanding physical and chemical properties as well as a wealth of potential applications. A particularly interesting class of low-dimensional nanostructures are two-dimensional (2D) materials, i.e. individual layers of so-called van der Waals crystals. The research was triggered in 2014 by Geim and Novoselov through the isolation and characterization of graphene, a single layer of two-dimensionally arranged sp^2 hybridised carbon atoms. 2D nanomaterials can be obtained by various methods including bottom-up approaches such as chemical vapour deposition and top-down approaches such as liquid phase exfoliation (LPE) and mechanical exfoliation. In recent years, LPE has gained increasing attention due to the high production rates and broad applicability to a range of structures beyond graphene including transition metal dichalcogenides (TMDs), hexagonal boron nitride, metal phosphorus trisulfides and many more.

In LPE, high energy and shear forces (e.g. through sonication) are applied to reduce the dimensions of the crystal and the resulting nanosheets are stabilized in the liquid medium through appropriate solvents and surfactant systems. The resultant nanosheets are extremely polydisperse in lateral size and thickness so that LPE is typically coupled with size selection, for example through centrifugation. Due to this additional processing step, it is difficult to assess the impact of the stabilizer on for example the optical properties of the nanosheets which will be a function of both size and stabilizer. In addition, the number of pure organic solvents suitable to prevent reaggregation is very limited which is a bottleneck for further processing and deposition. The goal of the work conducted within the scope of this thesis is to establish protocols to make high quality 2D nanosheets from LPE accessible in a range of liquid media and to achieve a deeper understanding of the impact of the stabilizer on the optical properties of the nanomaterial. To this end, tungsten disulphide (WS_2), a semiconducting transition metal dichalcogenide was chosen as model substance due to unique optical fingerprints of the monolayers (e.g. narrow linewidth photoluminescence from exciton only in WS_2 monolayers).

Throughout this thesis, monolayer-rich dispersions of WS_2 nanosheets were prepared by sonication-assisted LPE in a common detergent solution in combination with liquid cascade centrifugation for size selection. In the first part, a protocol was developed to transfer these nanosheets into a range of additive/solvent systems. The advantage over a direct exfoliation in

this systems is that dispersions containing nanosheets of the same size/thickness can be compared. This allowed to assess the impact of various chemical environments on the optical properties and to study effects associated with the dielectric screening of excitons (e.g. changes in exciton energy and width). With this foundation established, the nanosheets were transferred into a range of common pure organic solvents using a modified protocol. This is more challenging due to aggregation taking place. Nonetheless, this broad screening made it possible to relate the changes in exciton response to physical parameters such as refractive index and dielectric constant. Importantly, it was confirmed that monolayers can be stable in solvents that are not suitable for the exfoliation itself greatly expanding the choice of solvent for further processing.

The third part focuses on precise deposition of the nanosheets on substrates using spin coating. Experimental difficulties such as aggregation and restacking of nanosheets in solvents are addressed in detail together with solutions to improve the colloidal stability of the nanomaterials. In the optimized samples, monolayer properties, such as exciton photoluminescence, are retained after deposition. At last, a new route for transferring nanosheets from water-based WS_2 dispersions into different media is introduced which greatly facilitates deposition. In this approach, water-insoluble polymers are added to the aqueous surfactant solution prior to sonication. Through hydrophpobic interaction, the polymer is driven to the interface between the hydrophobic part of the detergent and the nanomaterial. This polymer coating on the nanomaterial reduces aggregation after transfer to hydrophobic organic solvents, suitable for thin-film processing. Such techniques for nanomaterial processing are highly demanded for the integration of these materials into functional devices.

Zusammenfassung

Nanomaterialen spielen im aktiven Feld der Nanomaterialen eine wichtige Rolle. Durch die Möglichkeit diese Materialen in ihrer Größe zu kontrollieren entsteht eine breite Vielfalt überragender physikalischer und chemischer Eigenschaften und daraus resultierend, eine große Bandbreite an Anwendungsmöglichkeiten. Seit der Isolation und Charakterisierung von Graphen- einer einzelnen, atomar-dünnen Lage Graphit- in 2004, sind zwei-dimensionale (2D) Nanomaterialien in den Fokus vieler Forschungsaktivitäten gerückt. Verschiedene Methoden der Herstellung wurden erforscht und je nach Methode zeigen sich verschiedene Ergebnisse bezüglich Ausbeute, Reinheit und Größe der Nanomaterialen. Generell unterscheidet man bei 2D-Nanomaterial-Synthese zwischen „Bottom-up"-Methoden wie chemische Gasphasen-abscheidung und "Top-down"-Methoden wie mikromechanische Exfoliierung oder Flüssigphasenexfoliierung (engl. „Liquid phase exfoliation", LPE). LPE hat hier die vergangenen Jahre einen erheblichen Aufschwung erlebt, auf Grund der Skalierbarkeit des Prozesses und die Anwendbarkeit auf diverse Materialklasse, wie z.B. Übergangsmetalldichalcogenide (engl.: „transition metal dichalcogenides" TMDs), hexagonales Bornitrid, Übergangsmetallphosphortrichalcogenide und viele mehr.

In LPE werden hohe Energien und Scherkräfte in Lösung verwendet (z.B. durch Ultraschall) um die Mutterkristalle zu zerkleinern. Ein wichtiger Parameter in LPE stellt das Verhindern einer Reaggregation der Schichten dar, wozu geeignete oberflächenaktive Stoffe, Lösungsmittel oder Polymere zum Einsatz kommen. Die erhaltenen Nanomaterialien sind extrem polydispers in Bezug auf deren Größe und Lagenzahl, so dass typischerweise eine weitere Aufreinigung und Größenselektion, z.B. durch Zentrifugation durchgeführt wird. Auf Grund dieser zusätzlichen Arbeitsschritte ist es jedoch sehr schwierig den Einfluss des Stabilisators auf die (optischen) Eigenschaften des Materials zu untersuchen. Zudem sind nur wenige reine organische Lösungsmittel als Medium geeignet, was die weitere Prozessierung erschwert. Ziel dieser Arbeit ist es LPE Methoden weiterzuentwickeln um qualitativ hochwertige Nanomaterial Dispersionen auch in organischen Lösungsmitteln zugänglich zu machen und einen tieferes Verständnis auf den Einfluss des Stabilisators/Lösungsmittels auf die optischen Eigenschaft zu erhalten. Auf Grund vorteilhafter optischen Eigenschaften (z.B. schmal-bandige Emission von Monolagen), wurde Wolframdisulphid als repräsentatives Material gewählt.

Dazu werden zunächst Monolagen-reiche Dispersionen von WS_2 in wässriger Detergenz Lösung mittel LPE und Kaskadenzentrifugation hergestellt und ein Protokoll erarbeitet, die Nanoplättchen in verschieden Lösungsmittel/Additiv Systeme zu überführen. Im Gegensatz zu einer direkten Exfoliierung in verschiedenen flüssigen Medien wird hier sichergestellt, dass die zu untersuchenden Nanoplättchen die gleiche Größe und Dicke haben. Der Einfluss der chemischen Umgebung spiegelt sich in den optischen Eigenschaften wider (z.B. Variation in Exzitonenenergie und Breite). Im weiteren Verlauf wurde ein ähnlicher Transfer in reine organische Lösungsmittel durchgeführt, der auf Grund von Aggregation der Plättchen zwar schwieriger zu kontrollieren ist, aber es erlaubt die Änderungen der optischen Eigenschaften auf physikalische Parameter, wie Brechungsindex oder Dielektrizitätskonstante zurück zu führen. Zudem wurde beobachtet, dass durch diese Vorgehensweise eine größere Bandbreite organischer Lösungsmittel zugänglich ist.

Im dritten Teil der Arbeit steht die Abscheidung der Plättchen im Vordergrund mit dem Ziel eine Überlappung der Schichten auf dem Substrat zu vermeiden. Besonderes Augenmerk bei diesen Untersuchungen gilt der Aggregation bereits in der Lösung, die sich negativ auf die Abscheidung auswirkt. Zu guter Letzt wird ein neues Verfahren aufgezeigt, den Transfer der Nanomaterialen in organische Lösungsmittel zu verbessern, um die Präparation hochqualitativer Dispersionen und Filme zu vereinfachen. Hierbei kommen wasserbasierte WS_2 Dispersionen und wasserunlösliche Polymere zum Einsatz. Die Nanomaterialen werden dabei durch das hydrophope Polymer beschichtet und stabilisiert, wodurch es möglich ist, diese besser in hydrophoben organischen Lösungsmitteln zu überführen. Diese verbesserte Prozessierbarkeit ist ein wichtiger Schritt um die Integration der Nanomaterialen in z.B. Anwendungen zu ermöglichen.

Table of contents

List of Acronyms

2D	two-dimensional
CVD	chemical vapor deposition
DGU	density gradient ultracentrifugation
g	earth's gravitational field
etc.	et cetera (and so forth)
Ext	extinction
h-BN	hexagonal boron nitride
L	length
LCC	liquid cascade centrifugation
LPE	liquid phase exfoliation
IPA	isopropyl alcohol
PVA	poly(vinyl alcohol)
PS	polystyrene
PMMA	poly(methyl methacrylate)
PVP	polyvinylpyrrolidone
HA	hyaluronic acid sodium salt
CTAB	hexadecyltrimethylammonium bromide
SDC	sodium deoxycholate
SDBS	sodium dodecylbenzenesulfonate
SDS	sodium dodecyl sulfate
COV	coverage
Eq.	equation
VB	valence band
CB	conduction band
OD	optical density
FL	few-layered
NMP	N-methyl-pyrrolidone
FWHM	full width of the half maximum
PGMEA	propylene glycol methyl ether acetate
DMSO	dimethylsulfoxid
Abs	absorbance
AFM	atomic force microscopy
BP	black phosphorus

CMC	critical micelle concentration
ML	monolayer
N	layer number
PL(E)	photoluminescence (emission / excitation)
RCF	relative centrifugal force
SC	sodium cholate
SDS	sodium dodecyl sulfate
THF	tetrahydrofuran
TMD	transition metal dichalcogenide
UV	ultra violet
Vf	volume fraction
Vis	visible
VS.	versus
W	width
TX-100	triton x-100
PVK	polyvinylcarbazole
PFO	polydioctylflourene
HA	hyaluronic acid
MeOH	methanol
DME	dimethoxyethane
DMF	dimethylformamide

1 Introduction

Over the past decades, many remarkable properties and a wide range of potential applications of nanomaterials led to increasing interest in this class of materials. In this work, novel 2D materials beyond graphene are studied. In the past few years, intensive research on the extraordinary physical properties of graphene has triggered the interest in 2D materials with unique electronic and optical properties (inorganic 2D materials). While a single layer of graphene is probably the only truly 2D material which is atomically thin in one dimension, the term 2D material is commonly used to describe single or few-layers of so-called van der Waals crystals. These type of crystals have in common that strong, mostly covalent bonds exist in plane in combination with weak, mostly van der Waals interactions between the individual layers in the bulk crystal which enables the exfoliation into two-dimensional nanosheets down to single layered thickness..

In this thesis, layered materials with special consideration of transition metal dichalcogenides (TMDs) especially WS_2 (tungsten disulphide) have been studied to obtain deeper insights into their optical properties and in particular, in which way they are influenced by their chemical environment. Layer-number dependent physical and chemical properties of TMDs as one big family of 2D layered materials have attracted attention. Depending on the d-orbital configuration, TMDs can be semiconducting or metallic. Group VI-TMDs are semiconductors with a direct bandgap only in the monolayer making the materials an ideal model substances to track the impact of the environment through optical spectroscopy..

After an introduction to layered materials and their production with focus on the liquid-phase exfoliation (LPE). The result of the thesis are presented in four chapters. In the first chapter of the results and discussion section, the impact of the chemical environment on the optical properties of LPE WS_2 is reported. The second chapter describes a similar study using pure organic solvents which allows to relate the changes in the optical properties (e.g. exciton energy and width) to refractive index and dielectric environment, respectively. The third chapter focuses on deposition of the nanosheets in such a way that monolayer properties are widely retained. Here, aggregation of the nanosheets in the dispersion is identified as crucial aspect that needs to be prevented. To this end, chapter four describes a new route to make WS_2-polymer composites based on micellar swelling which greatly enhanced colloidal stability in organic solvents..

1.1 Background- Two Dimensional Crystals as a New Generation of Materials

Since 2004, 2D layered materials have been introduced as a new class of materials after the first report on mechanically exfoliated graphite into atomically thin layers, coined graphene by Geim and Novoselov.[1-2] The unique 2D layered structure of Graphene (hexagonal lattice structure) represents promising optical, electronic, mechanical and thermal properties which can be used in a broad range of applications such as solar cells, sensors, spintronics and (opto)electronics.[3-5] The single layer of graphite shows no band gap between the conduction and valence band for the monolayer graphene, due to the hexagonal arrangements of carbon atoms in the lattice.

Mechanical or chemical exfoliation of honeycomb graphite layers (from the bulk) leads to accessing fascinating properties strikingly different from the initial bulk material. By considering three directions of x, y (in plane) and z (out of plane) in such materials, while the carriers will be confined in one of these directions for example z, they freely move in other directions of x-y which results quantum confinement in the direction of e.g., z. Hence, these materials are referred to as 2D materials because there are only two directions in which the carriers can freely move.[6-7] Put in other words, they have two freedom degrees. In-plane chemical bonds along the x-y plane and out of plane van der Waals interactions, along the z-axis are typically observed for layered materials. Since covalent bonds are stronger than van der Waals bonds, such interaction allows for exfoliation to produce atomically thin layers. Some examples of such materials comprised of only one element which have been exfoliated down to a single layer are graphite,[1-2] hexagonal boron nitride (h-BN),[8] black phosphorus[9] or germanium.[10]

In addition to such mono-elemental materials, a whole host of layered structures exist with a combination of elements. For instance, in transition metal dichalcogenides, the transition metal (M, e.g. Mo, W) is sandwiched between chalcogen (X, e.g. S, Se) atoms. From the top view, a hexagonal arrangement of the atoms is observed in some of the TMDs (referred to as 2H polytype). The structure of the two main TMD polytypes, as well as examples of other layered materials are displayed in Figure 1.1-1.

Two dimensional material with superconducting,[11] insulating,[12] semiconducting,[13] semi-metallic[14] and metallic[15] properties are known to date which originates in the structural configuration and chemical compositions of the material in an atomically thin, two dimensional arrangements.

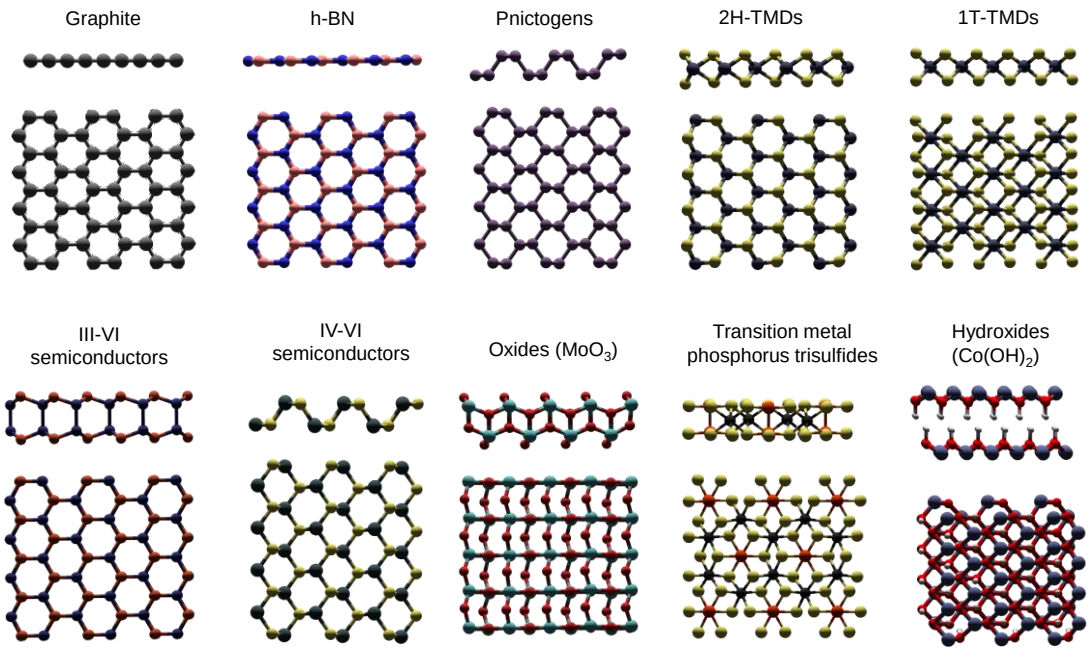

Figure 1.1-1: Examples of structures of 2D materials in side-view and top view. Reprinted from ref [16].

1.2 Two-Dimensional Transition Metal Dichalcogenides

The family of TMDs consists of roughly 60 different materials with different optical and electronic properties.[17-18] All TMDs have the unit formula MX_2, where M and X denote transition metal and a chalcogen atom respectively. Each TMD possesses its unique sets of properties: Depending on the combination of elements, different electronic properties arise. For example, TaS_2 is a semi-metal, WS_2 and MoS_2 are semiconductors and HfS_2 is an insulator. Different polymorph structures of two-dimensional TMDs can be formed, This refers to the geometric arrangement of the atoms in the unit cell. For TMDs, octahedral (tetragonal, T)[18-19], trigonal prismatic (hexagonal, H) and distorted (T0) crystal phases are known.[17, 20-21]

Already in the bulk, the TMDs are thus very versatile. In addition, quantum confinement effects lead to changes in the electronic properties on exfoliation. For the most commonly studied semiconducting group VI-TMDs, a systematic change of the band gap with layer thickness is observed. A wide study has been performed on the change of the electronic properties of TMDs with their layer number, first explored for MoS_2.[22-23] Decreasing the thickness from bulk to a single layer leads to a shift of the bandgap from and indirect (1.29 eV) to direct (~1.90 eV) band gap which gives rise to relatively intense photoluminescence in the monolayers. In this thesis, special attention is given to tungsten disulphide (WS_2), where similar effects are observed, i.e. a transition from an indirect semiconductors in the bulk with a gap of 1.4 eV for the bulk to a direct band gap

of 2.1 eV for the monolayered species.[14, 24] In addition to the changes in electronic properties with layer number, exfoliation of layered materials results in an increase of the accessible surface area of the material and hence pronounced effects from interaction with the environment. For example, MoS_2 on Si/SiO_2 substrates is commonly n-doped.[25]

In addition, theoretical and experimental studies confirm that two-dimensional monolayers and three-dimensional bulk semiconductors demonstrate different excitonic properties.[26-27] Typically, in semiconductors, photo-excitation generates excitons. These are quasi-particles formed through the Coulomb interaction between the hole in the valence band and the electron in the conduction band. In TMD monolayers, an exciton is confined to the monolayer plane which is not the case in the bulk form. Reduction of the dimensions (2D character) in TMDs leads to an increased Coulomb interaction[26, 28] which results in weak (reduced) screening of charge carrier thus creating strong excitonic effects. For example, the binding energy of excitons in TMD monolayers is in the order of a few hundreds of meV, while it is only 40 meV in the bulk.[29] Furthermore, the electric field lines of the bound electron-hole pair extend further into the surrounding environment in monolayers compared to bulk materials. Thus, varying the dielectric environment has an impact on the exciton resonance, which is more pronounced for thinner nanostructures not only because of the increased effective surface area. However currently it is not fully understood in which way the exciton resonance changes when varying the environment.

The most important excitonic transitions in group VI-TMDs are the lowest energy direct transitions which are associated with the K-point in the Brillouin zone. Spin orbit splitting results in two excitons referred to as A- (lowest energy) and B-exciton. In monolayers, recombination of the hole in the spin-orbit split valence bands with the electron in the conduction band typically results in a single photoluminescence (PL) peak. However, doping from the environment can lead to the formation of tightly bound trions, i.e. charged excitons, which are red-shifted compared to the neutral exciton.[25] In addition, in substrate supported TMDs, the higher energy emission from the B-exciton can also sometimes be observed, in particular in earlier works.[30] In this thesis, the focus is on WS_2 as a model system, since it has some advantageous properties over other members of TMDs. This includes large spin-orbit splitting between the A and B exciton (0.4 eV) and electronic transition which show narrow linewidth in both absorption and emission.[29, 31]

In brief, the excitonic and electronic properties of these materials are thus strongly influenced by exfoliation: First, quantum confinement changes the band structure and for monolayers, the band gap is increased. Second, the binding energy of the exciton is increased through enhanced interactions between the electron and the hole.

1.3 Overview of Production Methods

2D layered materials can be produced through several different methods. The fascinating properties of these materials can only be recognized when they are scaled-down in one dimension.[31-34] The production methods are categorized into two groups: bottom-up and top-down methods. Examples of bottom up methods are chemical vapour deposition (CVD),[33, 35] Here, 2D materials such as Graphene and TMDs mono- or few layered nanosheets with uniform thickness and extensive lateral area can be produced on substrate from precursor molecules. For instance, in the case of graphene, a copper substrate is heated to a high temperature of about ~1000 ˚C, which results in an increasing domain size of the metal. Over the substrate, a precursor molecule, typically methane (as a carbon-based gas) is passing over the surface and decomposes due to the high temperature, which leads to the deposition of carbon atoms on the surface of the substrate.[36] For TMDs, a similar process can be used with metal oxide precursors as substrate and sulfur vapours, which results in gas-phase reactions on the oxide-precursor. The resulting materials can be of high optical quality as well as of a low density of defects which are considered as two major advantages of the chemical vapour deposition technique. However, the nanosheets are hard to transfer to substrates other than the material they were grown on, which highly limits their application potential. Another example of bottom-up techniques is the self-assembly approach, which includes the principle of molecular self-assembly where molecules spontaneously are organized under thermodynamic equilibrium conditions which results in the formation of a stable structure.[37-38]

The original top-down exfoliation is cleaving the layers mechanically, for example using tape. In scotch-tape-based microcleavage, the material is mechanically exfoliated from a bulk form through scotch-tape, transferred to a substrate (typically Si/SiO_2) and ultimately, the residue of scotch tape is removing by suitable solvents like acetone and methanol. This affords the highest quality material (if high quality bulk crystals are available), but with very limited throughout and lateral size.

Although TMDs and graphene are commonly produced via micromechanical exfoliation or chemical vapour deposition as typically larger sizes of nanosheets can be produced, more attention is drawn to the optimization of liquid exfoliation techniques as they offer solution processing of the nanomaterial in form of nanosheet inks.[35] These also belong to the category of top-down methods. While many production techniques of high quality nanosheets lack scalability (e.g. micromechanical exfoliation), other techniques focused on high throughput of the nanomaterial production which typically lacks in the required optical and electronic properties, as defects are

typically introduced to the system. In the liquid phase, individual layers can be produced by increasing the layer distance for example through intercalation and subsequent dispersion in solvents through mild agitation. In the case of TMDs, this is commonly achieved through treatment with *N*-butyl lithium[39] and referred to as chemical exfoliation. This leads to the production of a large number of monolayers. However, within the intercalation process, structural defects are introduced and in the case of group VI TMDs, the layers are typically negatively charged and undergo a transition to the metastable, metallic 1T polytype.[39]

Layered nanosheets in organic solvents as well as water with an additional stabiliser can be produced via liquid phase exfoliation methodology (LPE). It was initially developed by Coleman et al. for graphene[40] and later on TMDs[41] and other materials. Here, the bulk crystal is subjected to high energies and shear forces, for example through sonication to break the bonds in the crystal. The resultant nano-objects are then stabilized against reaggregation through suitable solvents. While this technique produces laterally relatively small few and monolayered nanosheets (in solution), it has become increasingly popular to the broad applicability to a range of materials, the potential for scale-up.[42] However, to date it is still challenging to produce materials suitable for optical applications in this way.

1.4 Production of Nanosheets by Liquid Phase Exfoliation

Among all production methods, the focus of this work is on liquid phase exfoliation and a deeper look at the mechanics of this approach is given in Chapter 1.4. Graphene and any layered materials such as (transition metal dichalcogenide (TMDs), transition metal oxide (TMO), (hexagonal boron nitride (h-BN) and layered III-VI semiconductors can be exfoliated through this methodology that first reported by Coleman et al in 2008.[40] Initially, graphite nanosheets were dispersed in N-methyl pyrrolidone (NMP). The capability of the LPE method to produce nanosheets in solution is interesting, as it allows post-processing of the nanosheets in a liquid medium. The biggest strength of this method is that it can easily be scaled up. [18, 41, 43] However, the exfoliation mechanism is still not fully understood.

Layered nanosheets in a liquid medium can for example be produced by sonication of the bulk crystals which leads to a separation of the material into individual packages of sheet stacks of decreased thickness. After breaking the starting material into smaller crystallites and eventually nanomaterials, the dispersion has to be stabilized which is based on solubility parameters. As already discussed, the quantity and quality of material plays an important role for later

applications. In the bulk materials, there are van der Waals interactions (cohesive force) between the layers that could be overcome when the energy is exerted on the system by sonication. However, the supplied energy should be equal to or greater than the interlayer attraction of the nanomaterials to overcome the van der Waals forces. One of the main disadvantages of probe sonication refers to decrease the process effectiveness with increasing sample volume, making it difficult to scale up the process in contrast to other techniques such as shear exfoliation.[44] However, on the laboratory scale, sonication is still most widely used.

Using liquid phase exfoliation for nanomaterial production, the exfoliation can be performed in any appropriate solvent.[18, 40] However, it should be considered that the decision if a solvent is appropriate is based on the nanomaterials surface energy. Few- and mono-layered nanosheets can be stabilized if the surface energy of the solvent matches the surface energy of the nanomaterial.[11, 43] The nanomaterial will aggregate if no stabilization is achieved by the solvent. Dispersions can be stabilized either by using pure solvents like isopropyl alcohol (IPA), *N*-methyl-2-pyrrolidone (NMP) and *N*-cyclohexyl-2-pyrrolidone (CHP), blends or by adding surfactants or polymers as long to stabilize the dispersion.[45] Details are given in chapter 1.4.1-1.4.2.

A major issue with LPE is that samples are extremely polydisperse in lateral size and thickness after the exfoliation making size selection an important post-exfoliation processing step.[46] To this end, centrifugation is typically applied. In the simplest form, dispersions can centrifuged in a homogeneous centrifugation with a given centrifugal acceleration. The speed and time of the centrifugation directly affects the nanosheets size with higher speed and longer times producing smaller nanosheets. It should be noted that other centrifugation-based separations exist, as will be outlined in chapter 1.4.3. The availability of dispersions containing nanosheets with distinct sizes and thicknesses is an ideal foundation to investigate size-depending properties. Examples with be given in chapter 1.4.4.

1.4.1 Stabilization in Solvents in the Framework of Solution Thermodynamics

The solvent-based liquid exfoliation method has evolved since initially introduced by Hernandez et al. in 2008.[40] The initial work built on the previously elaborated theoretic understanding of related physics that leads to de-bundling and stabilising of carbon nanotubes in the liquid environment.[18] Prior to the application of LPE to layered materials, it has already been studied that re-aggregation in dispersions of carbon nanotubes can be prevented by using polymers or surfactants which results in stabilizing of dispersion. However, without these stabilizers, the bundles are aggregated and the dispersed samples aggregate and flocculate, which leads to a

sedimentation of the nanomaterial. In 2006, it was described that certain solvents can also lead to sufficient stabilization.[47]

The exfoliation and stabilization process can be described in the framework of solution thermodynamics. In general, the Gibbs free energy of mixing ($\Delta\bar{G}_{mix}$) describes the solubility of materials. [24, 48] If the Gibbs free energy is below zero, mixing is spontaneous. This principle under isothermal condition is given by:[49]

$$\Delta\bar{G}_{mix} = \Delta\bar{H}_{mix} - T\Delta\bar{S}_{mix} \qquad \text{(Eq. 1)}$$

where ($\Delta\bar{H}_{mix}$) is enthalpy, ($\Delta\bar{G}_{mix}$) is the Gibbs free energy of mixing, ($\Delta\bar{S}_{mix}$) is the entropy and T is the absolute temperature in Kelvin. In the case of small molecules, very often, a gain in entropy results in spontaneous mixing/dissolution. However, in the case of polymers or nanomaterials, the objects are relatively rigid and the gain in entropy is small. In such cases, it is important to minimize the enthalpie of mixing.

This is the case, when solubility parameters of solvent and solute match. This is described by the Hildebrand-Scratchard equation which says that the enthalpy of mixing is given by:[49]

$$\frac{\Delta\bar{H}_{mix}}{V_{mix}} \approx \phi\,(1-\phi).\,(\delta_a - \delta_b)^{\,2} \qquad \text{(Eq. 2)}$$

where δa, δb are the Hildebrand solubility parameters of solvent and solute (e.g. WS_2 nanosheets), respectively and ϕ is the solvent volume fraction. To produce a dispersion of high colloidal stability and minimal aggregation, it is thus important to match the solubility parameters. The Hildebrand solubility parameter is defined as the square root of the cohesive energy density of a system. Another possible descriptor of solubility is the surface energy which is related to the surface tension.[18]

Equation 2 only strictly holds for molecules, but a model was derived [49] taking into account the dimensionality of the objects (rods or sheets). This is given by:

$$\frac{\Delta\bar{H}_{mix}}{V_{mix}} \approx \frac{2}{T_{flake}}\,(\partial_{nanosheet} - \partial_{solvent})^{\,2}\phi \qquad \text{(Eq. 3)}$$

where T_{flake} is nanosheets thickness, $\phi = V_{nanosheet} / V_{mix}$ is the volume fraction of nanosheets and in general, ∂_a is the square root of surface energy corresponding to phase "a", which is the solvent or the solute, respectively.

While the solubility parameter of solvents are tabulated, the solubility parameters of the nanomaterial cannot be simply derived. However, it is possible to obtain an experimental estimate by dispersing a given material in a broad range of solvent and measuring the concentration of stably dispersed nanomaterial (e.g. through absorbance spectroscopy).[50] When plotting the dispersed concentration as function of solubility parameter, a peak (with a Gaussian envelope is observed with the centre being the estimate of the solubility parameter of the solute.[49] It was found that only minor differences are seen across different nanomaterials.[51]

However, when performing such dispersion screening studies, it is clear that not all solvents with matching surface tension or Hildebrand parameter are solvents that result in sufficient stabilization. This is because there are different types of interactions between the solute and solvent, e.g. hydrogen bonding (EH), polar cohesive energy (EP) and dispersive force (non-polar, ED) as Charles Hansen identified as the most important interactions. The solubility is increased in the case that the nanosheets and solvents are matched for all three of the mentioned parameters. This means that only a limited number of solvents are suitable for LPE. As will be shown in this thesis (Chapter 3.2), the range of possible solvents can be expanded when performing a solvent exchange rather than direct exfoliation in different solvents.

1.4.2 Stabilization in Surfactant and Polymer Solutions

Alternatively, it is possible to achieve a stabilization using surfactant or other additives that adsorb on the nanosheet surface. Examples include detergents in aqueous media. These are made of a non-polar tail and polar head group. In water, these amphiphilic molecules have a tendency to absorb at the hydrophobic nanomaterial surface through the tail group with the polar, often charged headgroup pointing into the liquid.[52-53] Different types of surfactants can be categorised as non-ionic, cationic and anionic. A critical parameter to describe detergents is the so-called critical micelle concentration (cmc), above which the detergent molecules form aggregates with the hydrophobic parts being shielded from the water molecules through the polar groups. Surfactant type, as well as pH and temperature of the solution, affect the micelle's geometry. Micelles can be differently formed including inverted micelle, ellipsoid, cylinder or sphere.[53-54] While it can be anticipated that this would also have an effect on nanosheet stability/dispersibility, experimental work showed that the effect of the cmc is not pronounced in the case of 2D materials.[55] Apparently, a coating on the nanosheet surface below the cmc of the surfactant results in efficient stabilization of the colloid through Coulombic and steric repulsion. In the case of charged, small molecule

detergents, Coulombic repulsion which can be described in the framework of the DLVO theory is the dominant factor.[56]

Graphene and other 2D materials can also be stabilized by using a broad range of polymers as a substitute for small molecular surfactants. Different effects such as electrostatic and lyophilic interactions can be created by using polymers. However, steric is the main mechanism of stabilization with the functionality of adsorbing polymers on the surface of nanosheets in an irregular way which results in sticking polymers tails and loops out the solvents.[57] In general, the free energy increases (chain confirmations number is lower) when the sticking out polymers occupy a similar space. This increased energy plays an important role in repulsive energy which leads to a stabilization of the system.[57-58] Observations from a comparative study on exfoliation of various 2D materials in the presence of different polymers could prove that polymer stabilization can also be described in the framework of solution thermodynamics: when solubility parameter of solvent and polymer are matched, an improved stabilization due to the matching of Hildebrand parameters is observed.[57] In addition, a correlation between dispersed nanosheets concentration and polymer molecular weight is observed.

Overall, this means that nanosheets can be stably dispersed in a range of organic solvents using polymers as additives, in this case solubility mediating functional groups. Typically, this is achieved by adding a polymer into a solvent with solubility parameters matching to the polymer and performing the exfoliation e.g. through sonication. Unfortunately, in the case of TMDs, the monolayer contents were reported to be lower than in the case of small molecule detergent stabilization.[45] In this thesis (Chapter 3.4), a new route towards making a high-quality WS_2-polymer composite is introduced to address this point.

It should be noted, that intrinsic properties of nanosheets can be influenced by doping effects from the stabilizers. For instance, a sign of doping was reflected in the appearance of trion emission in photoluminescence spectra obtained from WS_2 monolayer embedded in a polymer matrix of poly vinyl alcohol (PVA).[45] In contrast, an exciton PL with narrow linewidth is observed when nanosheets are embedded in a different polymer matrix, i.e. polymethylmethacrylate (PMMA).[59] To date, a comprehensive study on the impact of the solvent, or solvent/additive system on the excitonic properties of LPE nanosheets is missing. This will be addressed in this thesis in Chapter 3.1 and 3.2.

1.4.3 Size Selection Methods

As already mentioned, layered crystals of TMDs (transition metal dichalcogenides) can be exfoliated through the liquid-phase exfoliation approach, but this method of exfoliation produces polydisperse samples with broad size and thickness distributions. Since the size and particular thickness determines the properties, specific sizes of nanosheets have to be selected from the polydisperse mixtures to meet requirements in different application areas, e.g. catalysis, energy storage, polymer reinforcement or (opto)electronics. Most size selection technique are based on centrifugation techniques, which separate nanosheets by mass in first approximation. This makes the selection of thin and large nanosheets a major challenge. This is further complicated by the fact that small sheets tend to be thin and large sheets tend to be thick so that large/thin sheets are a minority population.[42]

While some centrifugation techniques such as density gradient ultracentrifugation (DGU) can potentially sort nanosheets by their layer number, the intrinsic relationship between size and thickness mentioned above implies that sedimentation-based approaches can be equally suitable. In this regard, the multi-step and versatile approach of Liquid Cascade Centrifugation (LCC) is an efficient method to select liquid phase exfoliated nanosheets by size in large quantities. This methodology was also used throughout this thesis. The concept is illustrated in Figure 1.4-1. The centrifugation speeds indicated are an example and can be adjusted depending on the types of samples that are targeted.

In brief, LCC is a multistep centrifugation procedure with sequentially increasing speed in each step. After each run, the supernatant and sediment are separated, the supernatant is transferred to the next stage at increased centrifugal acceleration and the sediment containing is collected in fresh solvent. As such, nanosheets in each run are trapped between two centrifugation boundaries (speed of centrifugation) which removes small/thin sheets from samples where large/thick sheets are collected and *vice versa*. The higher the speed of centrifugation, the smaller/thinner the size of nanosheets in the collected sediment. Hence, the transferred supernatant to the proceeding step contains the smaller and thinner nanosheets while the left sediment behind contains larger nanosheets.[60-61] Comparatively large masses of exfoliated and size selected nanosheets can be produced by LCC compared to other size selection methods, such as DGU.[62-64] In addition, the nanosheet concentration can be increased by redispersing in a reduced volume, the solvent can be exchanged and it is applicable to both organic solvent and aqueous surfactant systems. While the separation occurs predominantly by mass, it has been reported, that specific cascades can be designed to selectively enrich certain nanosheet dimensions, in particular monolayers.[65]

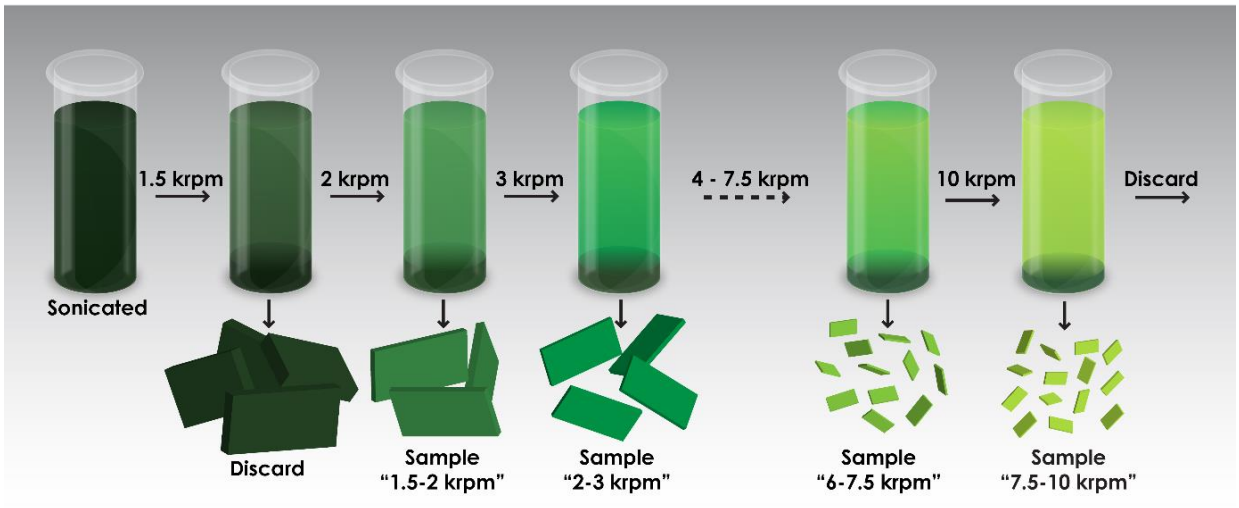

Figure 1.4-1: Schematic illustration of size selection by liquid cascade centrifugation. After each centrifugation step, supernatant and sediment are separated, the sediment collected and the supernatant subjected to centrifugation at higher centrifugal acceleration. Reprinted from ref. [65]

1.4.4 Size Dependent Optical Properties

After exfoliation and size selection procedures, dispersions contain different mean sizes of nanosheets that are well suited to track changes in optical properties with size. When size distributions and average sizes are quantified by atomic force microscopy statistics, the size information can be quantitatively linked to the spectral profile. The simplest spectroscopy in this regard is probably extinction and absorbance spectroscopy. In extinction spectroscopy, the attenuation of the light intensity through a sample is measured in transmission as function of wavelength. As such, it contains contributions from both light scattering and absorbance. The scattering is strongly size-dependent,[66] so that a size dependence of the spectra profile is expected. This has been described in detail for 2D platelets in the non-resonant regime, i.e. at energies below the electronic transitions.[67]

In addition, it was shown that the absorbance spectra, which can be acquired in the centre of an integrating sphere where scattered light is collected, also show a size dependence, in particular in the case of TMDs.[60, 65, 68] Importantly, it was found that the scattering in the resonant regime follows the absorbance in shape so that information encoded in absorbance spectra can be extracted from extinction spectra. In general, the systematic changes in optical extinction/absorbance spectra are related to both edge and confinement effects that result in different changes of the spectral profile. This is illustrated in the case of LPE WS_2 in Figure 1.4.2.

Figure 1.4-2A shows absorbance coefficient spectra of size-selected LPE dispersions of WS_2. Clearly, the intensity (i.e. absorbance coefficient) changes with nanosheet size differently for different excitation energies, i.e. the intensity profile changes. Empirically, it is found that the absorbance (and extinction) coefficient is widely constant at 235 nm so that this wavelength can be used to calculate the nanosheet concentration and yield using the Lambert-Beer law and the reported extinction coefficient of $\varepsilon_{235nm} = 47.7\ Lg^{-1}cm^{-1}$.[65]

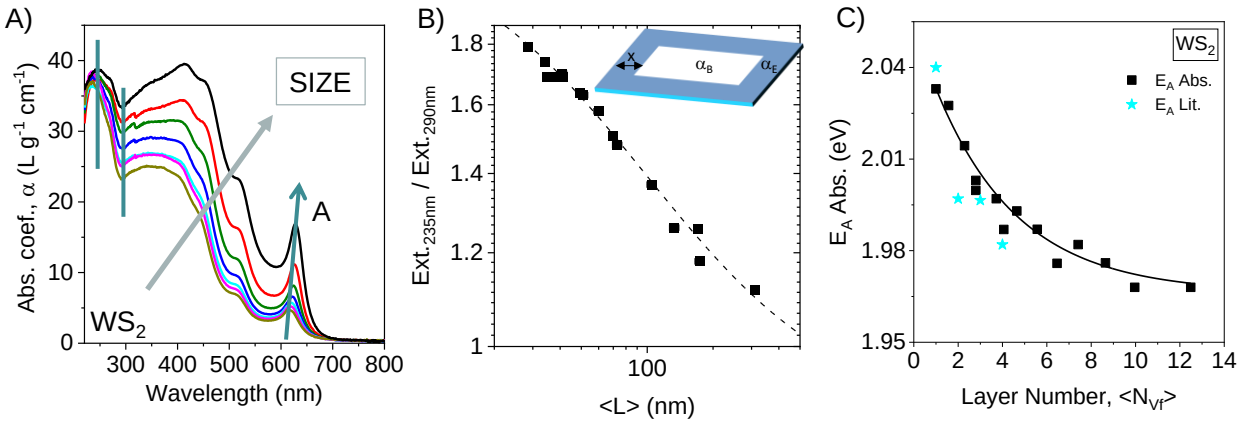

Figure 1.4-2: A) Absorbance coefficient of size-selected WS_2 dispersions in aqueous surfactant solution. The characteristic excitonic transitions are observed and size-dependent changes illustrated. B) Plot of extinction intensity ratio as function of average nanosheet length (measured from microscopy statistics). C) Plot of A-exciton energy as function of average (volume-fraction weighted) layer number showing an exponential dependence of the exciton energy with thickness. The black dots indicate dated from LPE measured in dispersion, while the cyan symbols show data from individual micromechanically-exfoliated nanosheets on substrate. Adapted from ref.[68]

It was suggested that these changes in the absorbance intensity as function of wavelength for the size-selected dispersions are due to edge effects.[60] Since edges are electronically different from the basal plane, they will have a different absorbance coefficient. At each wavelength, a combination of both basal plane and edge absorbance is observed, but to a different extent depending on the average lateral dimension. Therefore, nanosheets length can be calculated from the peak intensities ratio extracted from optical extinction spectra. This model is described by equation 4:

$$\frac{\mathrm{Ext}_{235}}{\mathrm{Ext}_{290}} = \frac{\alpha c(235nm)L + 2x(k+1)\Delta\alpha(235nm)}{\alpha c(290nm)L + 2x(k+1)\Delta\alpha(290nm)} \qquad \text{(Eq. 4)}$$

Table 1.4-1: Parameters used to calculate nanosheets length from the peak intensities ratio extracted from optical extinction spectra.

Symbol	Definition
x	Thickness of the edge region
k	Aspect ratio
L	Nanosheets length
α_C	Absorption coefficient of the nanosheets basal plane
$\Delta\alpha$	= αE– αC→ αE is absorption coefficient of the edge region

The correlation of the extinction intensity ratio at 235nm/290nm as function of average length is shown in figure 1.4-2B.[68] Fitting the data to equation 4 yields equation 5 which relates the ratio of peak intensities extracted from optical extinction spectra to the mean nanosheets length, <L>:[68]

$$\text{L (nm)} = \frac{2.3 - \frac{\text{Ext}_{235}}{\text{Ext}_{290}}}{Ext_{290}\ 0.02\ \frac{\text{Ext}_{235}}{\text{Ext}_{290}} - 0.0185} \qquad \text{(Eq. 5)}$$

This equation can be used for any WS_2 dispersion to extract the mean nanosheet length, <L> from optical extinction spectra.

In addition to the obtained information relevant to nanosheet length, mean nanosheet layer number <N> can be extracted from optical extinction spectra from the A-exciton peak position. This shift was originally assigned to confinement effects (i.e. changes in the band structure)[60], although more recent work suggested that dielectric screening effects of the excitons (i.e. changes in the binding energy) also play a role.[68] Reduction in thickness results in A-exciton shifts towards lower wavelengths, i.e. higher energy (Figure 1.4-2C). Empirical fitting with to an exponential decay yields equation 6, which can be used to extract the mean layer number of WS_2 nanosheets, <N> from the A-exciton wavelength, λ_A:[69]

$$< \text{N} > = 6.35 * 10^{-32} e^{\lambda_A\,(\text{nm})/8.51} \qquad \text{(Eq. 6)}$$

It should be considered that this equation only applies to WS_2 and for other TMDS like MoS_2, the same qualitative behaviour is observed, albeit with quantitative differences.

Furthermore, in monolayer-rich WS_2 dispersions some hidden spectral features are revealed in the second derivative of the A-exciton absorbance, i.e. a splitting of the monolayer component and the sum of the few-layers (more information is given in Chapter 3).

In addition to the metrics for nanosheet thickness and length from extinction spectra, a metric that corresponds to the monolayer content is desired. According to previous work,[65] this metric can be extracted from the PL (photoluminescence) of nanosheets. It is reported that the PL can be measured in a Raman spectrometer (for WS_2: λ_{exc} = 532 nm), which allows to simultaneously detect the PL from monolayers and the Raman modes stemming from all WS_2 units regardless of their thickness.[65] For exfoliated WS_2 nanosheets, 2461cm^{-1} is the wavenumber where the monolayer photoluminescence is observed which corresponds to ~611 nm for the 532 nm excitation. The higher the content of the monolayer, the higher the intensity of the PL peak (with respect to the Raman mode) and hence the lower the average thickness of the nanosheets.

It has been observed that increasing the speed of centrifugation yields a higher content of monolayers and hence, the intensity of the PL peak increases with respect to the Raman mode of the material.[65] By quantifying the monolayer content in a range of samples by AFM statistics, it was found that the monolayer volume fraction vs I_{PL}/I_{Raman} are linearly correlated. The monolayer volume fraction (in WS_2 dispersions) can be estimated by the following equation:

$$V_f = \frac{I_{PL}}{17\, I_{Raman}} \qquad \text{(Eq. 7)}$$

Where: V_f is the monolayer volume fraction, I_{PL} is intensity of PL peak and I_{Raman} is the intensity of Raman mode.

However, non-radiative decay can be observed by edges for small nanosheet sizes if the diffusion length of the exciton is in the same range as the nanosheet size.[65, 69] Furthermore, the PL quantum yield can also be affected by other parameters, such as defects.[70] Therefore, the PL/Raman intensity ratio should rather be considered as quality indicator of the exfoliated TMDs in dispersion. As will be shown in the next Chapters, it can also be influenced by the stabilizer due to doping

2. Objectives of the Thesis

The main goals of this thesis can be summarized as follows:

- Production of high-quality TMD dispersions suitable to study exciton physics.
- Develop protocols to modify the environment (dielectric screening and chemical doping).
- Identify optical fingerprints of dielectric screening and chemical doping.
- Use knowledge for controlled chemical doping of nanosheet in liquids and in thin films.

To this end, high quality WS_2 dispersions were first prepared by liquid exfoliation and subsequently transferred to a range of additive/solvent system. This is described in Chapters 3.1-3.2 bearing in mind the following fundamental scientific questions.

1. Can the A-exciton be used to track solvatochromism?
2. What is the best indicator to describe the interaction between WS_2 nanosheets with various chemical environments? The following options will be investigated: A exciton energy, Exciton or trion width, Exciton/trion ratio, scaling of A-exciton energy with thickness
3. Is a transfer to pure solvent in the absence of additives possible and allows to correlate the A-exciton response to physical parameters of the surrounding (static versus dynamic screening)?
4. Is a wider scope of solvents accessible on transfer compared to direct exfoliation?

With suitable organic, additives free solvents identified, the second part of the thesis (Chapter 3.3-3.4) was devoted to depositing the nanosheets in a controlled way with restacking between the sheets prevented. Such thin films are the foundation to study chemical doping from substrates. Here, aggregation that occurred over time was a major limiting factor. In the part, the following questions are discussed:

1. How can the coverage of deposited sheets be tuned efficiently?
2. How can aggregation and restacking be prevented (in dispersion and films)?
3. How can the optical quality in TMD thin films be improved?

3 Results and Discussion

3.1 Impact of Various Additives on the Optical Properties of LPE WS_2

3.1.1 Introduction

There is a fundamental difference between the excitonic properties of bulk semiconductor and the 2D monolayer of the same material. The electron-hole pair which forms the exciton is strongly confined to the plane of TMD monolayers. The electric field lines joining the electron and hole begin to extend outside of the sample which leads to an increase in the quasiparticle bandgap for monolayers and simultaneously in larger exciton binding energy as electron and hole interactions are enhanced.[29, 71] With this picture in mind, it is clear that the environment will also have an impact on the excitonic properties which is expected to be more significant in monolayer materials.

In this section, optical properties of tungsten disulfide (WS_2) nanosheets in different liquid environments are investigated. Based on previous works, WS_2 was chosen for this study due to some advantages, importantly the large spin-orbit splitting between the A and B excitons of about 0.4 eV which allows us to study the low energy excitons unobscured by features from higher-energy transitions. Secondly narrow spectral features are observed which facilitates an analysis of the A-exciton on absorbance spectroscopy in the case of mixtures polydisperse in thickness, as is the case in LPE dispersions. Solvatochromic and dielectric screening effects are studied by transferring WS_2 nanosheets produced by sonication-assisted LPE and size-selected by LCC into a broad range of additive and solvents systems. The transfer of the same dispersion greatly facilitates the analysis, as size-dependent effects can be taken out of the picture. Expected solvatochromic behaviour (e.g. A-exciton shifts and broadening) are probed by UV-Vis and Raman/PL spectroscopy. These investigations are performed to approach a deeper understanding of the interaction of WS_2 nanosheets with different chemical environments. It should also be noted that further processing such as fabrication of high-quality WS_2 thin films can be improved by selecting suitable solvent and additive systems which will be addressed in Chapters 3.3 and 3.4.

3.1.2 Preparation of the Dispersions

WS_2 dispersions were prepared by probe sonicating WS_2 powder in an aqueous sodium cholate (SC) solution in 80 mL batches using a two-step sonication procedure (see methods). This as-prepared dispersion is referred to as stock dispersion and contains nanosheets with broad size and thickness distributions which are subsequently narrowed by size selection through liquid cascade centrifugation (LCC). In this section, the following procedure was applied as also illustrated in

Figure 3.1-1. In a first centrifugation, unexfoliated crystallites are removed from the stock dispersion by low speed centrifugation at 400 *g*. This dispersion contains nanosheets with a broad distribution of sizes and thickness and a small but nontrivial population of monolayers with varying lateral sizes.[55, 69] The supernatant after the cleaning step at 400 *g* is subjected to further centrifugation at 1,000 *g*. The material in the sediment after this step contains the largest nanosheets. The supernatant is separated from the sediment and is subjected to a higher centrifugation rate at 5 k*g* to give a sediment with slightly smaller nanosheets. The sediment is collected in in fresh solvent (H_2O-SC at SC concentrations of 0.1 gL^{-1}) at reduced volume (3-8 mL) and subjected to 5 minutes bath sonication which leads to an efficient redispersion. Since the fraction was isolated between centrifugation rates of 1000 and 5000 *g*, we refer to this sample as "1−5k *g*".

The supernatant after the 5k *g* step was centrifuged again and the cascade continued for as many steps as are required with each step using an increasing centrifugation rate. In this work, the final sediment was collected after centrifugation at higher speeds, either 10,000 or 22,000 *g*. The resultant supernatants are more and more monolayer-enriched because the heavier, few-layer nanosheets are removed in each step of the size selection. As sample nomenclature, the lower and upper boundary of the centrifugation are indicated, as mentioned above. The final supernatant is discarded, as it mostly contains free surfactant and extremely small WS_2 nanosheets. In this section, four different fractions with narrowed size distribution, labeled as "0.4-1k *g*", "1-5k *g*", "5-10 k*g*", "5-22k *g*" were subjected to further analysis.

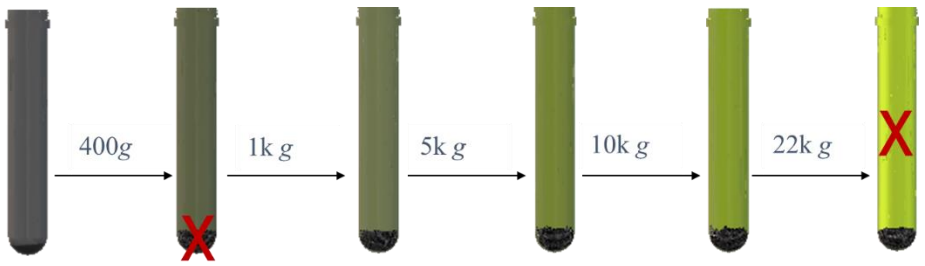

Figure 3.1-1: Schematic illustration of the size selection by liquid cascade centrifugation with the *g*-force iterations used in this study. Size-selected dispersions were prepared by redispersing the collected sediments in 0.1 gL^{-1} aqueous sodium cholate. The sediment discarded after the first centrifugation contains unexfoliated layered crystallites while the supernatant discarded after the last centrifugation step contains extremely small nanosheets.

After the size selection, the WS_2 nanosheets were transferred to several solvents/additives systems to investigate in which way solvatochromic effects can be tracked through the excitonic response.

Therefore, an effort was made to select a set of additives/solvents as diverse as possible including anionic, cationic and non-ionic molecular additives (surfactants) as well as ionic and non-ionic polymers.[60, 68] Note that we found that the choice was nonetheless limited, as not all additive/solvent dispersions yielded stable dispersions. The suitable systems are summarized on Table 3.1-1. To achieve the transfer, the size-selected dispersions (in 0.1 gL^{-1} aqueous SC) were diluted to an optical density suitable for the measurements and split in 1.5 mL aliquots and centrifuged again at centrifugal accelerations above the initial higher centrifugation boundary. After this step, the sediments were redispersed in the different liquid media. The detailed protocol is illustrated in figure 3.1-2.

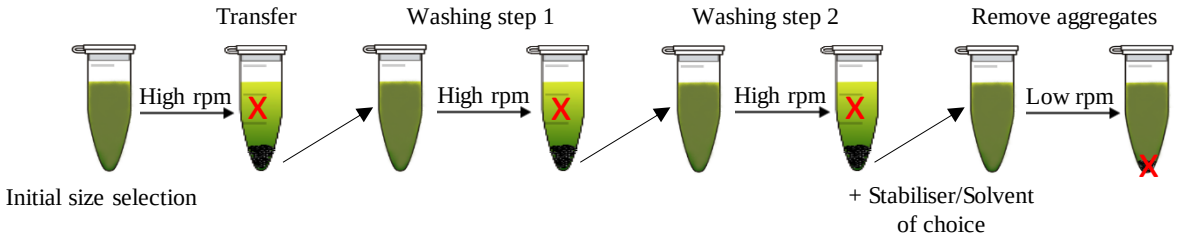

Figure 3.1-2: Schematic illustration of the protocol to transfer WS_2 nanosheets to a range of additives. After exfoliation in aqueous sodium cholate and size selection by liquid cascade centrifugation, the nanosheets in the sediment are redispersed in water. the mixture is distributed to small vials. the resultant dispersion centrifuged again at centrifugal accelerations above the initial higher centrifugation boundary. The supernatant is discarded and the WS_2 nanosheets in the sediment washed again with water and/or THF consecutively and the sediment redispersed in the stabilizer of choice. In a last step, aggregates are removed by centrifugation at 100 *g*.

Specifically, the following centrifugal accelerations were used: 30k *g* for the 5-22k *g* sample, 15k *g* for the 5-10k *g* sample, 7k *g* for the 1-5k *g* sample and 2k *g* for the 0.4-1k *g* sample. After this step, the supernatant was discarded and the WS_2 nanosheets in the sediments were washed through redispersing in distilled water or THF, depending on the solubility of the additive. After redispersion, the mixtures were sonicated ~3 mins in a sonic bath to account for re-aggregation and centrifuged again at high centrifugal acceleration (values as in the first step of the transfer see above). This step was performed twice to remove as much of the initial surfactant as possible. The washed WS_2 nanosheet sediment, was then redispersed in the desired solvent/additive mixture by using three minutes bath sonication. In the last step, aggregates were removed by centrifugation at low-speed centrifugation at 100 *g* for 30 min(Figure 3.1-2). All water-soluble additives were used as aqueous solutions, with the exception of poly(vinyl alcohol) (PVA) which was also tested in the organic solvents *N*-methyl-2-pyrrolidone (NMP) and dimethylsulfoxide (DMSO). For other polymers, either tetrahydrofuran (THF) or NMP were used as solvents. Small molecules were used

at typical surfactant concentrations of 2 gL^{-1}, whereas 0.1 gL^{-1} was used for polymers due to the lower solubility.

Table 3.1-1: List of all solvent/additive systems including the full name, abbreviation and their concentration. For some systems (e.g. Polystyrene-Toluene and Polystyrene-chloroform) too much aggregation appeared after transferring WS_2 limiting the choice of suitable systems.

Stabilizer	***Abbreviation***	***Conc.***	***Solvent***
Polymers			
Poly(vinyl alcohol)	PVA	0.1 gL^{-1} *and* 20 gL^{-1}	H_2O
Poly(vinyl alcohol)	PVA	0.1 gL^{-1}	Dimethylsulfoxide-DMSO
Poly(vinyl alcohol)	PVA	0.1 gL^{-1}	N-Methyl-2-pyrrolidone -NMP
Polystyrene	PS	0.1 gL^{-1}	N-Methyl-2-pyrrolidone -NMP
Polystyrene	PS	0.1 gL^{-1}	Tetrahydrofuran - THF
Poly(methyl methacrylate)	PMMA	0.1 gL^{-1}	Tetrahydrofuran - THF
Polyvinylpyrrolidone	PVP	0.1 gL^{-1}	H_2O
Hyaluronic acid sodium salt	HA	0.1 gL^{-1}	H_2O
Nonionic Surfactant			
Polyethylene glycol tert-octylphenyl ether	Tx-100	2 gL^{-1}	H_2O
Polyoxyethylenesorbitan monolaurate	TWEEN® 20	2 gL^{-1}	H_2O
Cationic Surfactant			
Hexadecyltrimethylammonium bromide	CTAB	2 gL^{-1}	H_2O
Anionic Surfactant			
Sodium cholate hydrate	SC (as reference)	2 gL^{-1}	H_2O
Sodium deoxycholate	SDC	2 gL^{-1}	H_2O
Sodium dodecylbenzenesulfonate	SDBS	2 gL^{-1}	H_2O
Sodium dodecyl sulfate	SDS	2 gL^{-1}	H_2O

3.1.3 Absorbance/Extinction Spectroscopy

Optical extinction measurements for all transferred WS_2 fractions in a range of additives and solvents systems were carried out. As outlined in chapter 1.4.4, optical extinction spectra of LPE TMDs are rich in information. In the case of the reference system in SC, quantitative metrics were established which allow to calculate the average lateral sheet dimensions from extinction intensity ratios and the layer number from the A-exciton energy which was found to blue-shift with

decreasing thickness.[65, 68] In this work, the goal is to understand in which way the environment has an additional impact on the A-exciton energy. Since the same nanosheet dispersions were transferred to a different liquid environment, the layer number should only vary across the size-selected fraction, but remain constant within one set of samples in different additive/solvent systems. Hence, it is known in all samples without the need for microscopy statistics. Similarly, the nanosheet length should remain constant.

In figure 3.1-1A, a selection of extinction spectra of the same WS_2 fraction (5-22k g) is shown after transfer to different environments. The overall spectral profile remains similar which confirms that the nanosheet dimensions do not vary significantly, as differences in peak intensity ratios are expected otherwise. In addition, it should be noted that no significant contribution from non-resonant scattering (> 650 nm) is observed which strongly suggests that aggregation effects are minor. However, as illustrated by the inset, even though it is the same population of the nanosheets, a slight shift of the A-exciton is observed. To analyze this in more detail, the second derivative of the A-exciton region was calculated for all samples (see Appendix Figure A6.1). For samples with a significant monolayer content (isolated at high centrifugation speed > 5k *g*), it is composed of two features, as illustrated in figure 3.1-1B. Previous work[65, 68] assigned the A-exciton resonance at 2.033 eV (612 nm) to WS_2 monolayers (in aqueous SC), while the second component at 622 nm relates to the average of all WS_2 few-layers as indicated in figure 3.1-1B by the grey and light blue shaded areas, respectively. Due to the relatively narrow linewidth of the excitonic resonances of LPE WS_2,[68] the monolayer contribution is very well separated from the few-layer component in the second derivative. Importantly, depending on the additive, a peak shift is observed. This shift appears more pronounced for the monolayers which results in a reduced splitting between the monolayer and few-layer component, as clearly observed for WS_2-PVP in figure 3.1-1B. From all data (see Appendix Figure A6.1), the positions and widths of the two components were determined from a fit to the second derivative of the sum of two Lorentzian as outlined in ref [65]. The fits are indicated as solid lines in figure 3.1-1B and figure A6.1.

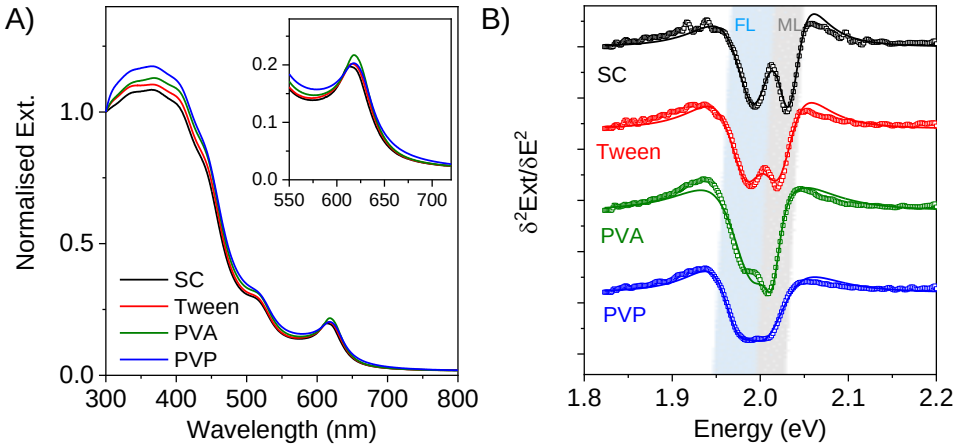

Figure 3.1-3: A) Selection of normalized optical extinction spectra of same size-selected WS_2 dispersion (5-22k *g*) transferred to different stabilizers. The inset shows a zoom-in to the A-exciton region of the optical extinction spectra. B) Second derivative of the A-exciton region of the same samples after smoothing the spectrum. A splitting into two components is observed which can be assigned to monolayer (ML) and few-layer (FL).

Since the layer number also results in a shift of the A-exciton, it is important to deconvolute the effect from the stabilizer from that of the layer number. This can be achieved by plotting the A-exciton energy, E_A, as function of layer number for the different stabilizer systems. For the different size-selected fractions, the layer numbers were calculated from published quantitative metrics of the SC reference systems.[60, 65, 68] A subset of the data is shown in figure 3.1-4A, for all data see Appendix Figure A6.2. While strictly speaking an exponential correlation of exciton energy with layer number was revealed,[68] the data can be fit well to an empirical power law as illustrated by the solid lines in figure 3.1-4A. This allows to extract the exponent, $Exp_{E\text{-}N}$ (i.e. the slope on the semi-logarithmic plot) and the A-exciton energy of the monolayer, $E_{A,ML}$ which is the intercept with layer number of 1. These two parameters are related to the average WS_2 layer number, <N> according to equation 8:

$$< N >= 10^{\left(\frac{E_A - E_{A,ML}}{Exp_{E-N}}\right)} \qquad \text{(Eq. 8)}$$

As can be seen from figure 3.1-4A, the additive changes both the exciton energy of the monolayer ($E_{A,ML}$), as well as the exponent relating the exciton energy with the layer number ($Exp_{E\text{-}N}$). This shows that thinner nanosheets are more affected by the environment, compared to larger nanosheets, since more of the material is exposed to the surrounding liquid.

We refer to this scenario as solvatochromism, since this is probably the more generalized term which includes changes in the effective dielectric environment, as well as potential chemical doping. Regardless of the origin of the solvatochromic effect, we would expect that the monolayer

exciton energy scales with $Exp_{E\text{-}N}$ in some way. To test this, the two fit parameters are plotted versus each other in figure 3.1-4B. Importantly, data points using different stabilizers fall on the same curve that can be described well be a linear relationship as indicated by the solid line. Figure A6.3 (Appendix) shows the same plot with the datapoints labelled with the respective solvent/additive systems. While it cannot be rationalized which system results in a stronger solvatochromic effect, some details will be pointed out: i) A combination of solvent and additive can be observed, since there is a stronger red-shift (interpreted as enhanced Coulomb screening) of the A-exciton in PS-NMP compared to PS-THF. However, this is not necessarily the case as shown by the data in PVA, which clusters in the same area ii) The effect is strongest in the cationic surfactant CTAB and the pyrrolidone-based polymer PVP suggesting a strong interaction with the nanosheets, i.e. due to chemical doping or dielectric screening, or a combination of the two. iii) The A-exciton is highest in energy for pure water, as well as the widely used surfactants SC and SDBS. This agrees well with previous investigations on suspended, free-standing monolayers of micromechanically-exfoliated MoS_2, where it was shown the A-exciton photoluminescence of monolayer and bilayer MoS2 is red-shifted by only ~10 meV, i.e. solvatochromism is negligible.[60]

While this correlation of $Exp_{E\text{-}N}$ and $E_{A,ML}$ is an interesting finding, it does not improve the understanding of the physics of excitons in 2D materials, since the exact nature of the surrounding (refractive index, dielectric constant) is not known in additive/solvent systems For example, it is unknown how the non-covalent interactions of the additive in the different environment change. Also we can observe a combination of the effect of solvent and additive. Furthermore, chemical interactions with the additives resulting in doping cannot be excluded. To achieve a more fundamental understanding, it is necessary to perform such experiments in neat solvents in the absence of additives which is more difficult, as there is a risk that dispersions are not colloidally stable resulting in aggregation of the nanosheets effectively changing the layer number. Experiments along these lines are described in chapter 3.2. Nonetheless, the data from the solvent/additive systems is useful for us as this enables to adjust the metrics related to the nanosheet thickness for different dielectric environments.

To generalize the thickness metrics for different environments, the correlation of $Exp_{E\text{-}N}$ with $E_{A,ML}$ in Figure 3.1-4B is empirically fit to a linear function yielding the following equation:

$$Exp_{E-N}[eV] = 1.667eV - 0.851\ E_{A,ML}\ [eV] \qquad \text{(Eq. 9)}$$

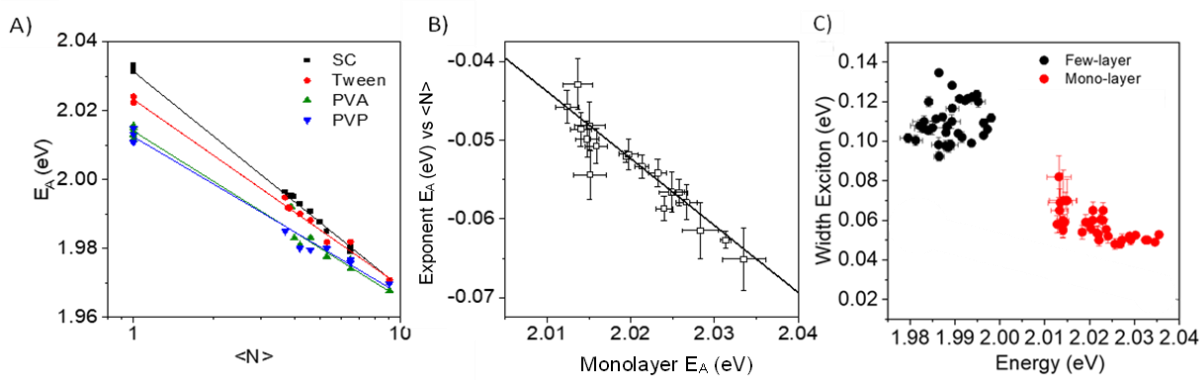

Figure 3.1-4: A) A-exciton energy plotted as a function of layer number. B) Plot of extracted fit parameters from all data shown in the appendix, figure A6.2. A linear relation between the exponent and the and monolayer A-exciton energy is observed. C) Scaling of the monolayer A-exciton width *vs.* the energy (eV) extracted from the width of the A-exciton second derivative.

An A-exciton position dependant-based equation for determining the number of layers is devised by inserting equation (9) in (8). This equation can be applied to all WS_2 samples, in unknown environments and is given by:

$$< N > = 0.434\, e^{\left(\frac{E_A\,[eV] - E_{A,ML}[eV]}{0.167\ eV - 0.851\ E_{A,ML}[eV]}\right)} \qquad \text{(Eq. 10)}$$

To determine the layer number of WS_2 in liquid environments, the only required input parameters are the A-exciton energy in the respective sample and the A-exciton of the monolayer which can be determined from fitting the second derivative of the A-exciton in a monolayer-rich samples (compare figure 3.1-3B). We note that such fits also yield the width of the monolayer and few-layer A-exciton response. This is plotted as function of A-exciton energy on figure 3.1-4C. The few-layer width is cluttered and larger than the monolayer width. This is can be rationalized, as this is the average value of all few-layers, i.e. the response does not stem from a single, defined layer number. This is in contrast to the higher energy component in the A-exciton which is exclusively from monolayers. Here, a rough scaling of exciton width and energy is observed. This suggests that the redshift associated with solvatochromism is accompanied by a broadening of the excitonic resonance.

In summary, a robust indicator for the interaction of TMDs with the environment was identified by evaluating the data obtained from UV-Vis extinction spectroscopy. Solvatochromic effects are best observed by plotting the A-energy as function of WS_2 layer number which reveals different exponents and ML exciton energies. Also, A-exciton width *versus* energy shows a rough, but scattered relation (at least for ML). However, probably the error from fitting the A-exciton second derivative is too large to observe this clearly. Overall, changes in the A-exciton energy-thickness

relation confirmed that solvatochromism can be observed from the A-exciton resonance. This was used for an improved quantitative metric to calculate the layer number of WS_2 from the optical spectra in various additive systems.

3.1.4 Photoluminescence spectroscopy

The A-exciton response can also be investigated with the aid of fluorescence spectroscopy which is potentially more sensitive to the environment than the absorbance. Thus, it is investigated how different additives affect the fluorescence spectra of the WS_2 nanosheets. Previous work suggested that the PL/Raman intensity is quantitatively related to the monolayer content as only the monolayers are luminescent.[65] However, it is unknown in which way this quantitative relationship is influenced by different stabilizers, or indeed different measurement conditions.

For the measurements, a Raman spectrometer (λ_{exc}=532 nm) was used. All samples with the smallest size of nanosheets (here 5-22k *g*) were investigated, since they have a sufficient quantity of monolayers. Samples were measured at high concentration, i.e. after redispersion in minimal volume after the transfer to eliminate the contribution from solvent to spectra. To avoid reabsorption and innerfilter effects, the laser was focused above the surface of the liquid droplet.[72]

It is reported that the PL is very sensitive to the dielectric environment and the defect content in the samples.[73] Therefore, in this study it is considered that photoluminescence peak position and width might be affected by various factors: i) defect content, ii) temperature, iii) dielectric screening from the different environment. In addition, a PL shift could be attributed to either doping or strain induced by the different additives.[73] In TMDs, doping is expected to result in the emission from trions, i.e. negatively charged excitons, which are observed at lower energies than the exciton.[25] Furthermore, the laser power will have an impact on the PL quantum yield and hence the PL/Raman ratio due to exciton-exciton annihilation at high power.[74] In addition, enhanced trion emission was reported at higher laser power.[75-76] Note that in additive systems, a photo-induced charge transfer[77] can also not be ruled out which is expected to significantly change the contribution from trions to the spectra as function of laser power (and additive).

To establish suitable measurement conditions, spectra were first acquired in the different WS_2/additive systems for different excitation laser powers. Some examples are shown in figure 3.1-5. The spectra are normalized to the 2LA(M) Raman mode at 355 cm^{-1}. In all cases, the feature at > 2000 cm^{-1} can be attributed to photoluminescence (from excitons and/or trions). In LPE WS_2 suspended in SC, emission from predominantly excitons was reported which is centered at 2525

cm^{-1} corresponding to ~612 nm.[65] In both Tween and SDBS, a second, red-shifted PL feature evolves at lower energy (*i.e.* larger Raman shift) at higher laser power which is attributed to emission from trions. The laser power threshold for this second component is different for the two surfactant systems shown and occurs at 5% (0.81 mW spread over ~4 x 35 μm^2) in Tween and a factor of 10 lower power in SDBS.

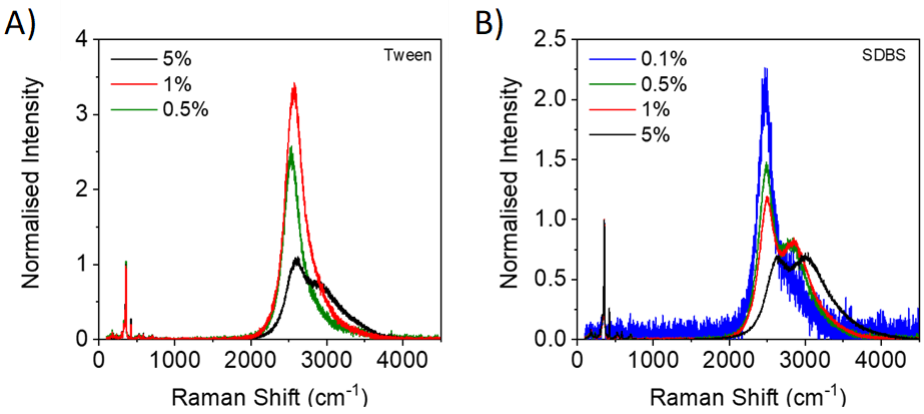

Figure 3.1-5: Impact of laser power on photoluminescence properties of standard samples. A, B): Selection of normalized Raman/ PL spectra (excitation at 532 nm) of size-selected WS_2 (5-22k g) transferred to different stabilizers (A- Tween; B- SDBS), showing non-systematical changes when the laser power is varied.

Similar effects have previously been observed in CVD grown WS_2 transferred by different techniques.[78] The reason for such behavior remains elusive. While different levels of strain were suggested in the work focusing of CVD-grown and transferred WS_2, this is unlikely in our case since the monolayers are laterally very small (< 50 nm) and still suspended in a liquid environment. If the environment induced any significant strain or doping effect in the WS_2, the $E_{2g}{}^1$ and A_{1g} Raman vibrational modes would shift[73] as well which is not observed in our data. While this merits further investigation in the future, in this work, we attempt to avoid this effect as much as possible and acquire the spectra below the power threshold of this effect, which was found as 1% laser power in most systems with the exception of SDBS where, the power was further reduced to 0.1%. We also note that the effective laser power is dependent on the focus of the laser on the surface. This is much more difficult to control in the measurements on the surface of liquid drops compared to solid substrates. Thus, the effective laser power cannot be considered identical for all samples. However, we focus our analysis on PL energies and widths which are widely unaffected to small

changes in laser power[78] (as long as the threshold is low enough to avoid the pronounced trion emission observable in some cases).

Figure 3.1-6A shows a selection of Raman/PL spectra of monolayer-enriched LPE WS_2 dispersions (fraction 5-22k *g*) transferred to different additive systems normalized to the 2LA(M) Raman mode (355 cm^{-1}). Note that high concentration samples were measured to avoid the contribution from the water Raman at 3000-3700 cm^{-1}. Peak shifts and broadening can be observed in the PL spectra due to changes of the environment by the different stabilizers. Note that this also dramatically changes the PL/Raman intensity ratio which had been suggested as metric for the monolayer content[65] due to negligible emission from few-layers. This clearly demonstrates that the PL intensity is strongly affected by the surrounding medium and that the reported metrics[65] are only valid for the WS_2-SC reference system that was previously investigated in detail.

While similar changes in position and width have been observed in the A-exciton response in the absorbance spectra, they are much larger in magnitude in the PL spectra. For example, the A-exciton energy of WS_2-in the absorbance spectra was centered at 2.015 eV, while the PL is centered at 2970 cm^{-1} which corresponds to 1.96 eV. Therefore, it is likely that the PL response is not only affected by dielectric screening, but also chemical doping which can result in an increase of the trion contribution (charged exciton). To analyze this in more detail, the PL spectra of the WS_2 dispersion transferred to the different additive and solvent systems is fitted to two Lorentzians, which have been assigned to originate from the radiative combination of the A^- trion and A exciton,[25, 73, 79] respectively. Examples fits are shown in figure 3.1-6B-E, for all data see figure A6.4, Appendix. The black dots represent the measured data, while the red and blue lines are the fit components of exciton and trion, respectively. In all cases, the measured data is described well by two Lorentzians as indicated by the envelope function in orange. In some surfactants, such as the SC reference system (Figure 3.1-6B), it is found that the PL is governed by excitonic emission as previously reported.[65] Other additives, such as the polymer PVA in water (Figure 3.1-6D) shows a mixture of exciton and trion emission. A previous study has shown that this is due to doping from adsorbed PVA.[45] The polymer PVP as an additive (Figure 3.1-6E) almost completely suppresses the exciton emission which suggests relatively strong chemical doping. Interestingly, this system also showed the most red-shifted A-exciton in the absorbance which might suggest that doping and dielectric screening are somewhat correlated in liquid-suspended nanosheets.

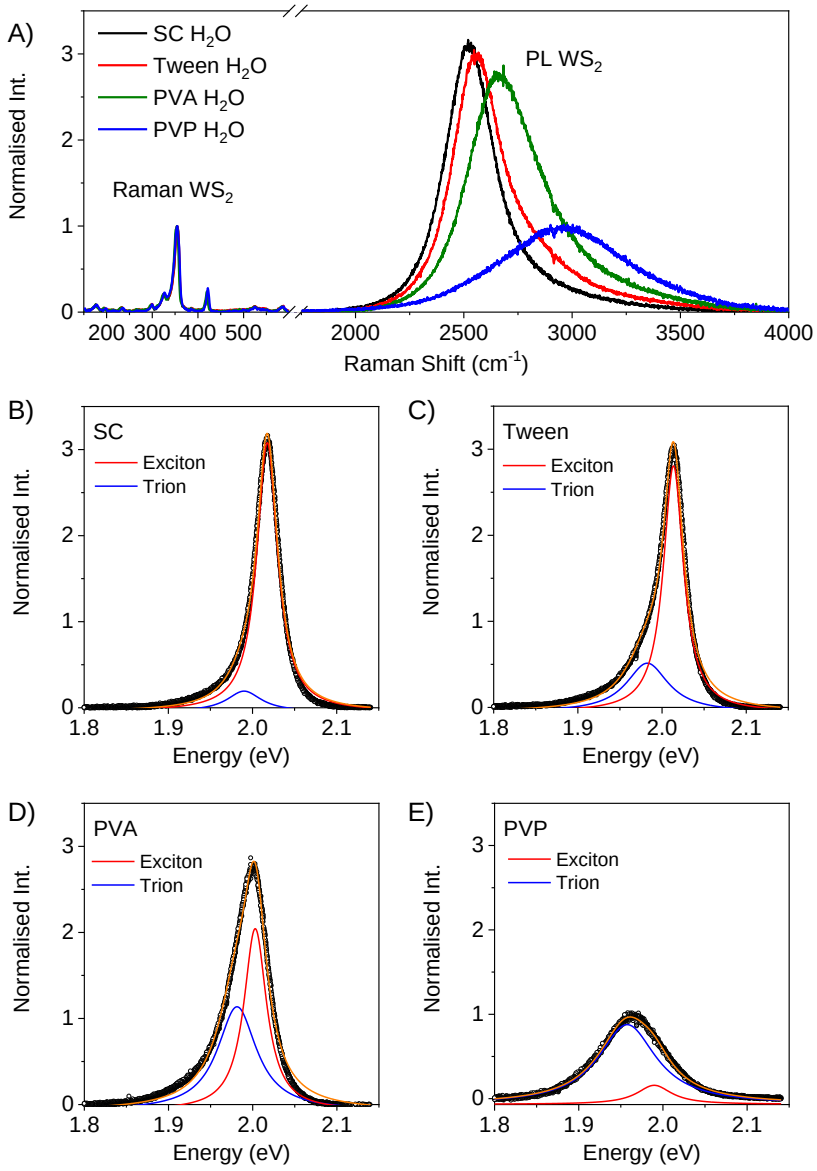

Figure 3.1-6: LPE WS_2 photoluminescence in different additive systems. A selection of spectra of the 5-22k *g* sample is shown. A) PL spectra of high concentrated WS_2 dispersions (532 nm excitation) normalized to the 2LA(M) Raman mode in four additive systems: H_20-SC (2 gL^{-1}), H_2O-Tween20 (2 gL^{-1}), H_2O-PVA (0.1 g L^{-1}), H_2O-PVP (0.1 gL^{-1}). At Raman shifts between 2000-4000 cm^{-1} (corresponding to 1.8-2.1 eV) the photoluminescence of WS_2 monolayers is observed showing significant differences across the samples. B-E) WS_2 photoluminescence fitted to two Lorentzian assigned to emission from excitons and trions, respectively. B) H_20-SC (2 gL^{-1}), C) H_2O-Tween20 (2 gL^{-1}), D) H_2O-PVA (0.1 gL^{-1}), E) H_2O-PVP (0.1 gL^{-1}).

From the fits, the energy, area and width of exciton and trion, respectively, are extracted. On the one hand, this allows us to test whether solvatochromism results in similar shifts and broadening of the response of both types of quasiparticles, *i.e.* excitons and trions. On the other hand, we can use the ratio of trion to exciton emission as indicator for chemical doping and test whether

chemical doping from the surrounding medium governs the shift/broadening. Since the effective dielectric constant of the environment is not known due to the use of additives, this is useful, as the presence or absence of correlations are an indication whether it is in principle possible to distinguish between chemical doping and screening of the excitons due to changes in the dielectric constant of the environment. Various correlations from fitting the emission of LPE WS_2 in different additive systems are displayed in Figure 3.1-7.

It is found that both exciton and trion energy (Figure 3.1-7A) and width (Figure 3.1-7B) roughly scale with each other, albeit with some scatter. In addition, Figure 3.1-7C shows that the width and energy of both exciton and trion are well correlated following a powerlaw dependence and all the fit data for both exciton (red) and trion (blue) fall on the same line. Thus, a red-shift is accompanied with broadening. We note that the quantitative relation is different from representative data obtained from the absorbance spectra (Figure 3.1-4C). This could be because we see the mean of exciton and trion in the absorbance spectra or because we expect a combination of various effects in the solvent additive system (e.g. dielectric screening of excitons and/or chemical doping) which is manifested differently in absorbance compared to emission spectroscopy.

At first glance, the data shown in figure 3.1-7A-C suggests that both exciton and trion respond in a similar way to the different chemical environment. However, the scaling of the trion energy *versus* the exciton energy in figure 3.1-7A follows roughly a linear correlation with a slope of ~1.5 in the lower energy regime (indicated by the dashed line) before saturating at an exciton energy of ~2.01 eV. If the shift of exciton and trion was attributed to doping, one would expect an increased separation of exciton *minus* trion energy as function of the Fermi level of the TMD.[25] In this case, the saturation occurring at the highest exciton/trion energies (~2.01 eV/~1.985 eV) could be related to an almost charge neutral state. It should be noted that the observed energy separation between exciton and trion energy at this point (20-25 meV) agrees well with literature on "charge-neutral" MoS_2[25] which was achieved by reducing the doping from the substrate electrically. Increased doping, in our case chemical doping, is expected to result in an increased energy separation between exciton and trion. This is exactly what is observed here: taking the lowest energy data point from this study, the exciton/trion separation is 30 meV which would be consistent with relatively mild doping and a shift in Fermi energy of ~10-15 meV.[25] This strongly suggests that the pronounced shifts in the emission of LPE WS_2 in different solvent/additive systems is a result of chemical doping. With this in mind, it is surprising to see a correlation of exciton/trion energy and their width in figure 3.1-7C, as the width is often regarded to be governed by the homogeneity of the surrounding[80] and that does not necessarily scale with the strength of doping.

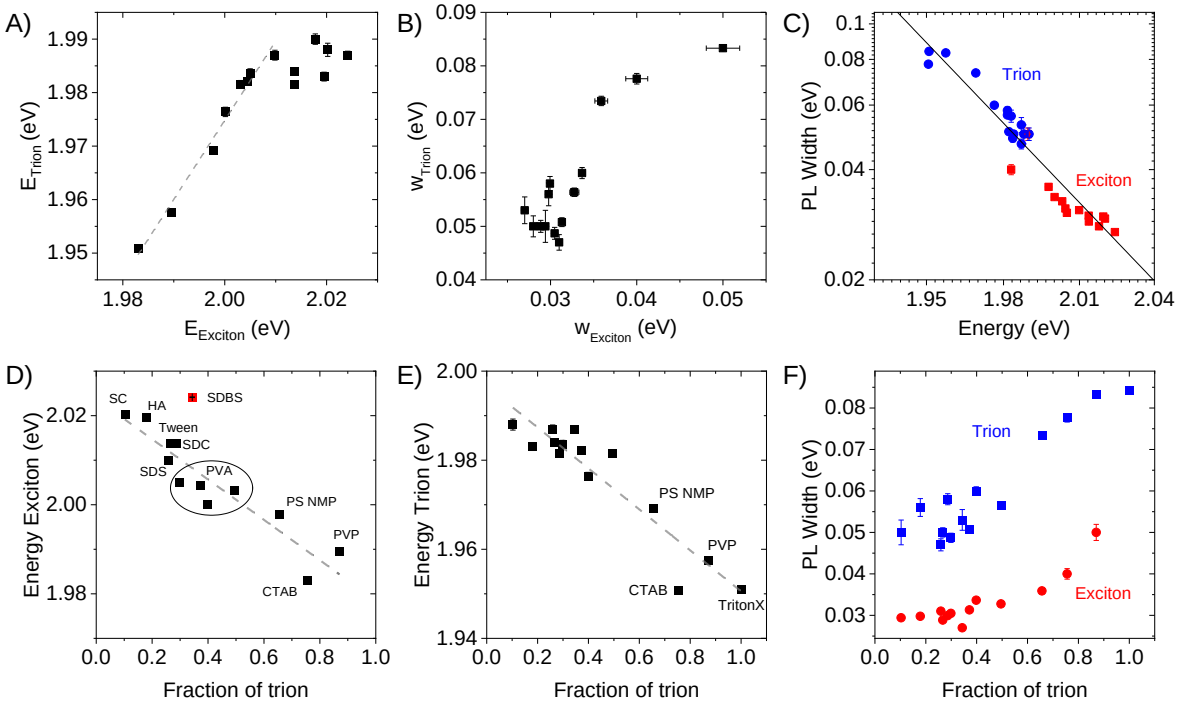

Figure 3.1-7: Impact of the stabilizer on WS_2 photoluminescence. Exciton and trion energies and peak widths are obtained from fitting the PL response as illustrated in figure 3.1-6B-E for all stabilizer systems. Plots of A) trion versus exciton energy, B) trion versus exciton peak widths and C) width as function of energy. Empirically we find that red-shifted exciton and trion emission is accompanied by broadening as indicated by the solid line. D-F) Plots of extracted fit parameters as function of the contribution of the trion to the overall PL which is indicative for charge transfer between stabilizer and WS_2. D) Exciton energy, E) trion energy and F) exciton and trion width.

While a quantitative analysis of potential chemical doping is not accessible in LPE WS_2 in different solvent/additive systems, we can qualitatively use the portion of trion emission to the overall PL response as indicator for doping of the nanosheets and test whether exciton and trion energy scale with this parameter. A clear scaling would confirm that the shifts in the PL are indeed related to doping rather than more subtle effects such as changes in the dielectric environment. To this end, the exciton (Figure 3.1-7D) and trion (Figure 3.1-7É) energy is plotted as function of trion emission to the overall photoluminescence. A linear relation is observed in both cases as indicated by the dashed grey lines. The data acquired in SDBS as additive is an outlier in the plot of exciton energy versus portion of trion emission (Figure 3.1-7D) which can be attributed to the sensitivity of this WS_2-surfactant system to variations in the laser power as discussed above. In addition, figure 3.1-7F shows a plot of the exciton and trion width as function of the portion of trion emission. While a detailed analysis is beyond the scope of this work, the data clearly shows that a broadening of both exciton and trion PL occurs with increasing fraction of the portion of the trion emission to the overall PL response. Overall, the data suggests that the PL position and widths are sensitive

indicators for chemical doping. Hence, in the case of PL, doping from the additive/solvent system governs the optical response and more subtle differences in the environment (dielectric constant, refractive index of the medium) are hardly discerned in these type of samples.

In spite of this discussion, it should be noted that PL measurements in a Raman spectrometer on liquid-suspended nanosheets are difficult to perform in a reproducible manner due to effects from focusing/defocusing, heating, laser power etc. For example, when the water in the sample evaporates due to heating, it results in broadening of the PL peak and evolution of more of the low energy components (assigned to trion) which might not be related to the nanomaterial/solvent-additive system, but to higher trion emission efficiency when the sample is accidently drying resulting in different heat dissipation. In light of this, absorbance spectra might be more suitable to reveal subtle differences in the A-exciton response as function of solvent/additive, in particular in systems with negligible chemical doping.

3.1.5 Conclusion

In summary, the first part of this thesis devoted to the additive/solvent system tracked several goals: 1- Producing high optical quality TMDs dispersions. 2- Modification of environments surrounding the material. 3- Investigation of solvatochromic effects on WS_2 as a function of layer thickness (dimension). 4- Identifying spectroscopic fingerprints for controlled chemical doping of nanosheets in liquid. It is confirmed that transferring WS_2 nanosheets from water/surfactant to different stabilizer and solvent systems gives indeed deeper insights into the effects of the environment on the optical properties of WS_2 nanosheets. In addition, the suitability of the transfer process and size selection method are highlighted.

Solvatochromic effects from the liquid environment are observed in the A-exciton absorbance, as well as A-exciton emission. However, it is not clear whether this is due to Coulomb screening of the excitons or other factors such as doping. In absorbance spectroscopy, shifts and broadening of the monolayer A-exciton are observed, but to a lower magnitude compared to the emission. Since thinner sheets have higher surface to volume ratio, they are more affected which is manifested by a change in the exponent relating the exciton energy to the layer number. Interestingly, a linear correlation between the exponent and the A-exciton energy of the monolayer is observed which can be used to generalize metrics to determine <N> from optical absorbance/extinction spectra in unknown environments. The overall photoluminescence can be deconvoluted into emission from exciton and trion which presents a qualitative measure for chemical doping. Stronger chemical doping, which can be referred to as increased interaction strength of the environment with WS2

results in larger shift of both exciton and trion as well as more broadening. A linear scaling of exciton and trion energy with the fraction of trion emission to the PL response of observed. It can thus be concluded that the PL fingerprint is dominated by chemical doping rather than physical parameters of the environment (dielectric constant or refractive index). Currently, it is not clear whether this is also the case for the absorbance data, in particular for the linear scaling of the exponent relating the exciton energy with layer number and the monolayer A-exciton energy.

In a nutshell, all observed data confirms that exfoliation in liquids is a good starting point for subsequent chemical modification of the nanosheets. According to the observed absorbance and photoluminescence data, changes in exciton energy and width indicate the solvatochromic effect. It should be noted that the nature of the environment surrounding the materials is not known due to the presence of a mixture of surfactant and solvent making a more quantitative analysis impossible. In addition, in the solvent/additive system, it is not possible to distinguish between chemical doping and dielectric screening of the excitons. Therefore, to gain deeper insights into the physics behind the solvatochromic effects, further studies on pure solvent systems were performed which is explained in detail in the next Chapter.

3.2 Transfer to Additive Free Organic Solvents

3.2.1 Introduction

In this section, it is clarified that when liquid exfoliation and size selection is optimized, nanosheets can be used to fundamentally study the excitonic properties. The main aim of this study is to understand what governs the solvatochromic shifts of excitons. As outlined in the previous section, we initially attempted this approach by transferring WS_2 nanosheets exfoliated and size-selected in aqueous sodium cholate to a range of other water/additive systems. The problem was that it was not possible to distinguish between chemical doping and dielectric screening of the excitons since both effects can occur. In addition, the effective dielectric environment in solvent/additive systems is not known. Therefore WS_2 nanosheets are transferred to pure solvents without additives in this section. In such a scenario, chemical doping should be reduced and we can use physical parameters of the solvent (*e.g.* refractive index, dielectric constant) to identify the origin of the excitonic response.

3.2.2 Preparation of the Dispersions

In analogy to the previous section, monolayer-enriched LPE WS_2 dispersions are first prepared by established protocols. This is important, as it enables the investigation of the monolayer A-exciton response on both absorbance and luminescence. For this purpose, a centrifugation scheme by liquid cascade centrifugation is applied to enrich the samples in monolayer. The dispersion goes through a cascade of consecutive centrifugation steps. After each step, the relative centrifugal force is increased and the supernatant is separated from the sediment which is redispersed in fresh aqueous sodium cholate 0.1 gL^{-1}. The stock dispersion is prepared by the same protocol which as in the previous section by probe sonication of the powder in an aqueous sodium cholate (SC) solution in a two-step procedure. The size selection was adjusted slightly to produce more fractions with relatively high monolayer volume fraction. In this section, the following fractions were used: "1-5k *g*", "5-10k *g*", "10-30k *g*" were subjected to further analysis.

In the previous experiments, nanosheets were exfoliated in sodium cholate (in water surfactant) to prepare a high-quality sample. The sediments collected after LCC were diluted, split into the desired number of aliquots and transferred to the new solvent/additive system by centrifugation after centrifugation-based washing steps (Figures 3.1-2). In a last step, low speed centrifugation was used to remove aggregates.

A similar procedure was used here with minor adjustments. Specifically, the following centrifugal acceleration was used for the sedimentation prior to transfer: 35k *g* for the 10-30k *g* sample, 15 k*g* for the 5-10k *g* sample. 7k *g* for the 1-5k *g* sample. After this step, the supernatant was discarded and WS_2 nanosheets in the sediment were washed in 2 steps, with water and IPA consecutively. After each step, the mixtures were sonicated for ~5-10 mins in a sonic bath to account for reaggregation and centrifuged again at high centrifugal acceleration (values as in the first step of the transfer see above). This washed WS_2 nanosheet sediment, was then redispersed in 21 desired solvents by bath sonication (~5 minutes). In the last step, a low centrifugal acceleration (100 *g*) removal step was applied to remove nanosheet aggregation. In the case of the transfer to solvents, this step was performed for 60 min.

The following solvents were used for redispersion: Acetonitrile, Anisole, 1-Butanol, Cyclohexanone, Diethyl ether, Dimethylformamide (DMF), Dimethylsulfoxide (DMSO), Dimethoxyethane (DME), Isopropanol (IPA), Isopropoxyethanol, *N*-Methyl-2-pyrrolidone (NMP), Nitromethane, Methanol, , Propylenecarbonate, Propylene glycol methyl ether acetate (PGMEA), Terpineol, Tetrahydrofuran (THF), Water. Transfer to the following solvents was tested, but could not be achieved: Cholorform, Acetone, Ethyl acetate. In addition, the samples were redispersed in aqueous sodium cholate after the washing procedure as reference.

3.2.3 Colloidal Stability of WS_2 Nanosheets in Various of Solvents

In the previous section, solvatochromism was investigated in size- selected WS_2 nanosheets transferred to different solvent/additives. The environment was reflected in changes of the A-exciton energy and width which was observed in both PL and absorbance spectra. While the use of additives improves the colloidal stability of the dispersions and prevents aggregation, the problem is that the exact nature of the surrounding medium is unknown. Therefore it was decided to investigate solvatochromic shifts in A-exciton energy and width of WS_2 dispersions by transferring nanosheets to pure solvents which allows us to test which physical parameter (dielectric constant, refractive index…) governs the response. It should be noted, that transferring to pure solvents is more challenging, as not all solvents are "good solvents". Here, the term "good" refers to the temporal colloidal stability of the nanosheets in different solvents. In general, pyrrolidone-based solvents such as NMP or Cyclohexyl-2-pyrrolidone were found to efficiently prevent aggregation with > 90% of material remaining dispersed after 100 h.[43, 51] Thus, before analyzing the A-exciton response, it is important to assess whether the dispersions are colloidally stable enough.

The colloidal stability of nanomaterials in pure solvents is generally described in the framework of solution thermodynamics- for details, see Chapter 1.4.1. In brief, the definition of the free energy of mixing ($\Delta\bar{G}_{mix}$) is used to understand the mixing of solvent and solute. Nanosheets are considered as solute in these systems. Mixing of two components is favorable when the Gibbs free energy is negative. Here nanosheets are considered as a large and rigid solute, hence their entropy contribution is very small compared to small molecules. Therefore, it is of interest to minimize the enthalpy to favor the mixing. If the solubility parameter of solvents is very close to that of nanosheets, the energetic cost of dispersing the nanosheets is minimized and the dispersed concentration is maximized. To predict this maximum dispersed volume fraction the an equation was derived[51] which emphasized that dispersed concentration as a function of solvent surface tension should follow a Gaussian envelope function.[51] As suitable solubility parameters, surface energy, Hildebrandt parameter or Hansen parameter can be considered.[81]

To test the model, the dispersed concentration can be plotted as function of the respective solubility parameter which should result in a well-defined peak, described by a Gaussian envelope. The maximum of the peak is related to the solubility parameter of the nanomaterial which was found to vary only weakly across materials.[51] It is reported that many solvents give dispersed concentrations significantly below the (Gaussian) envelope. In addition, there is only a small number of solvents with surface tension above 45 mJ/m^2 and surface energy above 75 mJ/m^2. Note that surface tension Γ is linked to the surface energy (γ), by $\Gamma = \gamma_S - TS_S$, where S_S is the surface entropy and $TS_S \approx 29$ mJ/m^2 for almost all liquids at room temperature. This limitation makes the right-hand side of the graph hard to be populated.[51] In addition, it is unknown whether certain solvent parameters, such as viscosity or density would affect the exfoliability. For example, it is known that cavitation, which is the main driving force for exfoliation in sonication is affected by the viscosity of the medium.[82] Such effects can potentially be taken out of the picture by transferring an already exfoliated dispersion to different solvents, as performed in this study.

To test this, three size selected WS_2 fractions (10-30k *g*, 5-10k *g* and 1-5k *g*) were transferred from aqueous surfactant to different solvents (including solvents that are known not to be good solvents for TMDs or carbon nanotubes) and their extinction spectra measured to assess the nanosheet concentration and simultaneously analyze the A-exciton response. A selection of spectra of the reference sample in aqueous SC (after the same washing steps used for the transfer to organic solvents), isopropanol, anisole and NMP are displayed in Figure 3.2-1A-C, for all data see Appendix, A6.5. The insets show the region of the A-exciton, which will be analyzed and discussed further below.

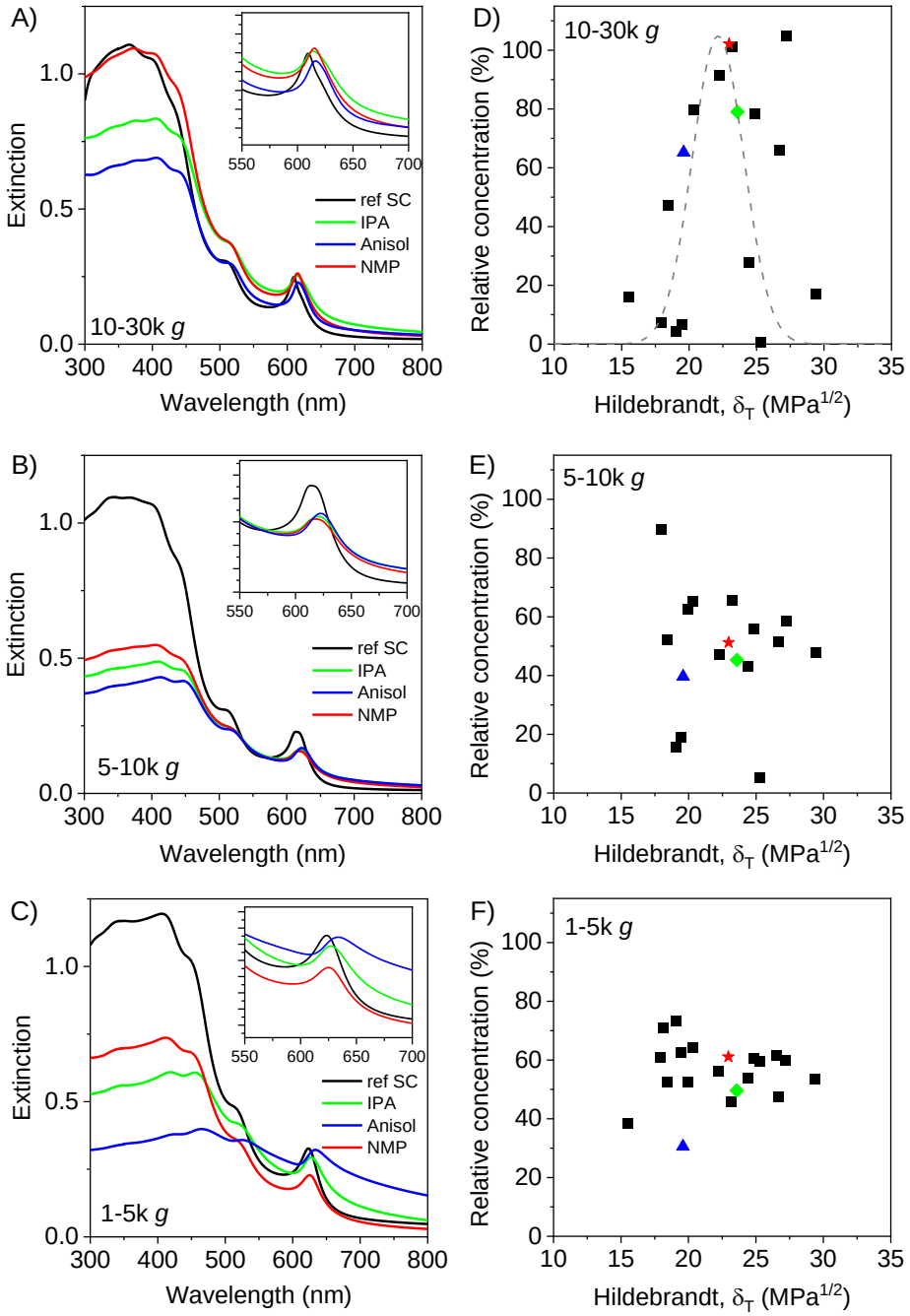

Figure 3.2-1: Impact of the solvents on WS_2 extinction spectra and dispersibility of exfoliated nanosheets. A-C) Selection of spectra of the 10-30k *g* (A), 5-10k *g* (B) and 1-5k *g* (C) samples are shown in 3 different solvent system (isopropanol, anisole, NMP) compared to WS_2-SC as reference sample. Insets: Zoom-in of the A-exciton. D-F): Dispersed concentration of WS_2 fractions transferred to different solvents plotted as a function of Hildebrand parameter for the three size-selected samples.

From the spectra, it can be observed that smaller nanosheets (10-30k *g*, Figure 3.2-1A) can be efficiently transferred to some solvents, such as NMP without loss of nanomaterial, which is not

the case for the fractions containing larger nanosheets. In spite of the centrifugation step at 100 g after the transfer to remove the majority of aggregates, an elevated non-resonant scattering background at > 650 nm can be seen in almost all transferred samples. This appears more pronounced for the WS_2 dispersion2 containing the larger nanosheets (1-5k *g*, Figure 3.2-1A). This suggests that larger nanosheets suffer more from aggregation during the transfer process. This will be discussed further below.

Information based on the transferring efficiency is obtained from the optical density of the extinction spectra after removal of aggregates. To calculate the relative concentration of size-selected WS_2 nanosheets, the optical density of the sample is determined at 400 nm from the optical extinction spectra, multiplied by the dilution factor and finally divided by the optical density of the initial sample at 400 nm (*i.e.* the nanosheets in SC aqueous solution before transferring to the desired environment). Figure 3.2.1D-F shows the relative dispersed concentration (in %) as a function of the Hildebrand parameter. As described above, it is suggested that the dispersibility in pure solvents without stabilizers can be described in the framework of solution thermodynamics which means that the dispersed concentration should be highest at the point where the solubility parameter of the material matches that of the solvent. Essentially, what this means is when we plot relative concentration as the function of solubility parameter we should see a peak if the data was consistent with solution thermodynamics.

The 10-30k *g* sample (Figure 3.2.1D) indeed shows a peak at ~22$MPa^{0.5}$ which can be described by a Gaussian envelope function. This suggests that the colloidal stability is governed by solution thermodynamics after transferring one sample to different environments in this case. Interestingly, opposed to direct exfoliation in solvents only few data points deviate significantly from the envelope. However, this is clearly not the case for the size-selected fractions containing larger nanosheets (Figure 3.2.1E-F). Here, the dispersed concentration after transfer varies only weakly across solvents. In the case of the 15k g fraction, roughly 60% of the nanosheets are retained after transfer regardless of the solvent. While this might suggest the presence of some residual solvents, this means that a broader range of solvents is accessible for further processing when the samples are transferred compared to direct exfoliation in the respective solvents.

For sake of completeness, the relative nanosheet concentration is plotted as function of various solubility parameters in figure 3.2-2. In figure 3.2-2A, the relative dispersed concentration is plotted versus surface tension. There is no clear correlation in both fractions 1-5k *g* and 10-30k *g* which is illustrated as blue stars and black squares, respectively even though solution thermodynamics predicts the dispersed concentration vs function of solvent surface energy to

display a Gaussian-shaped peak.[51] According to literature,[51] this should be centered at ~40 mN/m. While the data of the smallest fraction of WS_2 nanosheets (10-30k g) could evolve to a peak (with few exceptions) if solvents with higher surface tension were accessible, this is clearly not the case for the fraction containing larger nanosheets.

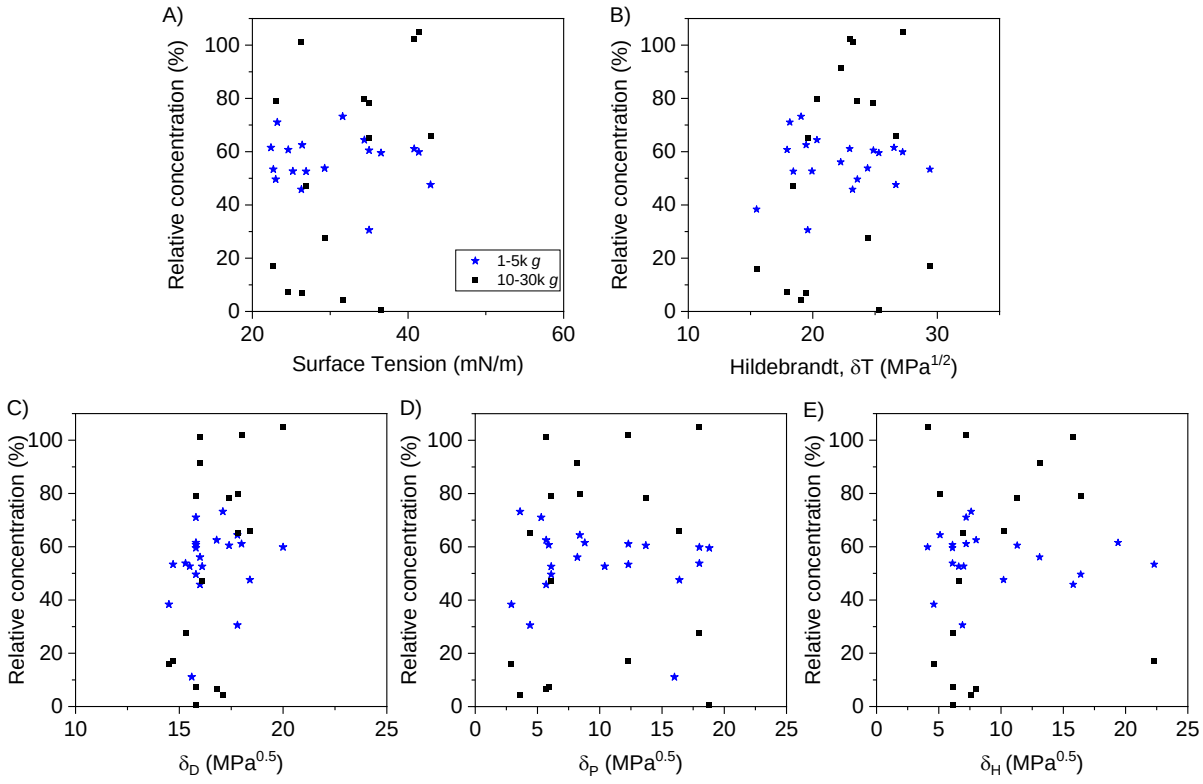

Figure 3.2 -2: Dispersibility of two different fractions of exfoliated WS_2 nanosheets (1-5k *g* and 10-30k *g* illustrated as blue stars and black squares, respectively) in a range of solvents. A) Relative concentration of dispersed nanosheets vs surface tension. B) Relative concentration plotted as a function of the Hildebrand parameter. C-E) Relative concentration as function of Hansen solubility parameters. C) Dispersive component, D) Polar component, E) Hydrogen bonding component. There are no clearly discernible correlations in both fractions, whereas it is assumed that the dispersed concentration plotted as a function of solubility parameter displays a Gaussian-shaped peak.

Also the dispersed relative concentrations as a function of the Hansen solubility parameters (i.e. the dispersive, polar and H-bonding solubility parameters) are illustrated figure 3.2-2C-E. In all cases the Gaussian envelope function is not observed. Similar to the surface tension, the data might evolve to a scattered peak in the case of the 10-30k *g* sample of more solvents were included. This further confirms that colloidal stability of the nanosheets transferred to different solvents cannot well be described in the framework of solution thermodynamics opposed to direct exfoliation and stabilization in different solvent systems.

Aside from potentially present small residues of surfactant, different levels of aggregation occurring during the transfer could be the origin for this. To assess the level of nanosheet aggregation in the dispersions, the optical density at 800 nm in the extinction spectra, which is non-resonant with electronic transitions and thus purely attributed to scattering, was divided by the optical density at 400 nm, where absorbance of WS_2 is dominant. This nonresonant/resonant ratio can be regarded as a qualitative measure for the presence of aggregates. In Figure 3.2-3 this ratio is plotted as a function of surface tension, Hildebrand parameter and solvent viscosity, respectively for the 1-5k *g* and 10-30k *g* fraction. If solvents with matching solubility parameters were efficiently suppressing aggregation after transfer, we would expect to see a minimum at the matching solubility parameter in Figure 3.2-3A-B. This is clearly not the case. To test whether the viscosity has an impact, *i.e.* due to different sedimentation behavior in the low speed centrifugation after the transfer that served the purpose to efficiently remove aggregates, the nonresonant/resonant extinction ratio is plotted as function of solvent viscosity in figure 3.2-3C. Again, no correlation is observed. As such, the origin for the presence of aggregates could not be identified. A potential source for experimental error is that it was not possible to acquire all extinction spectra immediately after the transfer so that different time intervals have passed prior to the measurement in which aggregation potentially happened to a different extent in the different solvents.

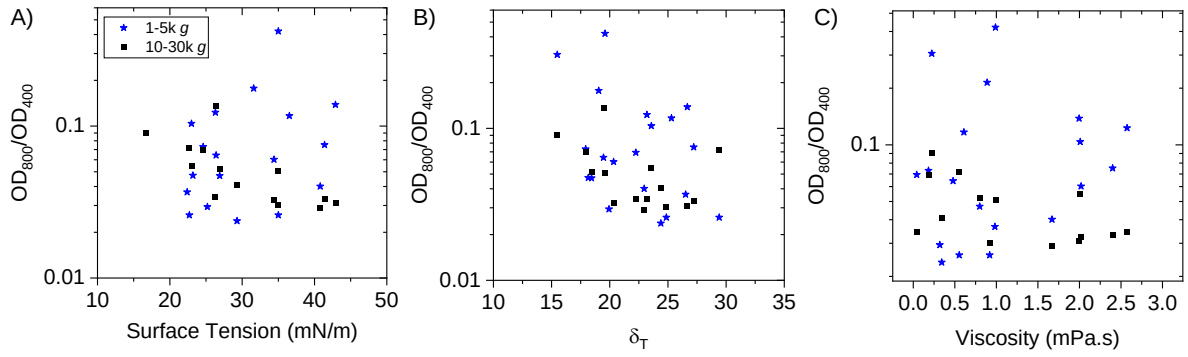

Figure 3.2-3: Extinction intensity ratio at 800 nm and 400 nm of size-selected WS_2 dispersions transferred to different solvents as indicator for aggregation in the samples plotted as function of the A) the solvent surface tension, B) the solvent Hildebrand parameter and C) the solvent viscosity.

In summary, solubility theory predicts that nanomaterials are effectively stabilized in solvents with matching solubility parameters. However, this is only observed for the fraction of smallest/thinnest nanosheets after transfer. While the origin of this behavior is unclear, it should be noted that

colloidally stable dispersions could be obtained in a broader range of solvents after transferring already exfoliated nanosheets. This is potentially useful for further processing.

3.2.4 Excitonic Response from Absorbance

The dielectric environment has been found to strongly influence both, the electrical and optical properties of low dimensional materials.[60, 65, 83-84] In the additive system, it was not possible to completely understand the nature of the surrounding due to the presence of surfactant. In the following, the intrinsic influence of the dielectric constant of the chemical environment of the nanosheets on the exciton behavior of size-selected WS_2 nanosheets will be discussed. A range of different solvents were chosen with a maximum spread of dielectric constants from 2.8 to 78.4. As a second parameter, the polarizability is considered which is a dynamic parameter in contrast to the static dielectric constant. Some reports[84-87] suggest that solvatochromic shifts are primarily influenced by the polarizability–polarizability interactions and therefore the refractive indexes of these different solvents are used to calculate the induced polarization which can be described by the Onsager polarity function:

$$f(\eta^2) = \frac{2(\eta^2-1)}{(2\eta^2+1)} \qquad \text{(Eq. 11)}$$

Where: η is the refractive index of the solvent.

To track solvatochromic shifts, the data of size-selected WS_2 nanosheets transferred to different solvents is analyzed in analogy to the data in the additive systems described in Chapter 3.1. First, the second derivative of the A-exciton absorbance is calculated. Figure 3.2-4A shows a selection of the second derivative of the A-exciton region after smoothing the spectrum for a subset of the data of the 5-10k *g* sample. For all data, see Appendix, Figure A6.6. The A-exciton splits into two components assigned to monolayers and few-layers. Depending on the solvent, a peak shift is observed. The data is fit to the sum of the second derivative of two Lorentzian which made it possible to extract information on the energy and the width of the monolayer and few-layer contribution. As before, the exciton positions of the few-layer component of the reference system in aqueous SC was used to calculate the layer number from published quantitative metrics.[60, 65]

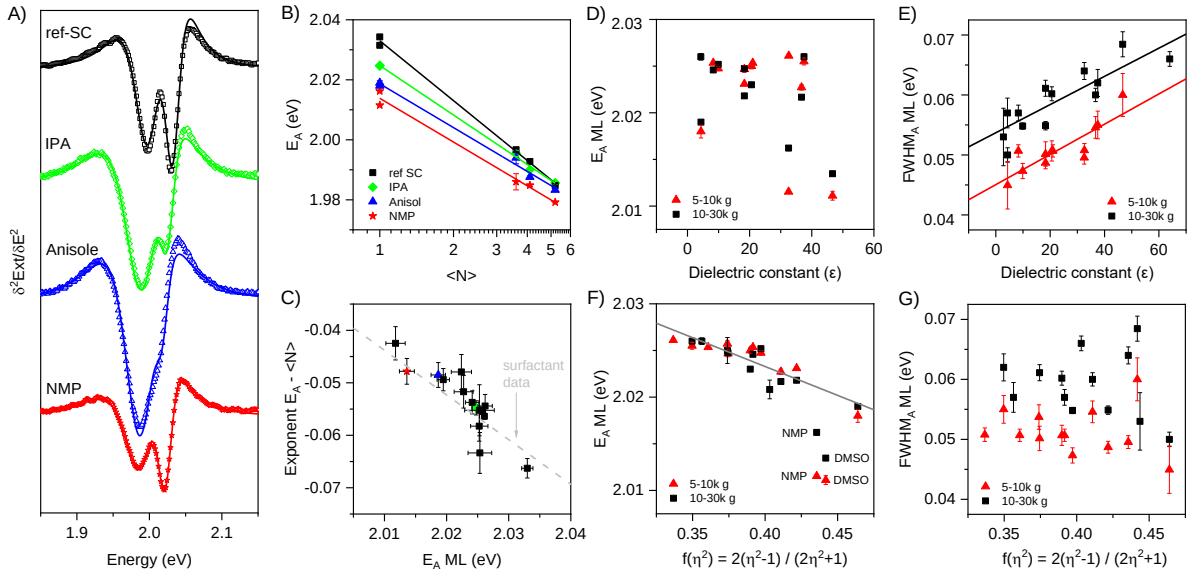

Figure 3.2-4: Impact of the solvents on WS_2 excitonic properties and investigation of solvatochromic shifts. A) Selection of the second derivative of the A-exciton region of the same samples (5-10k *g*) transferred to different solvents after smoothing the spectrum. The A-exciton splits into two components, assigned to monolayers and few-layers. Depending on the solvent, a peak shift is observed. The data is fit to the sum of the second derivative of two Lorentzian (solid lines). B) Plot of the A-exciton energy as a function of WS_2 layer number. The layer numbers were calculated from published quantitative metrics of the SC references system. The data is fit to an empiric power law to extract the exponent and the A-exciton energy of the monolayer. C) Plot of the fit parameters from figure (B) plotted *versus* each other for all solvent systems under study. The previously found linear correlation is confirmed as indicated by the solid line. D-E) Energy (D) and width (E) of monolayers *versus* dielectric constant of the solvent. It is shown that exciton energy does not scale with the dielectric constant, unlike the exciton width which scales with this parameter. F-G) Exciton energy (F) and width (G) *versus* the Onsager polarity function. The refractive index governs the solvatochromic shift based on the linear scaling of the energy as a function of the polarity function in contrast to the width of the exciton where no scaling is seen.

This allows to plot the exciton energy as function of layer number as shown for a subset of the data in figure 3.2-4B (all data see Appendix, Figure A6.7). While the data is more scattered than the data after transfer to solvent/additive system, a similar relation is observed even though with aggregation occurring, an artifical red-shift of the excitonic resonance is expected.[29, 88] Overall, a change in both monolayer A-exciton resonance is observed in combination with a different exponent relation E_A to the average layer number. The data is fit to an empiric power law to extract the exponent and the A-exciton energy of the monolayer. As before, the fit parameters (exponent and A-exciton energy of the monolayer) are plotted versus each other for all solvent systems under study in figure 3.2-4C. A roughly linear correlation is found, albeit with some scatter. Importantly, the data quantitatively correlates with the result found for the solvent/additive systems as indicated

by the grey dashed line which is the empirical fit from Chapter 3.1. While PL spectroscopy of the solvent/additive systems revealed issues with chemical doping, the quantitative agreement between the dataset is encouraging and strongly suggests that the relation between exciton energy with layer number is a manifestation of screening of the excitons, irrespective of doping. This also implies that the generalized metrics for thickness determination from the A-exciton energy derived in Chapter 3.1 are also applicable to pure solvent systems.

In contrast to the solvent/additive system, dielectric constant and refractive index of the environment are known in case of the pure solvents. This allows us to test, which physical parameter governs changes in exciton energy and width. In figure 3.2-4D, the exciton energy is plotted as a function of the dielectric constant of the solvents for two batches of monolayer-enriched WS_2 (5-10k *g* and 10-30k *g*). Clearly, the data shows no clear correlation. Note that this is distinct from literature reports on the impact of the solvent on the PL spectra of CVD-grown MoS_2 which had suggested a scaling of the excitonic shift with the dielectric constant.[73] This suggests that the magnitude of the excitonic shift is not related to the dielectric constant. For the width of the A-exciton monolayer, a similar study was performed (Figure 3.2-41E). In contrast to the energy, the width seems to scale with the dielectric constant. The higher the dielectric constant, the more broadening is observed. The two sample batches are offset from each other with smaller sheets (10-30k *g*) displaying a broadened linewidth. This is what we often observe and relate it to different lateral dimensions which can have an impact on the width of the exciton.

Since the static dielectric environment does not seem to determine the magnitude of the shift of the exciton, it is important to test other possibilities. As outlined above, a reasonable possibility is the Onsagar polarity function which is related to the refractive index as described above. Note that a study on single-walled carbon nanotubes suggested that exciton energy scales with the polarizability[84] function, even though this is still in debate also for liquid-suspended nanotubes. The plot of the monolayer A-exciton energy as function of the Onsagar polarity function shows a reasonable lines scaling (Figure 3.2-4F). Importantly, here, the two-samples fall on the same line. Note that there is two exceptions that do not follow the linear scaling: the solvents NMP and DMSO as a solvent. These are known to be quite efficient in stabilizing the nanosheets[65, 72, 84, 89] and as such, it is well possible that there are additional chemical interactions in place which would explain why NMP and DMSO do not follow the same curve as the other ones. For example, it was suggested that LPE-MoS_2 is particularly stable in NMP in the presence of trace water due to an interaction of NMP with water bound to nanosheet edges.[89] Further, it is clearly shown in figure

3.2-4 G, that there is no scaling when plotting the monolayer A-exciton width as a function of the Onsager function.

Before attempting a discussion on the origin of this behavior, it should be noted that the situation is rather complex. This is particularly because the exciton energy is determined in the measurements which is a result from both changes in the binding energy due to Coulomb screening from the environment, as well as bandgap renormalization. Both effects typically go hand in hand, but with opposite sign.[80] In addition, in polar semiconductors, longitudinal optical phonons produce a macroscopic electric field which interacts with electrons (and excitons). This coupling, known as Frohlich interaction, is relatively long range and thus expected to be particularly sensitive to the environment.

It is important to realize that excitonic relaxations, regardless of potential Frohlich interaction, are highly dynamic. Exitons are typically pictured as electrons circling around a hole in a quasiparticle. While dielectric properties of the environment can be described by the static dielectric constant, many realistic dielectrics are characterized by a dielectric function with a pronounced frequency-dependence. This is referred to as dynamic screening and better described by the polarizability. While progress is made in developing an analytical framework for dynamic screening of excitons, also in the case of 2D materials,[90] a full theoretical description is currently lacking. Nonetheless, awareness is growing that screening of excitons is not a static, but dynamic process, as also experimentally confirmed in few cases.[90-91] That the exciton energy scales with the polarizability function rather than static dielectric constant is a strong indication that dynamic screening has to be considered also in the case of liquid-suspended nanosheets. As such, it makes sense that the exciton energy shifts with the optical index- it is a matter of time scales. We have to consider the optical index at the frequency corresponding to the binding energy of the exciton. As for the linewidth, it would be expected that some slower mechanism like the spectral diffusion (spectral wandering) can contribute to the average linewidth of the system. In that case, the time scale can extend of 2 micro- or miliseconds.[73, 91] Then the dielectric constant which includes the contribution of the orientation of permanent dipoles (*e.g.* in polar solvents can contribute as well). While this explanation is currently a bit superficial, the results are encouraging. Importantly, the overall sample preparation and analysis is relatively straight forward and can potentially be applied to a range of other materials which could be the foundation for a more detailed understanding of screening of excitons in 2D materials in the future.

3.2.5 Excitonic Response from Photoluminescence

In contrast to the solvent/additive system described in Chapter 3.1, we expect only negligible chemical doping from pure solvents (with some exceptions such as NMP). It is thus interesting to test whether shifts in the A-exciton photoluminescence can also be related to the solvent dielectric constant or refractive index. According to the Franck–Condon principle,[92-95] solvent reorientation is too slow to be observed during absorption, but can often be observed in the emission. This could result in a discrepancy between data from absorbance and PL.

To investigate this in our samples, PL measurements were carried out. Since many solvents are volatile, the measurements could not be carried out on the surface of liquid drops in the Raman spectrometer, as solvent evaporation changes the focus of the laser on the sample during acquisition. Instead, dilute dispersions (maximum optical density at the excitation wavelength 0.4) were measured in a fluorescence spectrometer (see methods) with 425 nm excitation at room temperature. Note that such measurements can only be carried out for monolayer-rich dispersions with appreciable PL (e.g. 5-10k *g* and 10-30k *g* WS_2 fractions).

Figure 3.2-5 shows the impact of the solvents on the luminescence properties of size-selected WS_2 nanosheets transferred to different environments. In figure 3.2-5A-D, a selection of photoluminescence spectra of transferred WS_2 nanosheets to different solvent systems are shown: H_2O-SC (reference sample), isopropanol (IPA), anisole, N-Methyl-2-pyrrolidone (NMP). For all data see Appendix, Figure A6.9. The observed PL of WS_2 monolayers shows significant differences across the samples after transferring into the different solvents. The PL is at least partially retained after transferring to a range of solvents such as IPA, anisole or even acetone. This suggests that a significant portion of isolated monolayers is still present after the transfer, even in the case of solvents that are not very suitable for direct exfoliation. This is an encouraging finding and important for the fabrication of thin films with monolayer properties retained. This is addressed in the next Chapter.

In some cases, such as after the transfer to NMP, which is known to be a solvent very suitable for nanosheet stabilization, the PL is widely quenched (Figure 3.2-5D). This is in line with a chemical interaction with the nanosheets as suggested on the basis on the absorbance spectra. The PL response is fit to three Lorentzians, assigned to emission from excitons (blue) and trions (green) in addition to a broad background component (red) that stems from the solvent (red). Since the exciton emission with its narrow linewidth is most characteristic, the position was extracted and analyzed. Values are summarized in table 3.2.-1. Note that in almost all cases, the trion emission

is negligible compared to the exciton emission (Appendix, Figure A6.9) confirming a lower degree of chemical doping compared to the additive systems.

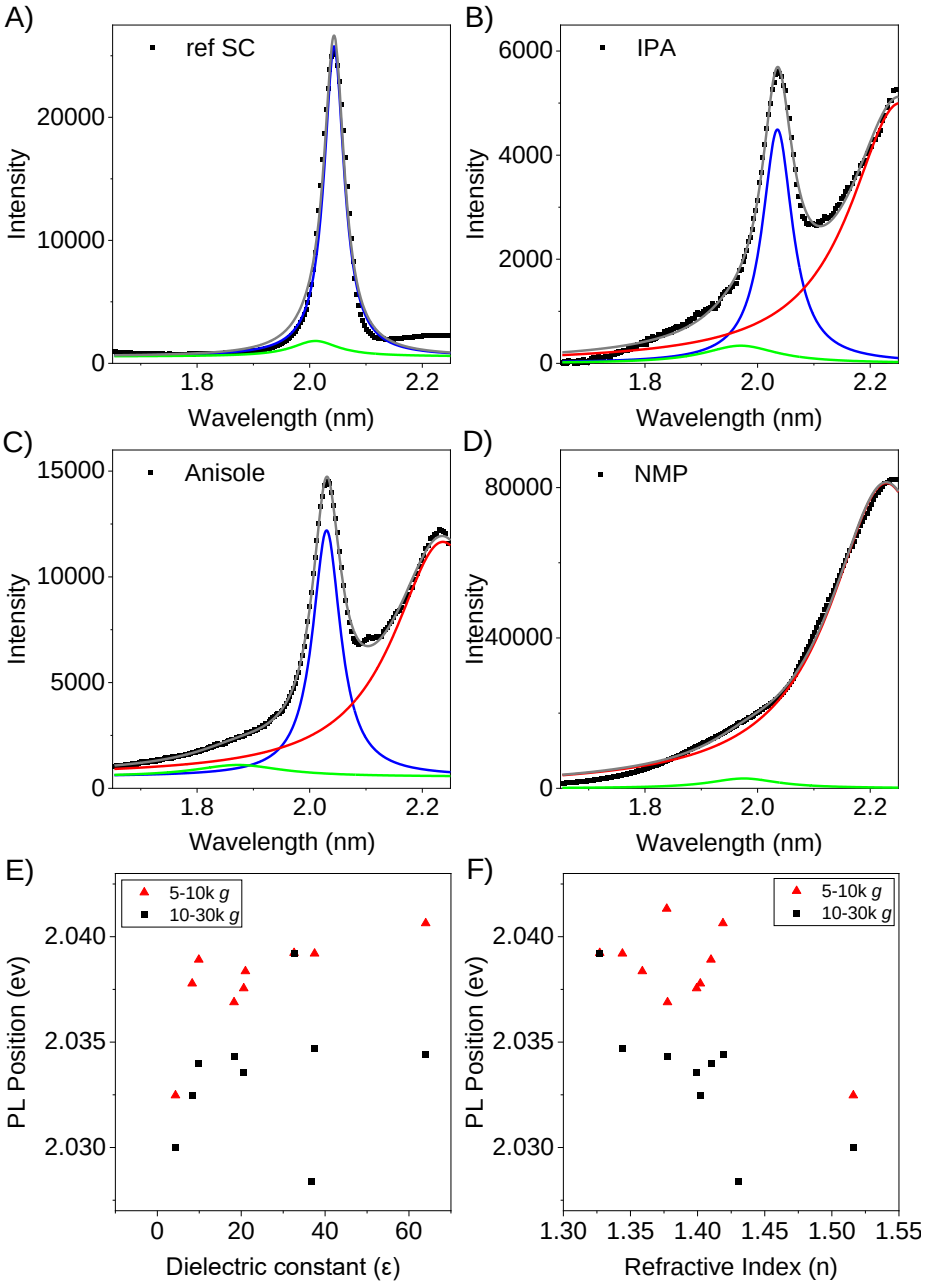

Figure 3.2-5: A-D) Photoluminescence spectra (excitation wavelength 425 nm) of transferred WS_2 nanosheets (10-30k *g*) to different solvent systems: H_2O-SC (A), Isopropanol (B), Anisole (C), N-Methyl-2-pyrrolidone (D) fitted to two Lorentzians assigned to emission from excitons and trions, respectively in addition to a broad feature for the background. E and F) Exciton and trion peak positions obtained from fitted photoluminescence spectra versus E) dielectric constant of the solvent and F) Refractive index. Data for two size-selected fractions is shown.

To test whether emission responds to the solvent environment in a similar way as absorbance, the exciton energy from all fit data for both WS_2 fractions (5-10k *g* and 10-30k *g* samples) is plotted as a function of dielectric constant and refractive indexes of solvents (Figure 3.2-5E and F). The

data is quite scattered and the PL peak position does not scale as a function of these solvent parameters. While there seems to be an overall red-shift with increasing refractive index (Figure 3.2-5F) which would be consistent with the trend from UV-Vis, the correlation is not clear. This suggests that the emission responds to additional factors beyond dielectric screening. Hence, it is confirmed that absorbance data is more suitable to study dielectric screening, while information of chemical doping can be extracted from PL (as discussed in Chapter 3.1).

Table 3.2-1: Tabulated values of the higher energy photoluminescence peak of the monolayer-rich WS_2 dispersions (assigned to the exciton) transferred to a range of solvents.

Solvent	**PL position (5-10k*g*) [eV]**	**PL position (10-30 k*g*) [eV]**
SC (reference)	2.055	2.052
1-Butanol	2.038	2.033
Acetonitrile	2.039	2.034
Anisole	2.032	2.03
DMF	1.96	2.028
DME	2.04	No PL
Isopropanol	2.036	2.034
Isopropoxyethanol	2.038	2.034
PGMEA	2.037	2.032
Propylene carbonate	2.04	2.034
Acetone	2.038	2.034
Methanol	2.039	2.039

It is noted that more evaluation has been carried on the obtained PL data to for example investigate a correlation between PL peak position (energy (eV)) and width or a scaling of exciton energy with trion energy from both 5-10k *g* and 10-30k *g* fractions. However, no obvious correlations between these parameters were observed.

One advantage of having nanosheets dispersed in a range of solvents is the opportunity of testing different solvents for nanosheet deposition into thin films, all the properties are explained in detail in the next section. In this work, the nanosheets are observed when the AFM image of such a spin-coated WS_2 dispersion is zoomed in and it is clear that there is roughly near one Layer coverage with not many aggregates. This (1L coverage) spin-coated WS_2 thin film could be used for

example to look at the photoluminescence. Also, properties of deposited WS_2 thin films on different substrates (glass and different polymer substrates) are investigated.

3.2.6 Conclusion

Further studies based on transferring nanosheets into different solvent system have been performed to investigate the nature of the surrounding medium which remained unknown in the additive system due to the presence of surfactant in the dispersion. Transferring to pure solvent allowed us to examine some physical parameters such as refractive index and dielectric constant that might govern the exciton shifts and broadening (dielectric screening). In general, transferring to pure solvents is more challenging, as matching the solubility parameters of solute (nanosheets) and solvent, which is believed to be a prerequisite for long term colloidal stability, cannot be achieved in all cases. Here, three size-selected WS_2 fractions (1-5k *g*, 5-10k *g* and 10-30k *g*) were transferred to in total 21 solvents each. In three solvents, no nanosheets remained stably dispersed and only in 15 systems, dispersions were stable enough to allow for a comprehensive analysis.

First, the efficiency of the transfer, which can be considered as measure for the colloidal stability, was analyzed in the framework of solution thermodynamics which is typically used to describe the stability of 2D nanosheets in additive-free systems. Solubility theory predicts that the dispersibility of nanomaterials is improved in solvents with matching surface energy, Hildebrandt or Hansen parameters, respectively. It is reported, that the dispersed concentration as a function of the respective solubility parameter is represented by a Gaussian envelope function. In this work, this Gaussian envelope was observed only for the smallest/thinnest nanosheets (10-30k *g*). In dispersions containing larger sheets, no correlation between dispersed concentration and solubility parameter was found. While this is surprising, it is useful, as it means that solvent transfer is possible to a wider range of solvents than accessible in direct exfoliation.

The extinction/absorbance confirmed that the shift of A- exciton with layer number follows the same signature as has already been seen with the surfactant systems. This suggests that the aggregation that was partially observed has an insignificant impact on the relationship of exciton energy and layer number. Importantly, the exponent relating the A-exciton with layer number and the monolayer A-exciton energy again shows a linear correlation that quantitatively agrees with the surfactant data. This means that the derived generalized equation for the thickness determination of the nanosheets based on the A-exciton energy can also be applied to pure solvents. To extract reasons for excitonic shifts in different solvents, the refractive index and the dielectric constant of the solvent were considered as two physical parameters. The data shows that

the results for A-exciton energy and width vs refractive index and dielectric constant are in contrast with one another. The monolayer A-exciton energy was found to scale linearly with the Onsager polarity function (related to the refractive index), while the width scaled linearly with the solvent dielectric constant. This scenario is interpreted as dynamic versus static dielectric screening of excitons. Overall, the data analysis suggests that these changes in the A-exciton response on extinction/absorbance are a manifestation of dielectric screening rather than chemical doping.

In addition, narrow linewidth PL assigned to emission from WS_2 monolayers is observed in some solvent systems, including solvents such as anisole and acetone which give very poor nanosheet stabilization when used during the exfoliation. This again confirms that more solvents are accessible when exfoliated nanosheets are transferred. In a subset of the solvents, the PL was quenched or overlapped from a strong background of the solvent. In the solvent systems that could be analyzed, only minor emission from trion was observed which confirms negligible chemical doping in pure solvents with some exceptions (such as NMP). In spite of this, no clear correlation between PL peak position as a function of such physical parameters of the solvent was found.

Taken together, Chapter 3.1 and 3.2 show that the UV-Vis data seems more suitable and robust to dielectric screening of excitons compared to the PL data. In turn, PL can give valuable information on chemical doping. Overall, exciton shifts in absorbance are governed by the refractive index/polarizability and not the static dielectric constant. The study also showed that high quality dispersions with monolayer PL retained can be produced in a range of pure organic solvents including low boiling point solvents such as isopropanol or acetone which will be exploited in the next chapter for deposition into thin films.

3.3 Production of WS_2 Thin Films Using Spin Coating

3.3.1 Introduction

Among top-down production techniques to obtain 2D nanosheets, liquid-phase exfoliation (LPE) has become increasingly popular especially due to its versatility making a whole host of nanosheets accessible. Major issues such as low monolayer contents and sample polydispersity could be addressed in the past years. However, one disadvantage of LPE is that nanosheets restack on deposition losing their monolayer characteristics such as photoluminescence of the single layers in TMD films. Here, we present progress towards the preparation of thin films from LPE WS_2 on arbitrary substrates with monolayer properties of the nanosheets retained. Nanosheets are produced by sonication in surfactant, followed by size selection to enrich the sample in monolayers (typically > 60%).[69] Following the procedure outlined in Chapter 3.1-3.2, the nanosheets can then be transferred to a wide range of organic solvents including solvent mixtures such as isopropanol-THF which is ideal for spin coating. While some aggregation occurs, mild centrifugation can be performed to remove aggregation.

The spin coater includes a chuck where the substrate is mounted on it and rotating the sample. The centrifugal force spreads the dispersion across the substrate which results in partial waste of the dispersion when entirely driving the material outward. The spin coating method consists of several steps that result in uniform deposition of material on the surface: 1. Fluid dispense, 2. Spin-up, 3. Stable fluid outflow, 4. Spinoff, 5. Evaporation.[96-97] For many materials, the desired thickness of the thin films is achievable by adjusting the coating parameters (time of spinning, viscosity and angular speed, surface wettability, solution density, solvent evaporation rate, material concentration) and a homogenous and uniform coating can be produced by this method without the need for tuning rheological properties of an ink unlike printing techniques.[98] Flat deposition on the substrate hardly depends on surface tension and viscous forces. Therefoe, spin coating is considered a simple and direct deposition method that is efficiently able to deposit the nanomaterial or organic molecule/polymer.

In this work, the goal is to approach controlling the surface morphology (*e.g.* tuning the network coverage) as well as thickness of LPE WS_2 nanosheets by the spin coating technique as relatively straight forward deposition method. It will be shown that the nanosheet density on the substrate can easily be tuned by the WS_2 concentration. In films with higher coverage, the photoluminescence per WS_2 unit decreases due to restacking. However, this can be prevented by adding additional stabilizers such as polymers. Such films will be interesting for integration into optoelectronic devices as well as to study heterostacks from various 2D materials. The aim of this

study is not to replace popular printing strategy for device fabrication, but rather the investigation of optical properties of WS_2 nanosheet thin films.

3.3.2 Initial Observations

Within this thesis, two series of WS_2 thin films were fabricated with the aim to tune the coverage by optimizing the WS_2 nanosheet concentration. The first series as prototype samples are described in this Chapter 3.3.2. Characterization by performing AFM measurements yielded the initial information on the morphology of these films and revealed the need to improve the protocol to fabricate thin films with less aggregation by applying different removal steps on a second series of films which will be described in Chapter 3.3.3.

3.3.2.1 Preparation and Characterization of the Dispersions

High quality WS_2 dispersions were prepared by probe sonication of the powder in an aqueous sodium cholate (SC) solution and subsequent size selection by LCC using the protocol in Chapter 3.2. The sample monolayer-richest fractions 5-10k *g* and 10-30k *g* were used throughout this section. After the comprehensive study about the transfer of WS_2 nanosheets in a range of solvents, isopropanol and THF (volume ratio 8:1) chosen as suitable candidates for the spin coating. The transfer from surfactant to solvent was performed as described in section 3.1-3.2 and detailed in the methods section. Here, the 5-10k *g* WS_2 fraction was chosen as a suitable candidate for approaching the goal of tuning the thin-film coverage.

The dispersion was initially characterized by extinction spectroscopy before and after transferring to the mixture IPA/THF (Figure 3.3-1A-B). The spectrum was measured at room temperature. A- and B-exciton peaks are seen at 613 nm (2.022 eV) and 513 nm (2.420 eV) in SC and 618 nm (2.010 eV) and 515 nm (2.410 eV) after transfer, respectively. Some presumably minor reaggregation occurred on transfer which can be observed as non-resonant scattering background at >650 nm in the optical extinction spectra. Note that this is in spite of an aggregation removal step by centrifugation at 500 *g* for 1 h as part of the transfer protocol.

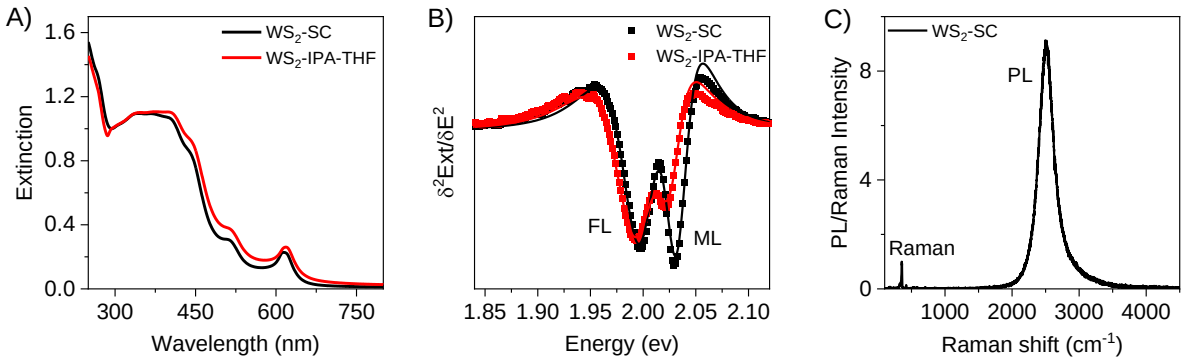

Figure 3.3-1: A) Normalized optical extinction spectra of WS_2 nanosheets trapped in the range of 5-10 k*g* in SC (conc: 0.1gL^{-1})-H_2O based dispersion (before transfer) and in a mixture of IPA and THF (after transfer). B) Second derivative of the A-exciton peak after smoothing the extinction spectra of the WS_2 dispersions before transfer and after transfer to IPA-THF. D) Room temperature PL and Raman spectra (excitation wavelength 532 nm) of a droplet the high concentration WS_2 dispersion (5-10k *g*) in water/SC. Raman/PL spectra after transfer cannot be measured in a comparable way to the volatility of the organic solvent mixture.

The second derivative of the A-exciton region after smoothing the optical extinction spectra typically shows a splitting into two components assigned to monolayers (ML) and few-layers (FL). The fitted second derivatives provide information based on the energy and width of the ML and FL nanosheets, as well as their relative population.[60, 69] It can thus for further investigation of reaggregation in WS_2 nanosheets transferred to solvents. Figure 3.3-1B shows that ML and FL features are separated even after transfer, but the intensity of the ML contribution is decreased due to reaggregation. The data can be fit to the sum of the second derivatives of two Lorentzian for both samples. Changes in linewidth and energy are related to solvatochromic effects (Chapter 3.2). The minimal change in linewidth (both samples ~55-57 meV in the case of the monolayer) is indicative of a high quality sample and is thus a confirmation of the choice of solvents.

As outlined in Chapter 1.4.4, extinction spectra of LPE WS_2 are rich in information and in combination with established quantitative metrics,[65, 69] nanosheet dimensions and concentrations can be calculated. In brief, the lateral size is obtained by considering extinction intensity ratios, while nanosheets layer number is extracted from the peak position of the A-exciton of the standard sample in sodium cholate. The WS_2 nanosheet concentration before and after transferis obtained from the size-independent extinction coefficient at 235 nm and the Beer-Lambert equation. Table 3.3-1 summarizes the parameters calculated from optical extinction spectra based on the empiric equations which were reported previously.

Table 3.3-1: Extracted information about nanosheet properties (average sheet length <L>, volume-fraction weighted layer number $<N>_{Vf}$, monolayer volume fraction ML Vf, concentration prior to and after transfer) from optical extinction spectra. All calculation have been done according to the established metrics.[65, 69]

<L>	$<N>_{Vf}$	ML Vf (from A-exciton fit)	Concentration prior to transfer	Concentration after transfer to solvent
46 nm	2.2	29%	~ 17 g/L	~ 0.12 g/L

As further quality check, the dispersion was subjected to Raman/PL spectroscopy. In figure 3.3-1C, the room temperature PL and Raman spectrum of a droplet containing nanosheets in SC-H_2O before transfer is shown (excitation wavelength 532 nm). Note that fast evaporation of the organic solvents under laser excitation made it difficult to record the PL and Raman spectrum for this sample after the transfer. The PL consists of a single symmetric peak centered at about 613 nm (2495 cm^{-1} or 2.021 eV) with a small shoulder extended towards higher wavelengths in agreement with literature.[65] The ML content is reflected in the PL/Raman ratios which makes it possible to assess the quality of the WS_2 dispersion. Here this ratio was ~ 9:1. The calculated ML volume fraction in H_2O-SC by considering previously established metrics based on Raman/PL spectra[65] is ~50%, i.e. larger suggested from UV-VIS spectra (table 3.3-1). However, as discussed in Chapter 3.1, the PL is sensitive to additional influences such as defect content, doping, laser power etc. Hence, the ML volume fraction from UV-Vis is probably the more realistic value. Nonetheless, the PL/Raman measurement confirms the high optical quality of the dispersion.

3.3.2.2 Initial Trials of Deposition

With this high quality sample, initial attempts of deposition through spin-coating were carried out. In this study, WS_2 was deposited on glass substrates by using a spin coater embedded inside a glovebox with inert nitrogen atmosphere to prevent potential oxidation of the deposited nanosheets. Deposited nanosheets were characterized by optical microscopy and atomic force microscopy (AFM) as tool to show the homogeneity and coverage. In an initial trial and error period, spin coating conditions were varied (rotational speed, deposition of the droplets on the substrate, dynamic versus static coating, nanosheet concentration) and the homogeneity tested. Eventually, this resulted in a homogeneous film with a dense coverage of one layer of deposited mono-and few-layer nanosheets (Figure 3.3-2). This was obtained using a dispersion with an optical density of 2.3 at 240 nm. Hence, this sample was used as reference for the subsequent

studies with the aim to tune the WS_2 coverage in thin films by systematic variations of the WS_2 concentrations.

The following spin-coating conditions were established: For the fabrication of each film, 1.5 mL of the WS_2 dispersion was used. To prevent the wasting of WS_2 dispersion in each spinning, 20 µL of optimized WS_2 dispersion as a droplet was deposited as close to the centre of the substrate as possible. The spin coater was set on 500 rpm for 2 s and followed by 8000 rpm for the 60 s. This will be referred to as multistep static dispense spin coating.

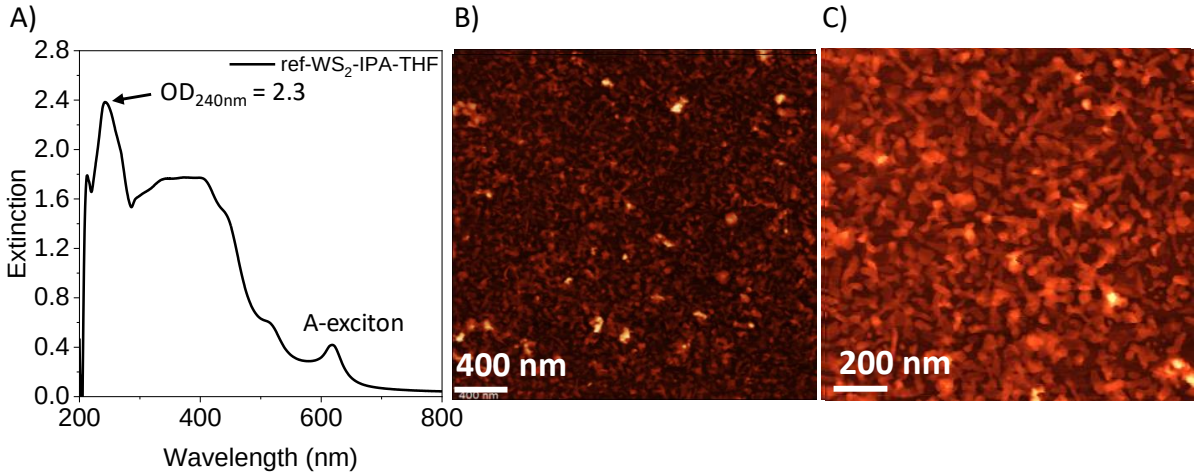

Figure 3.3-2: A) Optical extinction spectra of WS_2 nanosheets trapped in a range of 5-10k *g* transferred to a mixture of IPA/THF. This sample was used for initial spin coating attempts that eventually resulted in homogeneous films as shown in AFM. B-C) AFM images of the best spin-coated film obtained from the dispersion shown in (A). Here nearly complete single layer-coverage of the substrate is achieved.

3.3.2.3 Preparation of the First Set of Films With Tuned Coverage

To test whether it is possible to tune the coverage of deposited WS_2 using the multistep static dispense spin coating, dispersions with different concentration were produced and tested. Since initial experiments revealed that an optical density of 2.3 at 240 nm was in principle suitable to achieve a dense coverage with minimal overlap of sheets, this concentration was used as reference point denoted as "1L coverage". We expect a change in concentration to result in a variation of the coverage. In the following, this will be labelled as coverage 1 (COV1), coverage 2 (COV2), coverage 3 (COV3), coverage 4 (COV4) and coverage 5 (COV5). Coverage 1 uses the lowest and coverage 5 the highest WS_2 concentration in dispersion. The respective optical density of WS_2 at 240 nm are summarized in Figure 3.3-3.

Experimentally, after completing the transfer process including two washing steps and collecting all sediments in 8 mL mixture of IPA and THF, one centrifuge step at 100 *g* is performed to remove aggregates. This sample has the highest accessible nanosheet concentration with and optical density of ~6.9 at 240 nm. This would correspond to a concentration 3 times as high as the "1L" coverage. 1.5 mL of the sample with the highest concentration is kept, while the rest of this sample is diluted step by step with a mixture of IPA/THF (8:1) to obtain the lower concentrations. This procedure is repeated until the lowest concentration is reached with and optical density of 1.2 at 240 nm. All values were extracted from optical extinction spectra (rather than purely relying on dilution). These five dispersions with systematically varied concentration were used to fabricate five tuned coverage thin films. Bath sonication is applied for 5 minutes per sample prior to deposition to remove inhomogeneities or aggregation which might have occurred over time.

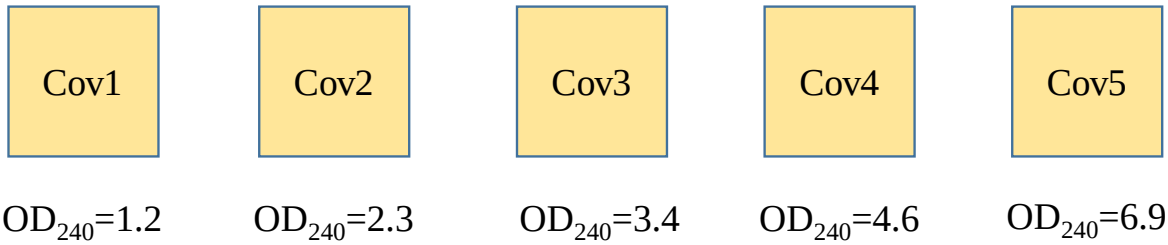

Figure 3.3-3: Schematic of the five different thin films that are produced from different WS2 dispersion with different concentration. The abbreviation of the resulting film and the optical density of WS_2 at 240 nm are given. Based on preliminary experiments, we expect COV2 to be dense and homogeneous. This is also referred to as "1L". As such, we can also use the nomenclature COV1=0.5L, COV2=1L, COV3=1.5L, COV4=2L and COV5=3L

As already indicated in Chapter 3.2, aggregation on transfer to solvents can occur. This can have a negative effect on the deposition which can best be revealed using AFM. Hence, all deposited WS_2 thin films were initially characterized by performing AFM measurements to rationalize if the current protocol is generally a promising way to fabricate thin films with tunable nanosheet coverage based on the systematically varied concentration of WS_2 in the dispersions. That it is in principle possible, was shown in preliminary experiments, but it is not clear whether the production of smooth films with minimal aggregation and stain is reproducible. The AFM images of this set of films are shown in Figure 3.3-4 along with photographs of the dispersions used. While the dispersions look homogeneous with no sign of aggregation visual to the eye, obviously, the AFM images of these spin-coated WS_2 thin films show significant aggregation in particular in COV5

what would have ideally been a “3L” coverage. It is also noted that large gaps are observed in the case of COV2-1L in contrast to the preliminary data.

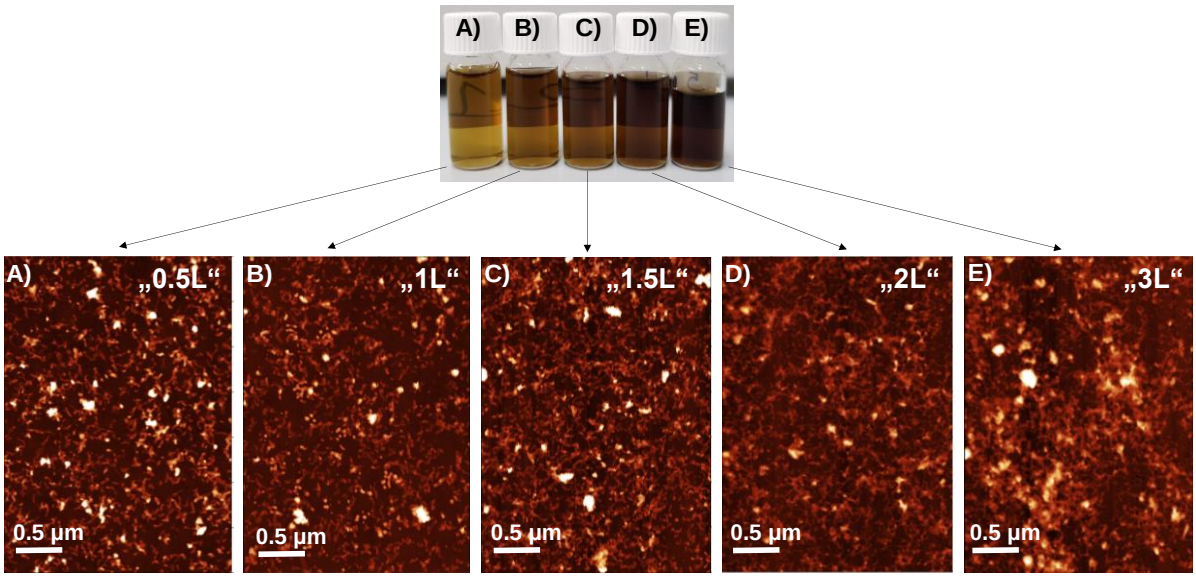

Figure 3.3-4: Attempts to tune the coverage of deposited nanosheets via the WS_2 nanosheet concentration. A-E) AFM images of the first set of films from different WS_2 concentration obtained from multistep static dispense spin coating. The concentration of these five dispersions were systematically varied which is visualized by. the color of these dispersions in the top row. An explanation of the sample labels is found in Figure 3.3-3.

The AFM clearly shows that there is a severe issue with aggregation over time leading to poor reproducibility of the films formation, as the quality of the thin films depends on the quality of WS_2 dispersion. Thus, in the following, the systematical removal of aggregated nanosheets by centrifugation steps on WS_2-IPA-THF dispersions is investigated. Note that in this first set of films, the aggregate removal step was performed on high concentration WS_2 dispersions. Apparently, this step was not sufficient to fabricate a high-quality thin film with minimal aggregation in a reproducible way.

3.3.3 Optimized Thin Films From Additive-Free Deposition

3.3.3.1 Preparation and Characterization of the Dispersions

The goal is to improve the quality of the thin films by applying additional centrifugation steps to the final dispersion transferred to IPA/THF prior to deposition as will be described in section 3.3.3.2. The initial WS_2 dispersion in aqueous SC was prepared by the same protocol and also a similar transfer procedure was applied (figures 3.1-1 and 3.1-2). However, the final step of the

transfer protocol, i.e. the removal of aggregated nanosheets was modified and centrifugation was performed at 500 *g* (instead of 100 *g*) for 60 min. Figure 3.3-5 shows the characterization of the WS_2 dispersion used for fabricating the second set of WS_2 thin films through spin coating. Optical properties of WS_2 dispersion before and after transferring to the mixture of solvents were characterized. The normalized optical extinction spectra of WS_2 nanosheets before and after transfer are shown in Figure 3.3-5A. No apparent changes are observed suggesting that the average nanosheet dimensions were not changed on transfer as before. The second derivative of the A-exciton region after smoothing the optical extinction spectra of both initially prepared and transferred WS_2 nanosheets to IPA/THF is depicted in Figure 3.3-5B. As before, the A-exciton splits into two components assigned to monolayers (ML) and few-layers (FL). Already in the as-prepared sample in aqueous SC surfactant, the ML content is higher than in previous batches. This is attributed to an improved decanting after cascade centrifugation used for the size selection. Energy and width of ML and FL are different in the two liquid environments due to solvatochromism (Chapter 3.2). However, importantly, after transfer, the ratio between ML and FL did not change significantly in contrast to the samples described in section 3.3.2.1. This strongly suggests that nanosheets were not re-aggregated by the time of the measurement and that the increases in the centrifugal rate in the last step of the transfer protocol is an important modification to the protocol.

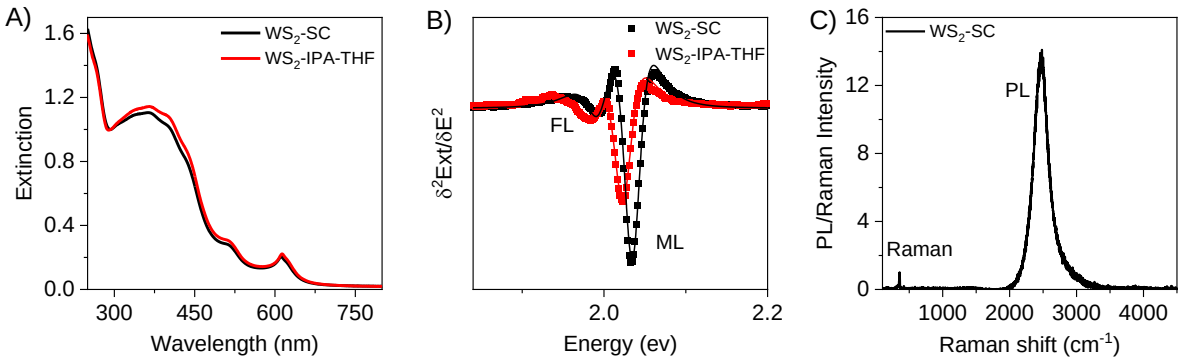

Figure 3.3-5: Characterization of the dispersions used in this section. A) Normalized optical extinction spectra of WS_2 nanosheets trapped in the range of 5-10 k*g* in SC (conc: 0.1gL^{-1})-H_2O based dispersion (before transfer) and in a mixture of IPA and THF (after transfer). B) Second derivative of the A-exciton peak after smoothing the extinction spectra of the WS_2 dispersions before transfer and after transfer to IPA-THF. D) Room temperature PL and Raman spectra (excitation wavelength 532 nm) of a droplet the high concentration WS_2 dispersion (5-10k *g*) in water/SC. Raman/PL spectra after transfer cannot be measured in a comparable way to the volatility of the organic solvent mixture.

The dispersion in aqueous surfactant was also subjected to Raman/PL spectroscopy (Figure 3.3-5A). The quality of the WS_2 dispersion is tracked by the PL/Raman ratio which is ~ 14 in this sample and confirms that it is a good quality sample. The metric for monolayer content suggested in literature[69] would imply a monolayer volume fraction of ~80% which is larger than the value suggested by the ratio of ML and FL A-exciton resonance in UVVis which gives ~63%. This agrees with the observation from the previous section and could be a result of different measurement conditions for the Raman/PL spectra in this work compared to literature.

Table 3.3-2 summarizes several parameters calculated from optical extinction spectra based on empirical equations (previously established metrics).[65, 69] The lateral size is obtained by considering extinction intensity ratios, while nanosheets layer number is extracted by considering peak positions of the standard sample in sodium cholate. In addition the volume fraction of monolayers is estimated from the A-exciton shape.

Table 3.3-2: Extracted information about nanosheet properties (average sheet length <L>, volume-fraction weighted layer number $\langle N \rangle_{Vf}$, monolayer volume fraction ML Vf, concentration prior to and after transfer) from optical extinction spectra. All calculation have been done according to the established metrics.[65, 69]

<L>	$\langle N \rangle_{Vf}$	ML Vf (from A exciton fit)	Concentration prior to transfer	Concentration after transfer to solvent
32 nm	2.2	63%	~ 15 g/L	~ 0.23 g/L

3.3.3.2 Tracking Aggregation by Repeated Centrifugation

Since an increase in the centrifugation rate from 100 *g* to 500 *g* in the aggregate removal step significantly improved the quality of the dispersion transferred to IPA/THF (*i.e.* similar ratio of ML to FL exciton response in UV-Vis in the transferred and original dispersion, Figure 3.3-5B), the impact of additional centrifugation steps was assessed in more detail. To this end, the dispersions in IPA/THF at different WS_2 concentration was repeatedly centrifuged at 1,000 *g* for 30 min. The WS_2 concentration was adjusted according to Figure 3.3-3.

After applying each aggregate removal step, optical extinction spectra of all transferred and optimized 5-10k *g* WS_2-IPA-THF based dispersions with different initial WS_2 concentrations were measured (Figure 3.3-6A). The noise in the spectra at extinction >3 is due to detector saturation at high optical densities. It is clear that concentration is reduced on repeated centrifugation as seen from a drop in the optical density. It is noted that the size of nanosheets are identical in all

dispersions with different concentrations (same initial dispersion), therefore no typical changes in spectral shape with nanosheet size and thickness due to edge and confinement effects are observed. This is best seen by the comparison in the Appendix, Figure A6.10 which shows the same data, but grouped by dispersion with different concentrations after each step in one panel. Interestingly, no significant change in the non-resonant scattering background is observed across all samples. This suggests that the chosen centrifugation conditions are sufficient to remove larger aggregates. This in turn implies that the drop in concentration on repeated centrifugation is due to aggregation occurring over time (*e.g.* during the time of centrifugation and decanting), but that the centrifugation simultaneously removes the majority of aggregates successfully under the chose conditions.

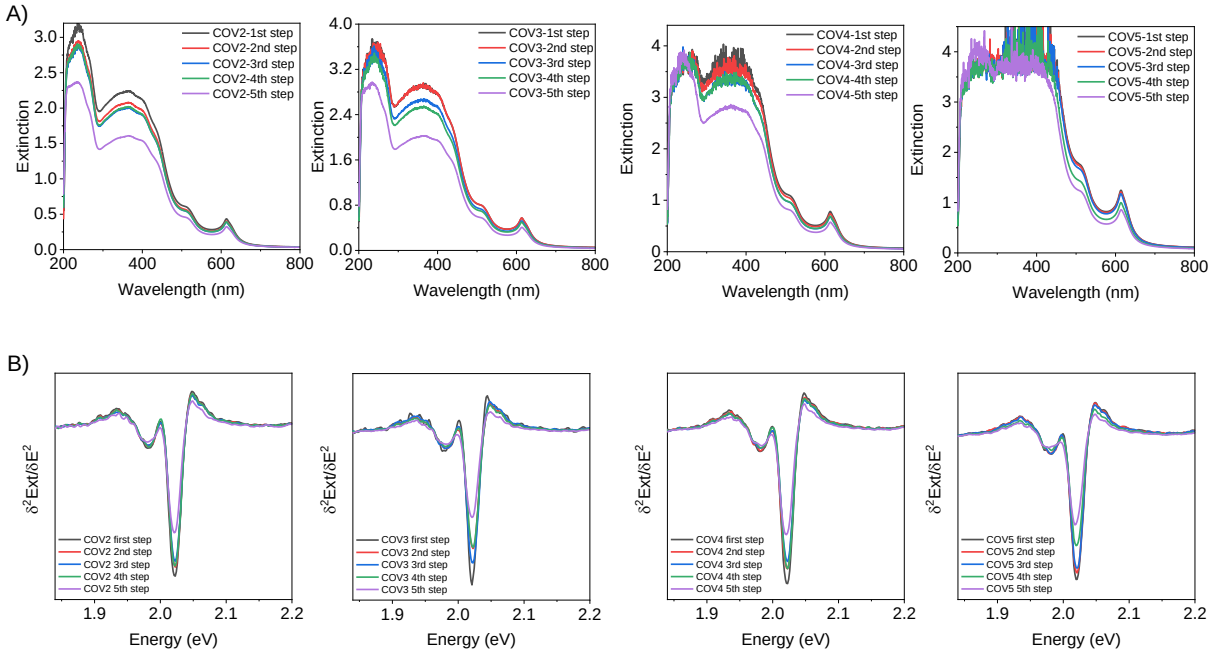

Figure 3.3-6: Impact of repeated centrifugation (1000 *g*, 30 min) on WS_2 (5-10k *g*) transferred to IPA/THF at different nanosheet concentration (denoted as COV2-COV5). A) Optical extinction spectra. Some material obviously sediments after each centrifugation step but there are no changes in spectral shape. The noise in the spectra at extinction >3 is due to saturation of the detector. B) Second derivative of the A-exciton region which is extracted from the respective optical extinction spectra after smoothing.

To analyze this in more detail, the second derivative of the A-exciton was extracted from the smoothed optical extinction spectra to give an indication of potential changes in the monolayer contents (Figure 3.3-6B). It is observed that the contribution of the ML to the A-exciton is reduced relative to the few-layer component with repeated centrifugation. This is consistent with the hypothesis that aggregation occurs (loss of monolayers) during the timeframe of the experiment (~2 h in each step with centrifugation, decanting, UVVis measurement), but that larger aggregates

are efficiently removed resulting in no obvious changes in the few-layer component. Note that aggregates would have a different effective layer number which would result in a significant shift and broadening of the response stemming from the sum of the few-layers due to the scaling of A-exciton energy with layer number.[65, 69]

These considerations imply that we can use the data obtained after repeated centrifugation to track the re-aggregation of WS_2 transferred to IPA/THF. To this end, the optical density (OD) of the A-exciton was extracted because the extinction is well below 2 in the region in all samples, even the highest concentration sample denoted as COV5 (Figure 3.3-7A), and plotted as function of centrifugation step in (Figure 3.3-7B). Clearly, any additional centrifugation run resulted in a decreasing A-exciton optical density due to sedimentation of (aggregated) nanosheets. A linear scaling is observed and the slope can be interpreted as indirect measure for the aggregation rate. It is expected that the aggregation rate is faster for higher WS_2 nanosheet concentration. This is indeed the case and manifested as a steeper slope when the optical density is plotted as a function of centrifugation speed. This dependence is best observed when plotting the slopes in Figure 3.3-7B as function of the initial optical density at the A-exciton (Figure 3.3-7C). This shows that how much material is lost linearly depends on the initial WS_2 concentration. This is very problematic for further processing because the dispersion might not be long term stable enough in IPA.

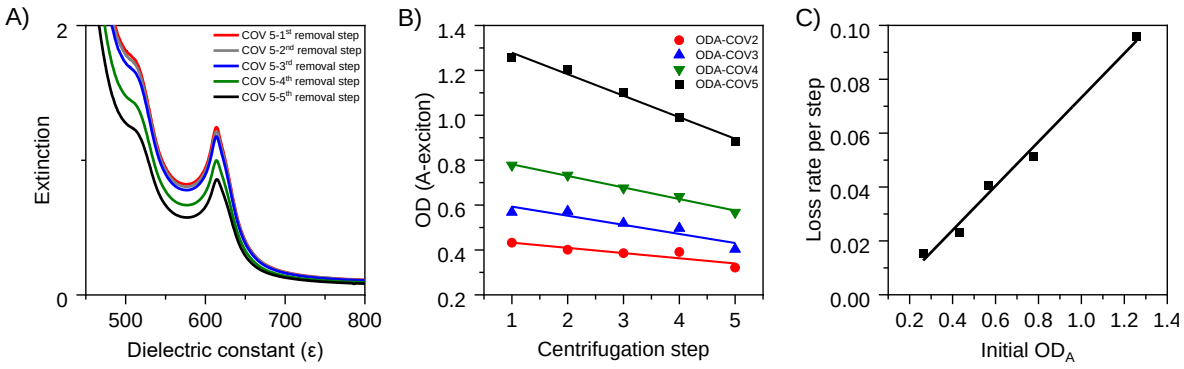

Figure 3.3-7: Impact of additional centrifugation on the optical response of WS_2 nanosheets transferred to IPA/THF. A) Comparison the extinction spectra in the region of the A-exciton for the highest WS_2 concentration used after performing five subsequent centrifugation steps at 1000 *g* for 30 min. A reduction of the WS_2 concentration is discernible after each step. B) Plot of the optical density at the A-exciton as function of the centrifugation step. A linear decrease in nanosheet concentration is observed. The slope can be interpreted as indicator of the aggregation rate. C) Loss rate per step (i.e. slopes in panel B) as function of initial optical density at the A-exciton visualizing that aggregation is concentration dependent.

As indicated above, the second derivative extinction spectra in the A-exciton region were also analyzed. All relevant extinction spectra were smoothed with the Lowess method before

differentiating twice. Due to the splitting of the A-exciton into two components, the monolayer content in the sample can be obtained by fitting the spectra to the sum of the second derivative of two Lorentzians. This also allows to investigate changes in the A-exciton energy and width after performing the additional centrifugation steps. In all cases, the data can be well described by the fit function as exemplarily shown in Figure 3.3-8A (all data, see Appendix A6.11). As illustrated by the sample set with the highest WS_2 concentration (COV5) in Figure 3.3-8A, subtle changes in A-exciton are observed.

It was previously observed (Chapter 3.1 and 3.2) that solvatochromism is manifested in a simultaneous shift and change in linewidth of the monolayer A-exciton. A redshift was typically accompanied by broadening. In some sense, aggregation can result in a similar response, since the solvent in the environment of an individual sheet is replaced by another nanosheet. Since the A-exciton response is very sensitive to the environment, it might be possible to use such information to even track beginning minor aggregation that has not yet yielded large enough particles that sediment under the chosen centrifugation conditions. To test this, the ML A-exciton width is plotted as function of the energy in Figure 3.3-8B. The data reveals a fairly clean correlation between width and energy which suggests that aggregation can have a similar effect on the A-exciton response as induced by different solvent environments. Overall, the higher WS_2 concentration samples show a more broadened and red-shifted A-exciton which, according to Chapter 3.2, implies a higher refractive index of the environment. Bearing in mind that few-layer nanosheets also show a broadened and red-shifted A-exciton absorbance, this can very well be an effect induced by aggregation. For completeness, the width of the contribution of the sum of few-layers to the A-exciton is plotted as function of the few-layer energy in Figure 3.3-8C. A scaling is also observed in this case, but in the opposite direction, i.e. a red-shift is a accompanied by a narrowing. This cannot be readily interpreted. Unlike the monolayer A-exciton response, the few-layers A-exciton is the average of all few-layers in the samples and position and width will therefore not only depend on the solvent environment, but also the effective number of layers which changes in the presence of aggregates. As such, various different effects can result in shifts and changes in linewidth which cannot be deconvoluted.

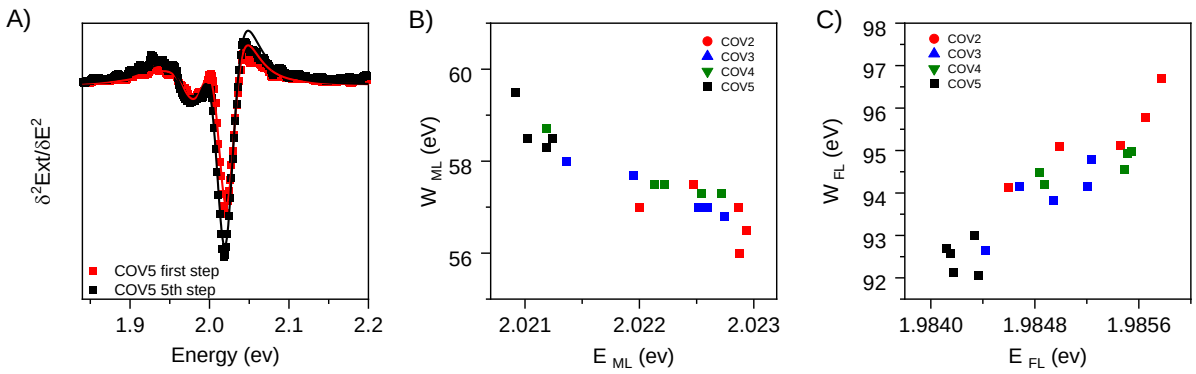

Figure 3.3-8: A) Comparison of the second derivative of the A-exciton region at the highest WS_2 concentration (COV5) after smoothing the extinction spectra after the first and last iterative centrifugation step. The A-exciton splits into two components assigned to monolayers (ML) and few-layers (FL). B) ML and C) FL width as function of energy for all samples. The different initial WS_2 concentrations are color-coded.

In summary, the systematic investigation of iterative low speed centrifugation steps showed aggregation is a severe issue after transferring the nanosheets to IPA/THF. While larger aggregates can be efficiently removed at 1000 *g*, 30 min centrifugation, aggregation occurs over the timeframe of the centrifugation, decanting and measurement. For further processing, it is thus important to perform the low speed centrifugation to remove aggregations immediately before the deposition. In addition, it was found that the aggregation rate linearly scales with the initial WS_2 concentration. This implies that aggregation might happen too quickly in high concentration samples. It is therefore of interest to test additional stabilizers as will be discussed in Chapter 3.3.4.

3.3.3.3 Characterization of Thin Films on Glass

As evident from the first set of thin films, it was important to investigate the removal of aggregated nanosheets systematically to approach the goal of this study which is the fabrication of WS_2 thin films with tunable coverage and with retained optical quality and minimal restacking of the sheets after deposition. With the knowledge gained from Chapter 3.3.3.2, a second set of films was made by spin-coating using dispersions of WS_2 in IPA/THF with different concentrations immediately after centrifugation at 1000 g for 30 min. Note that the concentrations were adjusted according to the description in Figure 3.3-3 before the additional centrifugation. While the optical density of 2.3 at 240 nm was previously found to yield a dense coverage with minimal nanosheet overlap and gaps, which was denoted as COV2, we expect a lower coverage from this sample after the additional centrifugation. Therefore, COV1, with even lower coverage was omitted as sample in

this section. Note that the labels COV2-5 refer to the optical densities summarized in Figure 3.3-3 before the additional centrifugation.

The network density and homogeneity was first investigated microscopically (Figure 3.3-9). In comparison to the first set of films, it is clear that aggregation was significantly improved in the new set of films by performing the additional centrifugation steps on the WS_2-IPA-THF dispersion. The progression in nanosheet density from sample to sample was observed. Both AFM and optical microscope images confirmed this improvement with minimal aggregation, homogeneous distribution of nanosheets on the surface and hardly any stains. Some patterns can be observed in the optical images due to solvent evaporation during the spin coating process (coffee ring effect), but these are relatively scarce. Consequently, it is shown that tuning of the coverage is in principle possible *via* the concentration of WS_2 using spin coating, although with restrictions due to aggregation of the nanosheets in dispersion occurring at high concentrations.

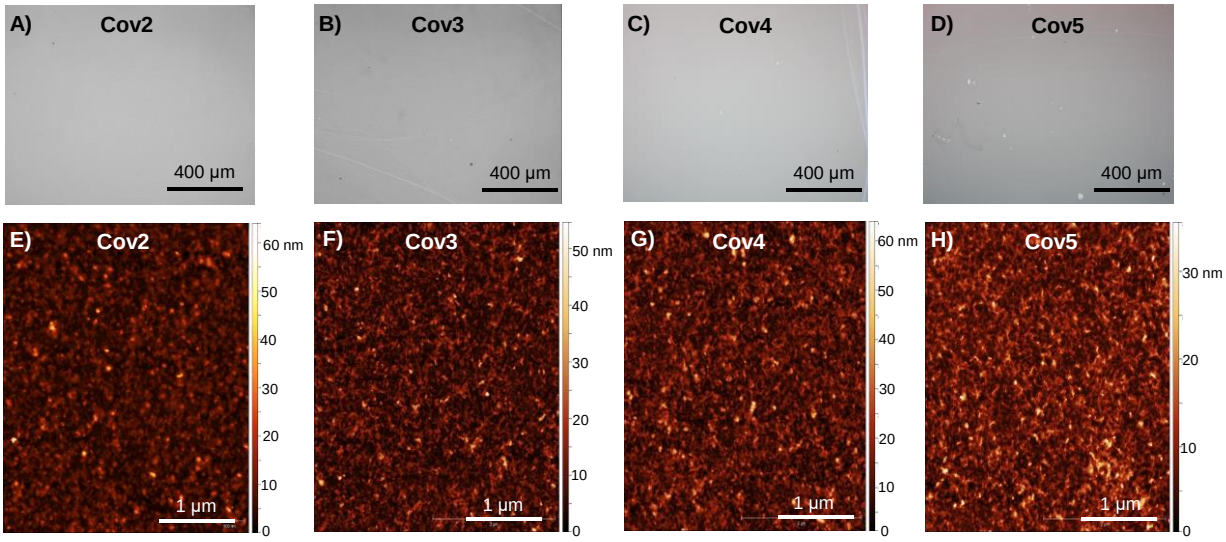

Figure 3.3-9: A-D) Optical microscope images of WS_2 nanosheets deposited on glass substrates by spin coating using different concentrations of WS_2 in IPA/THF. Films were made immediately after a centrifugation step at 1000 g for 30 min which successfully removed aggregations. E-H) Atomic force microscopic images on the WS_2 network density in the thin films.

The WS_2 thin films were also characterized by UV-VIS spectroscopy to measure extinction spectra (Figure 3.3-10A-B). The extinction in the films increased with increasing initial WS_2 concentration from COV2-COV5 (Figure 3.3-10A). This confirms that more nanosheets are indeed deposited using concentration dispersions, i.e. that the coverage is tunable. In the extinction spectra, a relatively large area (~ 1 cm^2) is probed so that this information is complementary to the microscopic picture described above. It should also be noted that the non-resonant scattering background (> 650 nm) is minor in the extinction spectra for all coverages which also confirms

improved optical quality in the thin films by performing additional aggregate removal steps prior to deposition. Second derivatives were calculated after smoothing extinction spectra (Figure 3.3-10B). According to the characterization of WS_2 dispersions, it is expected that these spectra are composed of two components as ML and FL. However in films, both features gradually broadened and merged so that it is not possible to resolve the splitting. This could also suggest restacking of the monolayers in the films. At the highest WS_2 concentration (COV5) these components were red-shifted and broadened the most presumably due to a greater level of restacking which increases the effective layer number.

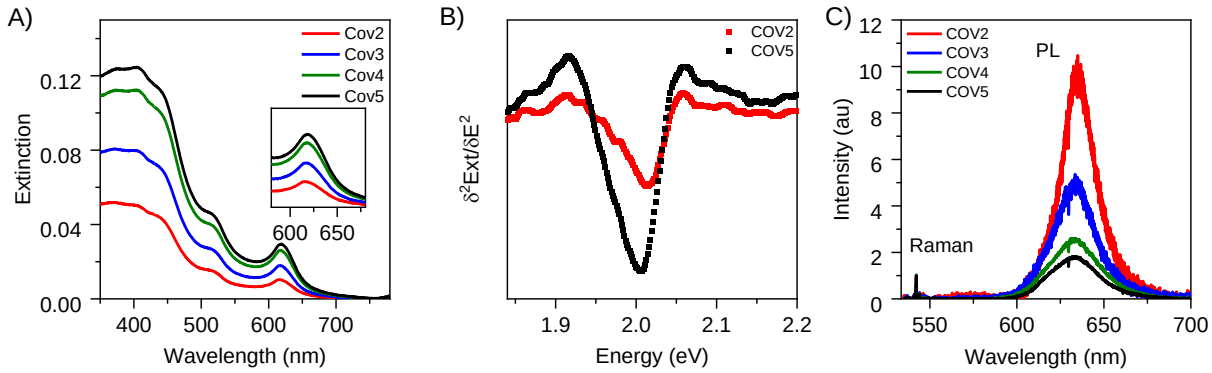

Figure 3.3-10: Optical thin-film characterization. A) Optical extinction spectra of WS_2 deposited on glass by spin coating using different initial WS_2 concentrations in the IPA/THF-based dispersions. There is an increase of the film optical density with increasing OD of the dispersion. Inset: Zoom-in at the A-exciton. B) Second derivative of the A-exciton region from films with two different coverages. The splitting between ML and FL cannot be resolved C) Photoluminescence of thin films measured by Raman spectroscopy normalized to the 2LA(M) Raman mode of WS_2. PL is detected in thinner films however the intensity gradually decreases in thicker films accompanied with a redshift.

UV-Vis extinction spectra cannot resolve the splitting of the ML and FL components in the thin films so that it is not clear whether monolayers are still present or whether too much random restacking occurred on deposition. To test this, Raman/photoluminescence spectroscopy was performed (excitation 532 nm) to investigate if the optical properties of WS_2 monolayers in a thin film are comparable to the dispersion. Note that complete restacking of monolayers would result in a loss of the PL. As discussed in previous Chapters, the PL peak position and width is influenced by a range of factors: i) temperature; ii) defect content, iii) doping and dielectric screening from different environments and iv) acquisition conditions (focus) and v) strain. Here the laser power kept as low as possible (1%) to avoid heating the sample. Contrary to measurements in dispersions where single spectra were measured, here roughly thousand spectra were collected from different spots of the films and averaged (Raman mapping).

The Raman/PL spectra of the thin films are shown in Figure 3.3-10C. Clearly, the PL is widely retained in thinner films, unlike the thicker ones where the intensity gradually decreased. The PL peak consists of a single peak centered at ~ 635 nm which is significantly redshifted compared to the dispersion (~615 nm) with a small shoulder extended towards longer wavelengths. In the COV2 film, a PL/Raman ratio of 10.5 could be achieved which is only 25% lower than in the initial dispersion. This suggests that at least 75% of the monolayers were retained. Note that these values need to be treated with care and are a lower estimate, since the PL is broadened in the film compared to the dispersion which effectively decreased the intensity ratio.

As mentioned before, broadening could be observed for different reasons such as reaggregation, doping, inhomogeneous broadening or heating, interference effects, or mechanical strain which can influence the electron to photon transition energy. Several studies have been carried out on the Raman and PL spectra of atomically thin WS_2 layers on various solid substrates and attributed the shift of the PL peaks to either doping or strain by the dielectric or metallic substrates.[99] If any strain[99-100] or doping[73, 101] effect was introduced in the WS_2, the $E_{2g}{}^1$ and A_{1g} Raman vibrational modes would also shift which is not observed here. While strain is often observed in 2D materials on substrates, the flakes in this work are relatively small (< 50 nm) and can presumably relax more easily than extended monolayers of tens of microns in lateral dimensions. Further, since the PL intensity gradually decreases with increasing coverage, we attribute the variations in the PL signal across the sample predominantly to restacking effects.

To investigate the shape of the PL in more detail, the PL was fitted to two Lorentzians (Figure Figure 3.3-11). The (gray) dots are experimental data, the red and blue lines are two fitted peaks. The sum of the fit peaks is represented by the black line, which matches the experimental data reasonably well. In dispersion, the PL signal originates solely from the monolayer nanosheets and in aqueous sodium cholate, only a minor contribution from trion emission at higher energy is observed. Note that the red-shifted trion emission can be significantly enhanced relative to the monolayer when chemically doping the sample by additives in dispersion (Chapter 3.1). In thin films, doping can occur on interaction with the substrate. However, as illustrated by Figure Figure 3.3-11, the redshifted PL component increases relative to the monolayer in thicker films with higher coverage where fewer nanosheets are in contact with the substrate. This is counterintuitive if the second red-shifted component was indeed due to trions. An alternative explanation is that it arises from restacked monolayers. In micromechanically-exfoliated TMDs, the PL intensity for a bilayer WS_2 is at least an order of magnitude weaker and further decreases with the number of layers.[59, 102] As already reported, the PL signal from multilayers would exhibit contributions from

the transitions via the indirect bandgap.[73] These multilayer signature is expected to be red-shifted by several hundred millielectronvolts, depending on the layer thickness with respect to the transition of the direct gap. After deposition, in particular for higher coverage thin films, we expect that random restacking occurs which will certainly have an impact on the PL response, but restacked nanosheets are not identical to few-layer sheets due to some disorder and increased stacking faults. As such, it is possible that the lower energy component is from restacked few-layers rather than trions in the thin films.

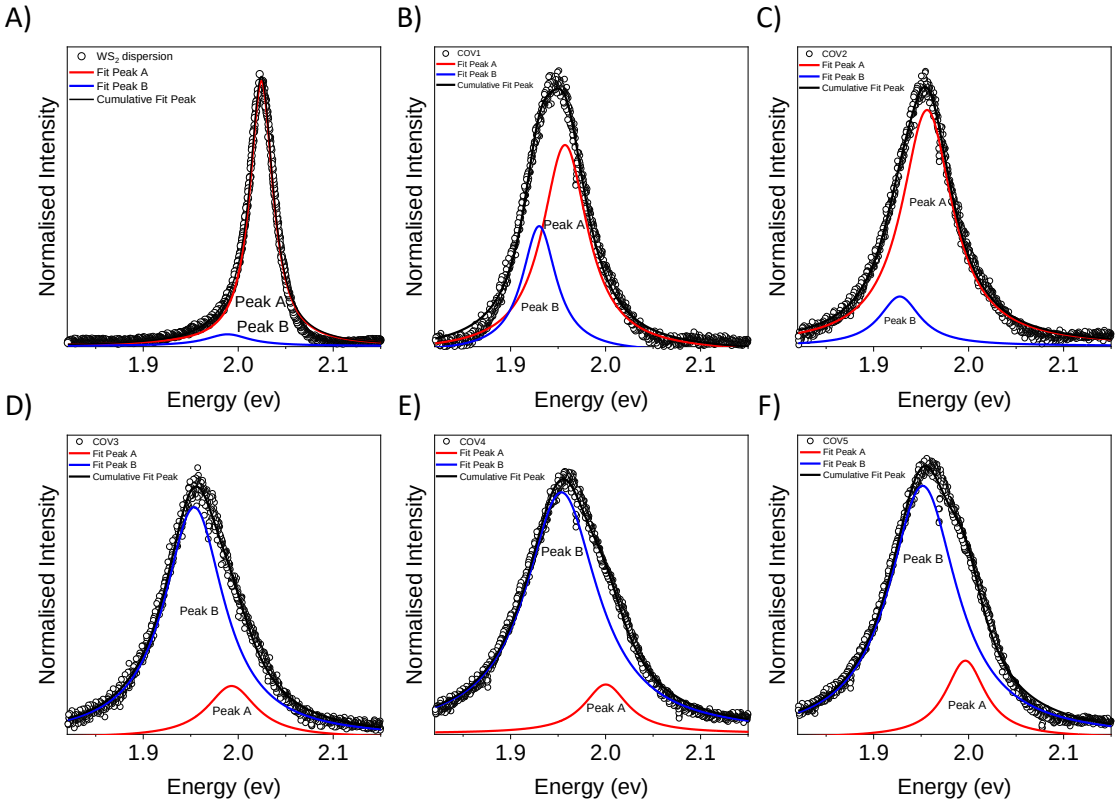

Figure 3.3-11: Fitted PL response of WS_2 nanosheets deposited on glass. A) Typical PL spectrum of a WS_2 dispersion in aqueous sodium cholate dispersion. (B-F)WS_2 deposited on glass using spin coating with different initial WS_2 concentration resulting in an increasing coverage. The black, red, and blue lines are the three fitted peaks by Lorentzian functions.

The results of the optical characterization is summarized in figure 3.3-12. As shown in figure 3.3-12A, the optical density of the film is clearly dependent on optical density of dispersion (*i.e.* the nanosheet concentration) albeit with in a non-linear correlation. This suggests that it will be extremely challenging to make thicker films with this technique limiting the practical relevance of the work. In figure 3.3-12B, the A-exciton peak position is plotted as function of the optical density of the film. The observed well-defined scaling is consistent with restacking of the sheets in thicker films which leads to an increased effective average layer number and hence a redshift of the A-

exciton. Similarly the PL/Raman intensity ratio (Figure 3.3-12C), decreases with increasing coverage (expressed as optical density at the A-exciton in the film), likely due to a loss in PL when nanosheets overlap in the film.

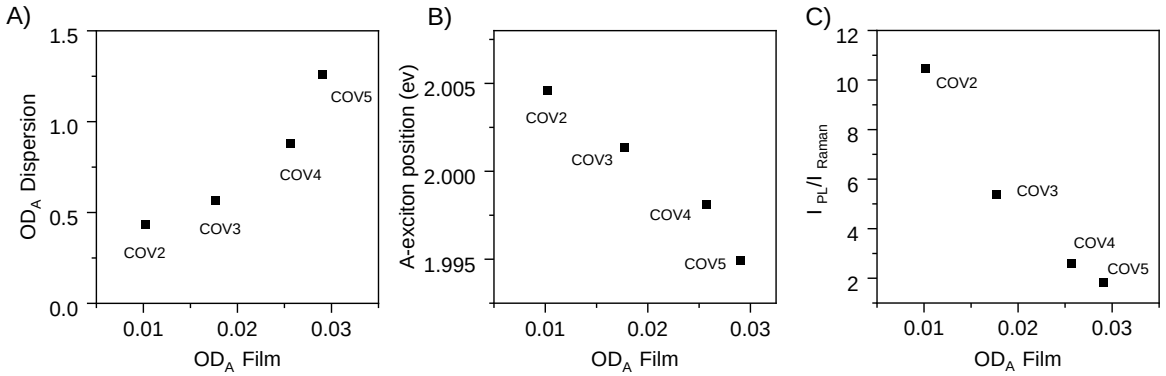

Figure 3.3-12: Impact of WS_2 concentration on the optical properties of the films. A) Optical density of the WS_2 dispersion at the A-excition in dispersion as function of the optical density of the film. B) A-exciton peak position as a function of the optical density of the film . C) PL/Raman intensity ratio as a function of films optical density at A-exciton.

In summary, the improvement in the protocol enabled the fabrication of high quality thin films of WS2 nanosheets on glass through spin coating. A tuning of the coverage was accessible through the initial WS_2 concentration. An increase of the coverage is correlated with an increased restacking of nanosheets can be optically tracked through the A-exciton in response. In thicker films, a reduction of the intensity and broadening of the PL peak is observed. This can be considered as an inherent limitation. A possible route forward is the deposition of WS_2 covered with an additional stabilizer, such as a polymer to prevent restacking in the thin film which should retain the optical quality. This is discussed in Chapters 3.3.4 and 3.4.

3.3.3.4 Deposition on Polymer-Coated Glass

The spin coating should allow for deposition in arbitrary substrates with different surface energies. To test this, the WS_2 IPA/THF dispersion was deposited in glass substrates that were previously coated with different polymers (also through spin coating). The polymers PEDOT:PSS (poly(3,4-ethylenedioxythiophene) polystyrene sulfonate) and PVK (polyvinylcarbazole) since these are popular hole injection and transport layers in light emitting devices.[103-105] A summary of the optical characterization is shown in figure 3.3-13. In Figure 3.3-13A, the optical extinction spectra are shown of WS_2 deposited on glass (COV2), as well as glass coated with a few 10s of nm thick layer of PEDOT:PSS, PVK and PVK on PEDOT:PSS, respectively. In addition to the extinction from WS_2, a background from PEDOT:PSS is observed in the spectra, e.g. at > 650 nm. Interestingly,

the optical density of the film is strongly dependent on the polymer. This suggests significant differences in surface adhesion of W_{S2} on the substrate. The film thickness under identical conditions increases in the order glass < PEDOT:PSS < PEDOT:PSS/PVK < PVK.

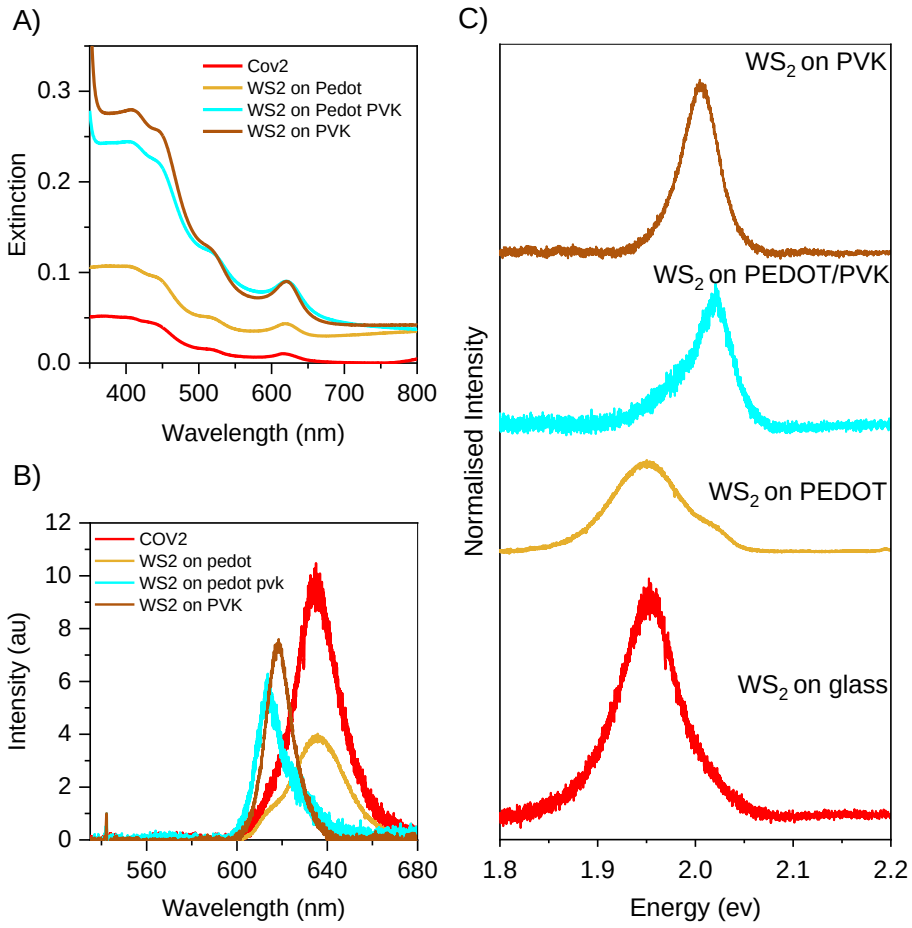

Figure 3.3-13: Optical characterization of WS_2 deposited on glass, and glass coated with different polymers. The optimized spin coating conditions of WS_2 were used in all cases. A) Optical extinction spectra. B) Raman/PL spectra (532 nm excitation) normalized to the WS_2 2LA(M) Raman mode. C) Normalized PL response of the different samples.

The Raman/PL spectra of WS_2 deposited on polymer-coated glass are shown in Figure 3.3-13B. Due to different film thicknesses (according to the optical densities), the PL/Raman intensity ratio cannot be properly evaluated. However, it is clear that there a significant changes in the PL lineshape when WS_2 is deposited on the different surfaces. This is further illustrated in the stacked plot in Figure 3.3-13C. On PEDOT:PSS, the PL of WS_2 has a dominant signal at ~1.95 eV (where the PL is also observed in case of the glass substrate) with a weaker shoulder at higher energy at ~2.02 eV. This gradually increases in intensity in WS_2@ PEDOT:PSS/PVK and becomes the dominant signal in WS_2@ PVK. Importantly, in WS_2@ PVK, a symmetric, narrow linewidth PL is observed similar to the initial dispersion. This suggests that minor doping occurs with PVK and that the nanosheets are efficiently shielded from the underlying substrate. In addition, the adhesion

of WS_2 was improved on PVK which makes this polymer an ideal candidate as stabilizer with the goal of retaining the optical properties of WS_2 in thin films.

3.3.4 Thin Films after Deposition in the Presence of Polymer Stabilizer

3.3.4.1 Preparation and Characterization of the Dispersion

As explained in the previous section, although good quality films were fabricated, the preparation is tedious and time consuming and there is always a risk of aggregation of the nanosheets in organic solvents. This encouraged us to examine a better way to prevent the aggregation. In this study, an additional stabilizer, the polymer (PVK) was added to the medium to make the dispersion long term stable in solvents. It is reported that polymers present the third main class of potentially suitable stabilizers for LPE nanomaterials.[106-107] Their main advantage lies in the ability to stabilize the dispersion in either an aqueous or organic environment, depending on the sidechains[100] of the polymer which govern the polymer's solubility. [54, 108-109] PVK was chosen due to the promising results when depositing WS_2 on PVK-coated glass.

Although PVK is a photoconductive polymer soluble in aromatic hydrocarbons, halogenated hydrocarbons and ketones and resistant to acids, alkalis, polar solvents and aliphatic hydrocarbons, the solubility in our solvent system IPA/THF was expected to be poor. However, a change in the selection of solvents would have made the previous optimization obsolete. Hence, it was tried to dissolve as much PVK as possible in a mix of IPA and THF (8:1) at a concentration of 10 gL^{-1}, by stirring on a hotplate set to 70°C for 5 minutes. This resulted in a transparent solution without noticeable Tyndall effect.

For the preparation of the WS_2 dispersion, the washing and transfer steps based on the established protocol was used except for the presence of PVK in the mixture of IPA and THF as medium at the last step of the transfer protocol. The 5-10k *g* WS_2 fraction was initially spectroscopically characterized before and after transferring into the IPA/THF/PVK mixture. Figure 3.3-14A shows the room temperature optical extinction spectra. In addition to the excitonic resonances of WS_2, a signal from PVK is observed between 300-350 nm and extending further in the UV region. There is no obvious non-resonant scattering background after transfer suggesting minor aggregation.

To confirm this, the second derivative of the A-exciton region of the optical extinction spectra (1.9-2.1 eV) is analyzed to track the degree of nanosheet reaggregation which might have occurred after the transfer to the polymer solution. This is shown in Figure 3.3-14B. The ML and FL features are well separated even after transfer, but the intensity of ML is decreased suggesting that some aggregation had occurred. According to the 2nd derivative plot, the line width remains relatively narrow which is a confirmation that PVK does not significantly alter the optical properties. Both components (ML and FL) are red-shifted compared to water surfactant as a result of solvatochromism, which is expected as the PVK contributes to the dielectric environment of the nanosheets.

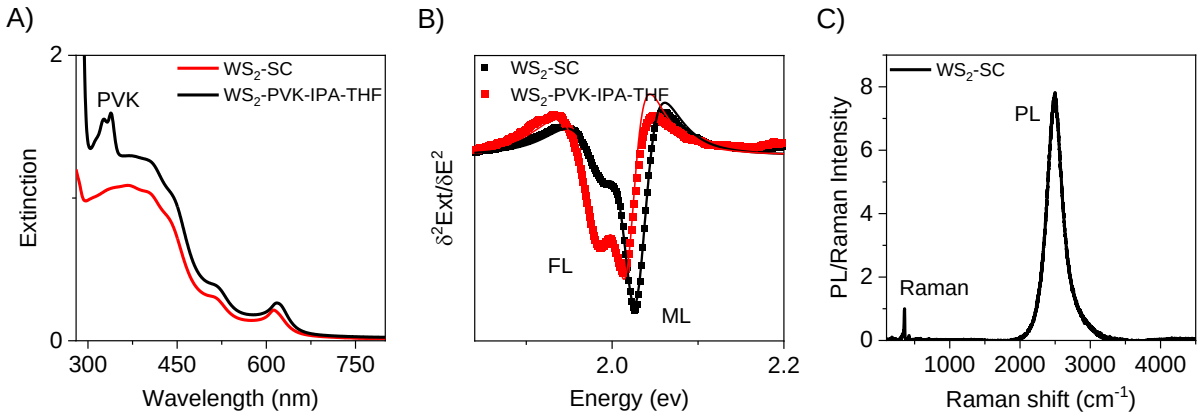

Figure 3.3-14: Characterization of the dispersions used in this section. A) Normalized optical extinction spectra of WS_2 nanosheets trapped in the range of 5-10 k*g* in SC (conc: 0.1gL^{-1})-H_2O based dispersion (before transfer) and in a mixture of IPA and THF in the presence of PVK (after transfer). B) Second derivative of the A-exciton peak after smoothing the extinction spectra of the WS_2 dispersions before transfer and after transfer to IPA-THF. D) Room temperature PL and Raman spectra (excitation wavelength 532 nm) of a droplet the high concentration WS_2 dispersion (5-10k *g*) in water/SC. Raman/PL spectra after transfer cannot be measured in a comparable way to the volatility of the organic solvent mixture.

Raman/photoluminescence spectroscopy was performed with a 532 nm excitation laser in air under ambient conditions on a droplet containing nanosheets in a SC-H_2O based dispersion before the transfer (Figure 3.3-14 C). As already explained further above, the PL/Raman ratio is a good candidate to track the quality of the sample. Here the initial ratio was ~ 8:1 confirming the high-quality of the sample. The PL consists of a single symmetric peak centered at about 613.5 nm (2498 cm^{-1} or 2.021 eV) with a small shoulder extended towards longer wavelengths in agreement with previous samples. The Raman peak of water is not observed due to the high WS_2 concentration used for the measurement.

3.3.4.2 Tracking Aggregation by Repeated Centrifugation

Evaluation of the obtained data from the second set of thin films described above emphasized the importance of systematic aggregate removal steps to improve the quality of WS_2 deposited by spin coating. It was found that aggregation occurred over relatively short time frames (< 2 hours). While these aggregates could be removed by centrifugation (1,000 *g*, 30 min) this step had to be performed immediately prior to deposition. Also, it was clear that the aggregation rate increased with the initial nanosheet concentration. In this section, it is investigated whether the nanosheets are stabilized by the adsorbed polymer after transferring nanosheets to a polymer-containing solvent. To test this, the same iterative centrifugation (5 steps at 1,000 *g*) was applied to nanosheet dispersions with different WS_2 concentrations and extinction spectra measured after each step.

All optical extinction spectra and the respective second derivatives of the A-exciton are displayed in the Appendix, Figures A6.12-6.13. In analogy to WS_2 transferred to IPA/THF in the absence of PVK, the concentration is reduced on repeated centrifugation (according to the optical intensity, Figure 3.3-1A). The second derivatives show a more significant difference across samples with different WS_2 concentration with the highest WS_2 concentration exhibiting a slight blue-shift, narrower line width compared to the lower concentrations (Figure A6.13-14). This is probably due to a different ratio of WS_2 and polymer in the surrounding. For non-specific interactions between stabilizer and nanosheet that we anticipate here, one would expect the adsorption/desorption equilibrium to be concentration-dependent. In this case, shifts and changes in lines width are likely due to solvatochromic effects stemming from the polymer (in addition to potentially different aggregation states of the nanosheets).

The most important information that can be extracted from the UVVis spectra in this context is the change in nanosheet concentration on repeated centrifugation which can be extracted from the optical density. When plotting the optical density at the A-exciton as function of centrifugation step (Figure 3.3-1B) the same trend is observed as in the samples in the absence of PVK (Chapter 3.3.3.2). This confirms that PVK as a stabilizer cannot prevent restacking of the nanosheets over time. In agreement with the data in IPA/THF in absence of PVK, at higher WS_2 concentration, more aggregation happened, resulting in a greater loss of WS_2 nanosheets from step to step which gives a steeper slope when the optical density plotted as a function of the centrifuge run. As before, we extract the slope from fitting this data to a linear function which we interpret as characteristic indirect measure for the aggregation rate. This is plotted as function of initial optical density of WS_2 in figure 3.3-1C showing a linear dependence. The data is compared to the reference system in IPA/THF in the absence of PVK. We find that the aggregation rate is even higher in the presence of PVK compared to the pure solvent mixture. This is very problematic because the dispersion is

even less stable when nanosheets are in the matrix of the polymer. This is surprising and we attribute this to the relatively poor solubility of PVK in polar solvents. Additional experiments are required to find a more suitable match of polymer and solvent. Nonetheless, the protocol established here can be applied in a straight forward manner to investigate this in future work. In this work, the unsuccessful stabilization through the PVK encouraged us to test a new idea to solve the problem with reaggregation occurring on transfer. This is described in Chapter 3.4.

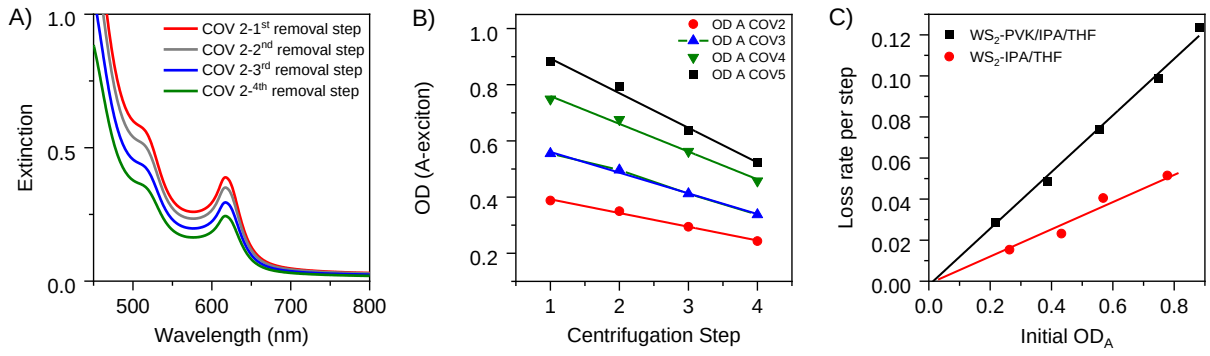

Figure 3.3-15: Impact of additional centrifugation on the optical response of WS_2 nanosheets transferred to IPA/THF in the presence of PVK. A) Comparison of the extinction spectra in the region of the A-exciton for the second lowest WS_2 concentration used after performing four subsequent centrifugation steps at 1000 *g* for 30 min. A reduction of the WS_2 concentration is discernible after each step. B) Plot of the optical density at the A-exciton as function of the centrifugation step. A linear decrease in nanosheet concentration is observed. The slope can be interpreted as indicator of the aggregation rate. C) Loss rate per step (i.e. slopes in panel B) as function of initial optical density at the A-exciton visualizing that aggregation is concentration dependent in comparison to the reference system in absence of PVK.

3.3.4.3 Characterization of Thin Films on Glass

Based on our recent obtained observations from the second set of thin films, higher coverages in thin films resulted in a loss of the WS_2 photoluminescence due to restacking of the sheets. While Chapter 3.3.4.2 revealed that aggregation of the sheets could not be prevented in dispersion by the addition of PVK, it is still possible that communication between the WS_2 monolayers is suppressed through the polymer layer. Such TMD-polymer composites are potentially interesting for applications exploiting the light emitting properties, such as light emitting diodes or field-effect transistors. While 2D materials have been widely investigated as in polymer composites for reinforcement, conductive fillers or as barrier enhancing agents,[5, 110-111] little attention has been given to understanding the optical properties in such composites. It has already been shown that PVA or PMMA can prevent communication between LPE WS_2 when embedded in a polymer

matrix.[45, 59] However, in the literature reports, the LPE TMD was embedded as guest, or filler in a polymer film. Here, in this work, we focus on the deposition of polymer-coated nanosheets, i.e. a significantly higher TMD:polymer ratio.

Thin films were prepared from the WS_2-PVK-IPA-THF dispersion immediately after centrifugation to remove aggregates using different WS_2 concentrations by spin coating as before. WS_2-PVK thin films were characterized by absorbance and Raman/photoluminescence spectroscopy (Figure 3.3-16). The non-resonant scattering background (> 650 nm) in the extinction spectra (Figure 3.3-16A) of the thin films is relatively low for all coverages, albeit higher than in the films produced in the absence of PVK. Unfortunately, the region of the polymer absorbance (300-350 nm) overlaps with a change in the filter during the measurement which can induce artifacts in the spectra. Therefore, it is not clear whether absorbance from PVK is still observed after deposition. However, clearly, it is lower relative to the WS_2 which suggests that nanosheets are preferentially deposited. Similar to the WS_2 deposition in the absence of PVK, the optical densities in thin films strongly depend on the WS_2 concentration in dispersion. It should be noted that, overall, the optical densities achieved in the films is lower for this set of films in the presence of PVK, but the optical density of the dispersion used was also lower due to stronger aggregation as discussed in Chapter 3.3.4.2.

Second derivatives of the A-exciton are extracted from extinction spectra (Figure 3.3-16B), like in the case of second set of thin films data. The A-exciton absorbance is not de-convoluted into the individual ML and few-layer peaks which are merged unlike in the dispersion where they could be well distinguished. Figure 3.3-16B shows that at the highest WS_2 coverage (COV5), the center of mass position is only slightly redshifted compared to lower coverages (COV2). This is in contrast to the films produced in the absence of PVK, where a stronger difference was observed. This is indicative that communication of restacked sheets is indeed prevented.

This can be best confirmed by the Raman/PL spectra of the WS_2-PVK thin films with systematically varied nanosheets coverages shown in Figure 3.3-16C. The signal to noise ratio in the spectra is lower than for the films produced in the absence of PVK since laser-induced damage was observed so that the laser power had to be reduced by a factor of 10. The observed PL peaks in all films with varying coverage are identical with similar PL/Raman ratio and linewidth and with only minor shift or broadening compared to the initial dispersion in aqueous SC (Figure 3.3-14). It should be noted that the PL/Raman ratio in the film is reduced compared to the dispersion by ~50%. While this could be an effect from the deposition, we mainly attribute this to the reaggregation occurring in dispersion rather than on deposition. If reaggreation on deposition was

responsible, we would expect films with higher coverage to have a reduced PL/Raman ratio. Overall, the optical properties of WS_2 are not severely affected by PVK and the homogenous dielectric environment from the polymer retains narrow linewidth PL, as nanosheets are isolated from each other by a polymer matrix which shields the environment and prevents restacking. Therefore, the optical properties of these films are mostly preserved.

Figure 3.3-16: Optical characterization of thin films produced from WS_2-PVK-IPA-THF by spin coating. A) Optical extinction spectra of WS_2 deposited on glass using different initial WS_2 concentrations in the PVK/IPA/THF-based dispersions. There is an increase of the film optical density with increasing OD of the dispersion. Inset: Zoom-in at the A-exciton. B) Second derivative of the A-exciton region from films with two different coverages. The splitting between ML and FL cannot be resolved C) Photoluminescence of thin films measured by Raman spectroscopy normalized to the 2LA(M) Raman mode of WS_2. PL remains

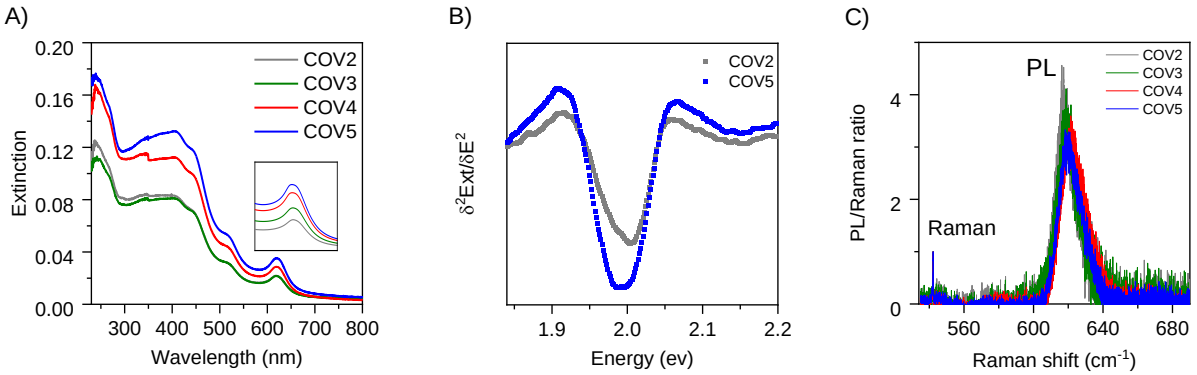

unaltered in all samples suggesting a reduced communication between restacked nanosheets through the polymer.

3.3.5 Conclusion

In summary, this section described significant progress towards making thin films of WS_2 through spin coating with homogeneous, tunable coverage and minimal nanosheet restacking in optimized samples which resulted in the observation of narrow linewidth photoluminescence from monolayers.

While preliminary experiments to optimize the spin coating conditions showed that homogeneous deposition is achievable by spin coating WS_2 transferred from aqueous sodium cholate to a mixture of IPA/THF (8:1), nanosheet aggregation was found to be a major obstacle. It was found that aggregation occurred after the transfer of size-selected WS_2 to the organic solvent mixture relatively quickly (< 1-2h) and that the aggregation rate scales with the nanosheet concentration. Centrifugation at 1000 *g* for 30 min was found sufficient to remove the aggregates, but preparation of thin films has to be carried out immediately after the centrifugation. These aspects clearly limit the applicability of the deposition method.

In spite of this, films with varying WS_2 coverage were fabricated by using WS_2 dispersions with different concentrations and the optical properties of WS_2 in the films assessed. With an optimized coverage (dense packing with minimal overlap of the sheets), ~75% of the monolayer photoluminescence was retained in comparison to the initial dispersion. The highest achievable PL/Raman ratio on glass was ~10. The PL/Raman ratio was decreased when increasing the WS_2 coverage due to nanosheet restacking and clear shifts in the PL were observed depending on the substrate as confirmed by deposition on glass coated with different polymers. Due to the issue with aggregation after transferring the nanosheets to the organic solvent, it was assessed whether the addition of a polymer to the organic solvent mixture during the transfer could prevent nanosheet aggregation. For the chosen system (PVK ind IPA/THF), this was not the case, but the presence of the polymer decoupled the nanosheets in the thin film resulting in a retention of the PL irrespective of the coverage.

While the deposition by spin coating has severe restrictions in its wider applicability due to tedious optimization, the films that can be produced in this way are suitable for fundamental studies, e.g. investigating the PL response as function of substrate. Further, a procedure was established based on repeated centrifugation that can be used to reliably track aggregation. This methodology is applicable to other systems and can be used to screen suitable solvent or solvent/additive mixtures. Finally, it was demonstrated that the communication between nanosheets can be successfully suppressed through the presence of a polymer coating which could be of interest for applications in light emitting devices in future work.

3.4 A New Route to Make WS_2 -Polymer Composites Through Micelle Swelling

3.4.1 Introduction

LPE is an attractive method to produce 2D nanosheets, as it can be applied to a whole host of layered structures and gives access to high-quality nanosheet dispersions in the liquid phase. Main issues such as low monolayer contents and sample polydispersity were addressed in the past years by improved post exfoliation size selection. It was shown that exfoliation and stabilization in aqueous surfactant yields dispersions with higher monolayer contents than accessible in solvents.[109] However, for some applications, such as the preparation of polymer composites, the exfoliated materials need to be compatible with organic solvents.[5, 111] When transferring from aqueous to organic media , restacking of nanosheets occurs and leads to the loss of their monolayer characteristics such as photoluminescence of single-layered TMDs. By using WS_2 as a model substance, it was shown in Chapter 3.3 that the rate of aggregation depends on the nanosheet concentration. While it is possible to remove aggregates by mild centrifugation and produce thin films with monolayer properties of the WS_2 retained, this procedure is only poorly reproducible.

In this Chapter, a new route is introduced to prevent aggregation on transfer that simplifies the preparation of thin films from liquid phase exfoliated WS_2 in a polymer matrix on glass substrates with monolayer properties of the nanosheets retained. The secret is to add a polymer that is not water-soluble (such as polyvinyl carbazole, PVK) to the aqueous WS_2 mixture prior to sonication. The sonic energy also "exfoliates" the polymer, *i.e.* it finely distributes the polymer in the aqueous surfactant medium. Due to the hydrophobic effect, the polymer adsorbs on the most hydrophobic area in the aqueous dispersion which is the interface between surfactant and nanosheet.[112-114] This is schematically illustrated in Figure 3.4.-1. The concept is conceptually similar to micelle swelling using liquid hydrophobic compounds (*e.g.* oils[115]) or gases[116] with the exception that a polymer is used that is allowed to arrange in the dynamic situation during sonication.

With this method, it is anticipated that a densely packed thin layer of the polymer is formed on the WS_2 nanosheets. As we will show, this facilitates transfer to organic solvents without aggregation occurring. When preparing nanosheet based thin films in this way, the polymer coverage also prevents communication between the sheets after deposition so that no loss of monolayer photoluminescence compared to the dispersion is observed. This new route can be applied for the range of polymers to produce films of outstanding optical quality which are interesting for integration into optoelectronic devices.

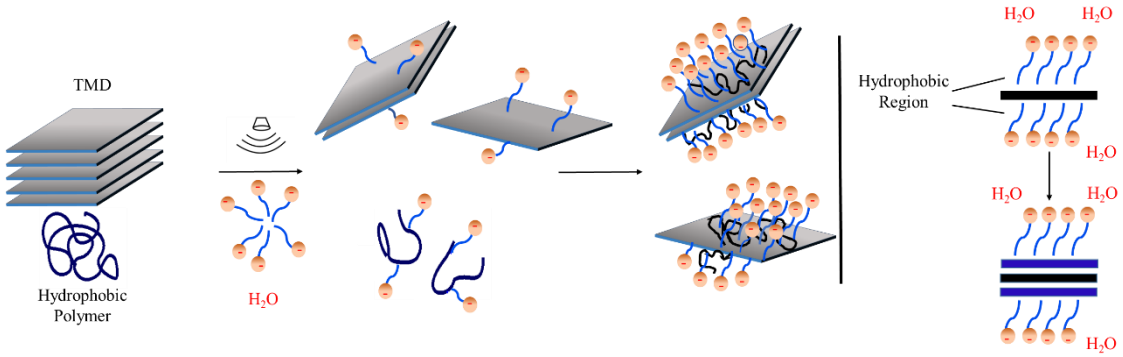

Figure 3.4-1: Schematic of the new route to fabricate WS_2-polymer composites by a procedure similar to the micelle swelling technique. Initially, a water insoluble polymer and the TMD are sonicated in the aqueous surfactant solution. In the dynamic situation of sonication, the polymer is also partially dispersed by the surfactant and can arrange in the most hydrophobic position in the vial which is the interface between 2D material and surfactant.

3.4.2 Sample Preparation

Sample preparation was performed according to the standard protocol described in the methods section. In brief, WS_2 powder (30 gL^{-1}) was immersed in an aqueous solution of sodium cholate (8 gL^{-1}). In addition, the non-water-soluble polymers is added to this mixture prior to sonication with a concentration of 0.01 gL^{-1}. PVK was used as the model polymer, but other non-water soluble polymers were also tested. The WS_2 exfoliation protocol is the same as described in Chapter 5 using a two-step sonication procedure. The same concentration of polymer (0.01 gL^{-1}) is added during both short and long tip sonication processes, respectively. To select nanosheets by size, the LCC method is used. Specifically, unexfoliated WS_2 and polymer not associated with the nanosheets were removed by centrifugation at 400 *g*. The supernatant was exposed to further centrifugation at 1,000 *g*. Next, the sediment was collected in water at reduced volume (5-10 mL), while the supernatant was centrifuged at 5,000 g. Again, the sediment was collected and the supernatant subjected to centrifugation at higher speeds at either 10,000 or 30,000 *g*. The final supernatant was discarded. Note that this procedure not only serves the purpose of size selection of WS_2, but also ensures that all non-soluble material is discarded (as sediment at low centrifugal acceleration) and any potentially "free polymer", *i.e.* polymer not associated with the WS_2 surface, is removed as supernatant at high centrifugal acceleration.

3.4.3 Characterization of Dispersions and Thin Films Using WS_2-PVK as Model System

First, the size-selected WS_2 dispersions prepared by the micelle swelling-type technique with PVK added during sonication were characterized in aqueous sodium cholate solution by extinction and Raman/PL spectroscopy. In figure 3.4-2, extinction spectra of three different sizes of exfoliated WS_2-PVK nanosheets denoted as large (1-5k *g*), medium (5-10k *g*) and small (10-30k *g*) are shown compared to the standard WS_2 dispersion (reference-exfoliated WS_2 nanosheets in the absence of polymer). Interestingly. The WS_2 concentration is higher when sonication is performed in the presence of PVK in all cases. The presence of PVK is well discernible in the UV-Vis as additional peaks in the spectral region of 300-350 nm. This confirms the presence of PVK in the sample. Importantly, much PVK relative to WS_2 is observed in the sample containing the smaller and thinner WS_2 nanosheets due to a higher surface area of WS_2. This strongly suggests the polymer is associated with the nanosheet surface.

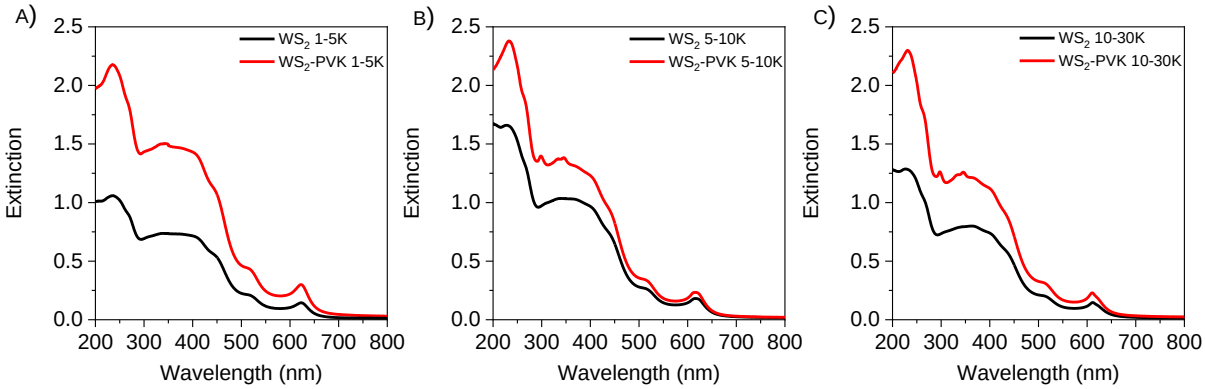

Figure 3.4-2: Optical extinction spectra of three size of WS_2 nanosheets in aqueous sodium cholate exfoliated in the presence of PVK compared to the reference sample (sample with no polymer) processed under otherwise identical conditions. A) 1-5k *g*, B) 5-10k *g*, C) 10-30k *g*.

Raman/PL spectroscopy was performed on exfoliated WS_2-PVK samples with 532 nm excitation wavelength. To prevent sample heating, the laser power is kept as low as possible (1% laser power, <10 µW). The data is shown in figure 3.4-3 for three different fractions of exfoliated WS_2 in the presence of PVK compared to the reference sample (standard dispersion in aqueous sodium cholate). A significant shift corresponding to the dominant WS_2 Raman mode (2LA(M)) located at ~355 cm^{-1} is not observed. As already discussed, the Raman mode can be observed in all WS_2 (from bulk to monolayer WS_2) but PL only stems from WS_2 monolayers (with direct bandgap). The fluorescence peak is located at ~2470 cm^{-1} (equivalent to 612.5 nm) in all samples, both in the absence and presence of PVK. Importantly, the PL/Raman ratio is even higher in all fractions when PVK was added during sonication. Taken together with the findings of higher concentration

based on extinction spectroscopy, it can be concluded that exfoliation is more efficient when PVK is added. Further, PL remains symmetric and is narrow and comparable to the PL peaks of the reference sample (no broadening- not affected by heating or etc). This confirms that optical properties of WS2 are not affected by the presence of the polymer and that high quality samples can be produced. Note that the PL/Raman ratio in the WS_2-PVK 10-30k *g* is the highest reported for LPE WS*2* to date.

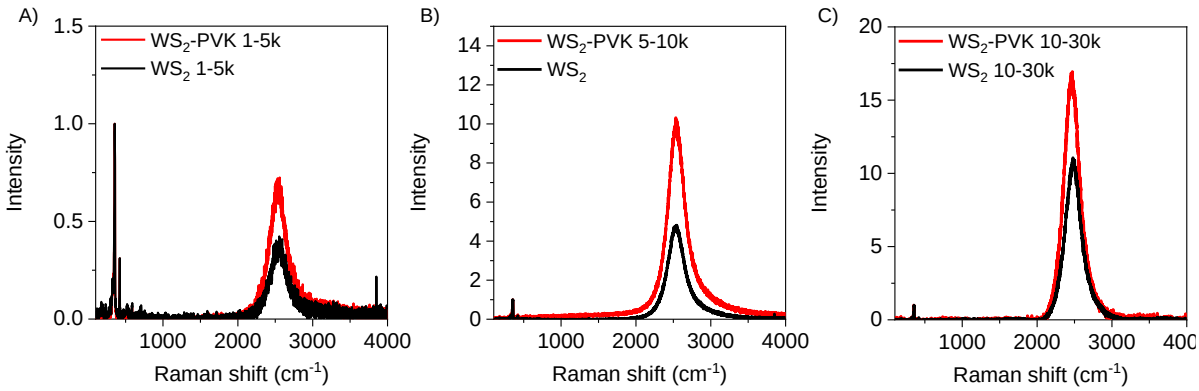

Figure 3.4-3: Raman/PL spectra (532 nm excitation) of three size of WS_2 nanosheets in aqueous sodium cholate exfoliated in the presence of PVK compared to the reference sample (sample with no polymer) processed under otherwise identical conditions. A) 1-5k *g*, B) 5-10k *g*, C) 10-30k *g*.

To get a deeper insight into the advantage of this new route and to test if our new liquid-phase exfoliated WS_2 in aqueous sodium cholate in the presence of PVK is able to overcome the aggregation challenge, the fabricated 5-10k *g* dispersion (after exfoliation and size selection of WS_2-PVK) was transferred to a mixture of IPA/THF medium following the established procedure. Subsequently, three additional low-speed centrifugation runs (1,000 *g*, 30 min) were applied on the polymer-based sample and extinction spectra measured to investigate how much material is lost after each run. The protocol is already explained in the previous sub-chapters.

The extinction spectra are shown in figure 3.4-4A. In contrast to WS_2 exfoliated and size-selected in aqueous sodium cholate in the absence of PVK or WS_2 transferred to a mixture of PVK/IPA/THF, the optical density of this sample is not decreased by the subsequent centrifugation and hence there was no sedimentation. This observation confirms a significant suppression of aggregation likely because nanosheets are homogeneously covered by the polymer on the surface. Also, the second derivatives of A-exciton are extracted from the extinction spectra (Figure 3.4-4B). The splitting of the A-exciton in ML and FL is clearly observed. There is no change in energy and width of nor ML peaks neither FL peaks after performing multiple centrifugation runs and the ratio of the two components remains identical. This also confirms that no aggregation occurs after transferring WS_2-PVK to IPA/THF.

To further confirm that the polymer is associated with the surface of the TMD, the LPE WS_2-PVK dispersion (5-10k *g*) in IPA/THF (where the polymer is at least slightly soluble) was subjected to high speed centrifugation at 30k *g* to force sedimentation of WS_2. Then, the sediment was redispersed in fresh solvent and extinction spectra of supernatant and sediment measured. As it is shown in figure 3.4-4C, the PVK signature is observed in the redispersed sediment and there is no sign of PVK in the collected supernatant. This confirms that PVK remains on the surface of WS_2 after transfer to IPA/THF.

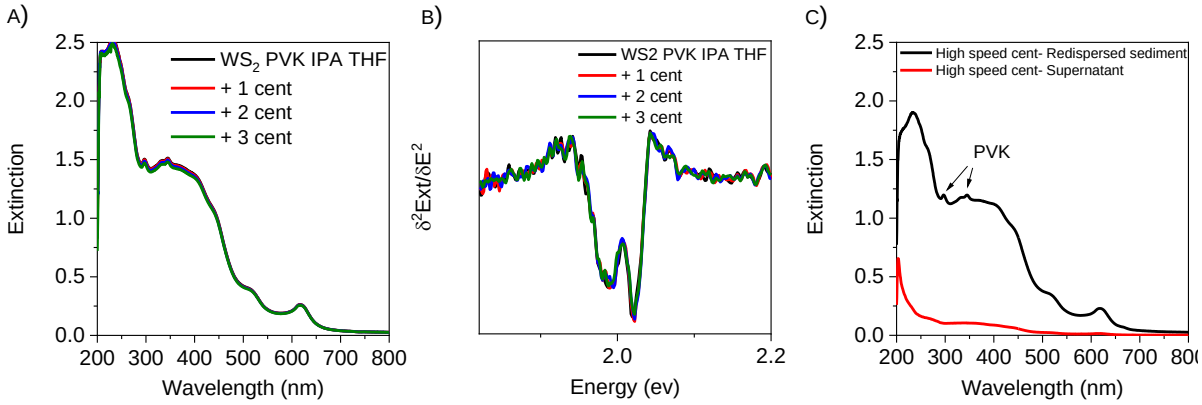

Figure 3.4-4: Impact of repeated centrifugation (1000 *g*, 30 min) on WS_2-PVK (5-10k *g*) produced by the micelle swelling-type technique transferred to IPA/THF. A) Optical extinction spectra showing no change in optical density, i.e. no sedimentation due to aggregation. B) Second derivative of the A-exciton region which is extracted from the respective optical extinction spectra after smoothing. C) Extinction spectra of both sediment and supernatant after subjecting WS2-PVK to high speed centrifugation at 30k *g*. The signature of PVK is only observed in the redispersed sediment (black) and not the supernatant (red). This suggests that PVK seems to remain on the WS_2 nanosheets surface.

The data confirms that the polymer tends to stick on the TMD surface which results in no pronounced aggregation after transferred to the IPA/THF mixture due to shielding from the solvent. These observations encouraged us to use a high quality exfoliated WS_2 nanosheet dispersion produced in the presence of polymer by the micelle swelling-type technique to investigate the possibility of fabricating WS_2-polymer thin films with promising and preserved optical properties. Figure 3.4-5 shows results with respect to the characterization of a spin-coated WS_2-PVK thin films. The film was produced in analogy to the method described in the previous section using an dispersion with optical density at 240 nm of 2.3. The obtained results confirm that the new polymer route can be used to produce films of outstanding optical quality. The extinction spectra of the WS_2-PVK thin film (Figure 3.4-5A) shows a spectral profile similar to the dispersion used, albeit with some background at > 650 nm. The optical density is similar to the SC-based reference sample transferred to IPA//THF and spin-coated under the same conditions. Importantly, the PVK signature is still observed in the extinction spectra of the thin film which affirms the

presence of polymer on the WS_2 surface. The Raman/PL spectrum with 532 nm excitation is shown in Figure 3.4-5B. The PL/Raman ratio as quality indicator breaks any record and is roughly ~ 23. This is attributed to polymer on the WS_2 surface which prevented nanosheets restacking, as well as interaction with the glass substrate and therefore the PL/Raman ratio is comparable to the dispersion. Further, as indicated in the previous section, there are no chemical doping effects with PVK and thus the PL linewidth remains narrow and the PL is symmetric with no sign of trion emission or inhomogeneous broadening. Overall, the optical response of WS_2 is not affected by PVK. Finally, the optical microscope image (Figure 3.4-5C) shows a homogeneous film with no visible aggregates. These results confirm that the micelle swelling type route is an interesting method to make WS_2-polymer composite films with promising optical quality.

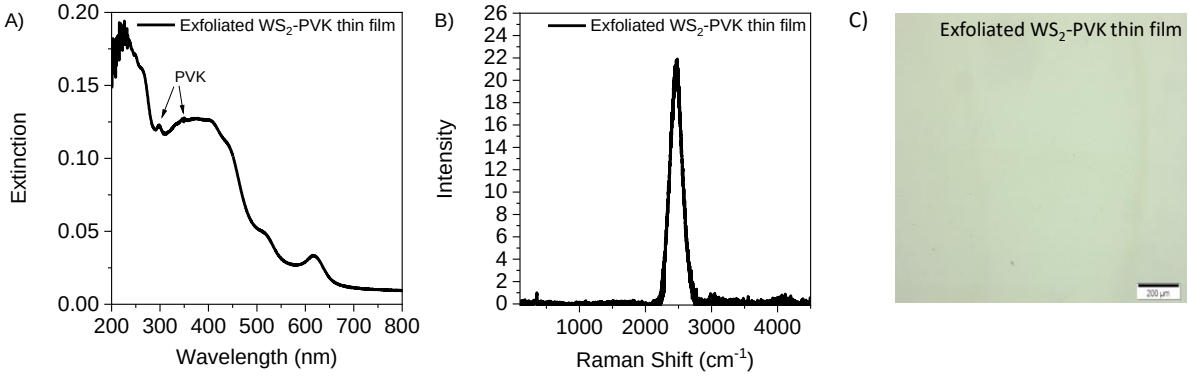

Figure 3.4-5: Characterization of a thin film on glass produced by spin coating using the WS_2-PVK in IPA/THF produced by the micelle swelling-type technique. A) Extinction spectrum. B) Raman spectrum (532 nm excitation). The PL/Raman ratio of the thin film fabricated with the new route is comparable to the dispersion in SC with narrow PL linewidth. C) Optical microscope image of the WS_2-PVK thin showing a homogeneous film with no visible aggregates.

3.4.4 Assessing the Applicability to Other TMD-Polymer Systems

To assess the applicability of this new route to make WS_2-Polymer hybrids, it is applied to other systems which include WS2 in the presence of other polymers such as polydioctylfluorene (PFO) and polymethylmethacrylat (PMMA) or other TMDs such as $MoSe_2$.

3.4.4.1 Different Polymer Systems

Figure 3.4-6 shows observations using different polymer systems applied in the micelle swelling type co-exfoliation route. WS_2 exfoliation is done by tip sonication in aqueous sodium cholate in the presence of PMMA and PFO, respectively, and then both samples are size selected and the monolayer-richest fraction (10-30k *g*) characterized. The extinction spectra (Figure 3.4-6A,D)

show signatures of PMMA (< 290 nm) and PFO (300-500 nm), respectively. The optical density of WS_2 is similar to the WS_2-PVK system, i.e. higher than the SC reference system in the absence of polymer. The WS_2-PFO spectrum shows an elevated non-resonant scattering background at > 650 nm. This is likely due to the presence of larger particles in the form of aggregates. It should be noted it could mean that the nanosheets are laterally larger. In future work, it will be important to assess this with AFM statistics. The smoothed second derivative of the A-exciton region extracted from the optical extinction spectra (Figure 3.4-6B,E) showed very nice splitting in both cases. The contribution from ML FL WS_2 are perfectly separated with narrow linewidth. This confirms that this new route prevents communication between the WS_2 even if aggregates were present which is likely the case in the WS_2-PFO sample.

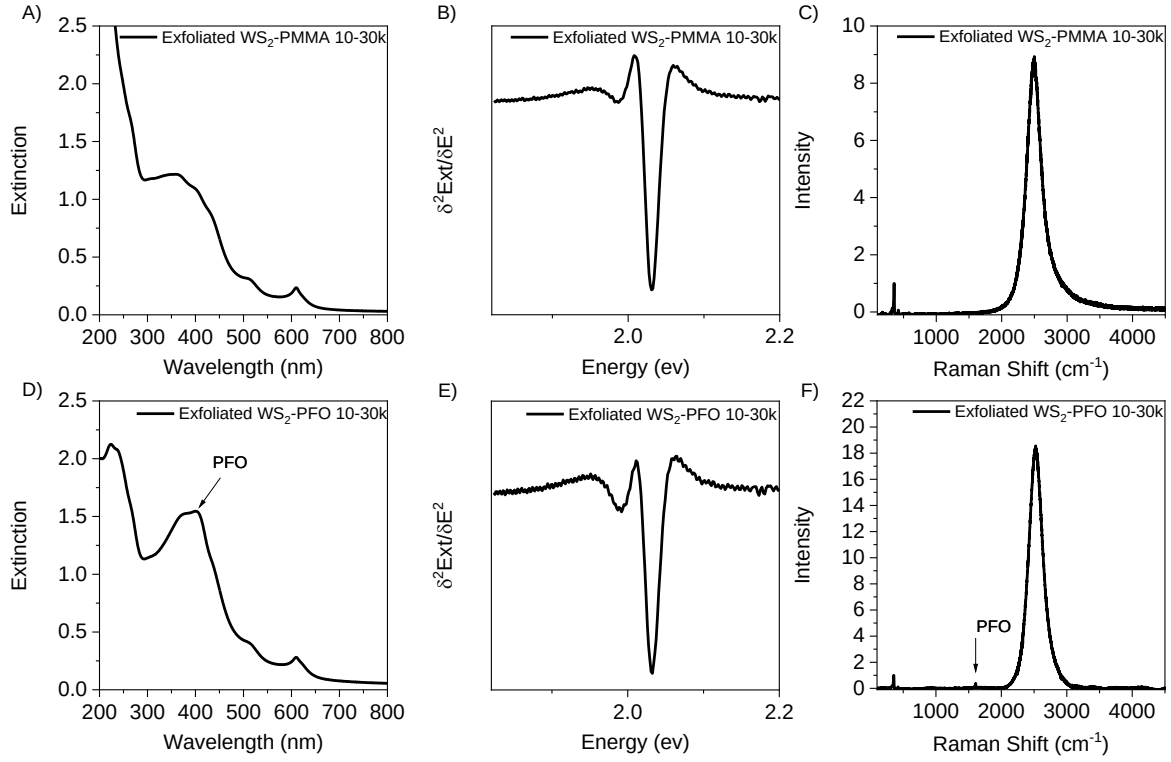

Figure 3.4-6: Applying the micelle swelling type exfoliation technique to different polymer systems. A, D) Optical extinction spectra of exfoliated WS_2 in the presence of PMMA and PFO respectively. WS_2 nanosheets are trapped in a range of 10-30k *g* in both cases (smallest/thinnest size of nanosheets). B, E) Smoothed second derivatives of the A-exciton correspond to the exfoliated WS_2 in the presence of PMMA and PFO, respectively. The peak is composed of two components: ML (a peak at ~ 611 nm or 2.033 eV) and FL (a shoulder at ~ 622 nm or 1.99 eV). C, F) Raman/PL of exfoliated WS_2 in the presence of PMMA and PFO respectively. The PL line width is narrow and symmetric. Therefore, the monolayer properties are maintained in both cases.

The exfoliated samples are also characterized by Raman/PL spectroscopy to better understand if the surrounding polymers are efficient enough to preserve monolayer properties by shielding the nanosheets and to test whether any chemical doping effects are discerned. Figure 3.4-6C, F shows narrow linewidth, symmetric photoluminescence of the A-exciton which is retained in both samples. In spite of similar ML contents according to the second derivative of the extinction spectra, the PL/Raman ratios vary. For WS_2-PVK, a PL/Raman ratio of ~17 was observed, while it is ~9 in WS_2-PMMA and ~18 in WS_2-PFO. Future work will be required to understand the origin of this behavior, e.g. an assessment of the lateral size of the monolayers which could be at the origin of this variation since edges are known to quench the PL.[65] An alternative explanation could be that the polymer coating is more or less homogeneous, since inhomogeneities often reduce the PL quantum yield.[29] To understand this, low temperature PL measurements would be of interest.

3.4.4.2 Different TMD Systems

The new route was also applied to other TMD systems. This is important, as it could be envisaged that a polymer layer on the surface of the 2D material shields the nanosheets from the environment which could also prevent degradation in the case of materials prone to degradation.

Figures 3.4-7A,B show, optical extinction spectra of molybdenum diselenide ($MoSe_2$, 10-30k *g*) exfoliated in the presence of PVK and PFO respectively. The absorption signature of the polymers are well discernible in both cases confirming the presence of polymer. When using PFO instead of PVK, there is a relatively intense/large PFO signal which appears more intense than in the WS_2 dispersions. However, the oscillator strength of the polymers and TMDs are different so that a quantification from UV-Vis spectra is hardly achievable. Also, a scattering background is discernible in the extinction spectra of $MoSe_2$-PFO. This could be due to polymer aggregates in the water-based dispersion, or indeed polymer-$MoSe_2$ aggregates. Future work will be required to understand which systems remain colloidally stable. Nonetheless the data shows that this new route is applicable to other TMDs such as $MoSe_2$.

To investigate whether the optical properties of the $MoSe_2$ monolayer are preserved after exfoliating in the presence of polymers, both samples are characterized by Raman/PL spectroscopy with an excitation wavelength at 633 nm, where the $MoSe_2$ PL is expected at ~3200 cm^{-1} corresponding to ~790 nm (1.57 eV). Figures 3.4-7C,D show Raman/PL of $MoSe_2$ exfoliated in the presence of PVK and PFO with excellent PL/Raman ratios of 20-25 and 70-75 respectively. In spite of the scattering background in $MoSe_2$-PFO, the PL is very intense with a factor of 3

improvement which is definitely interesting and promising, although further work is required for an understanding.

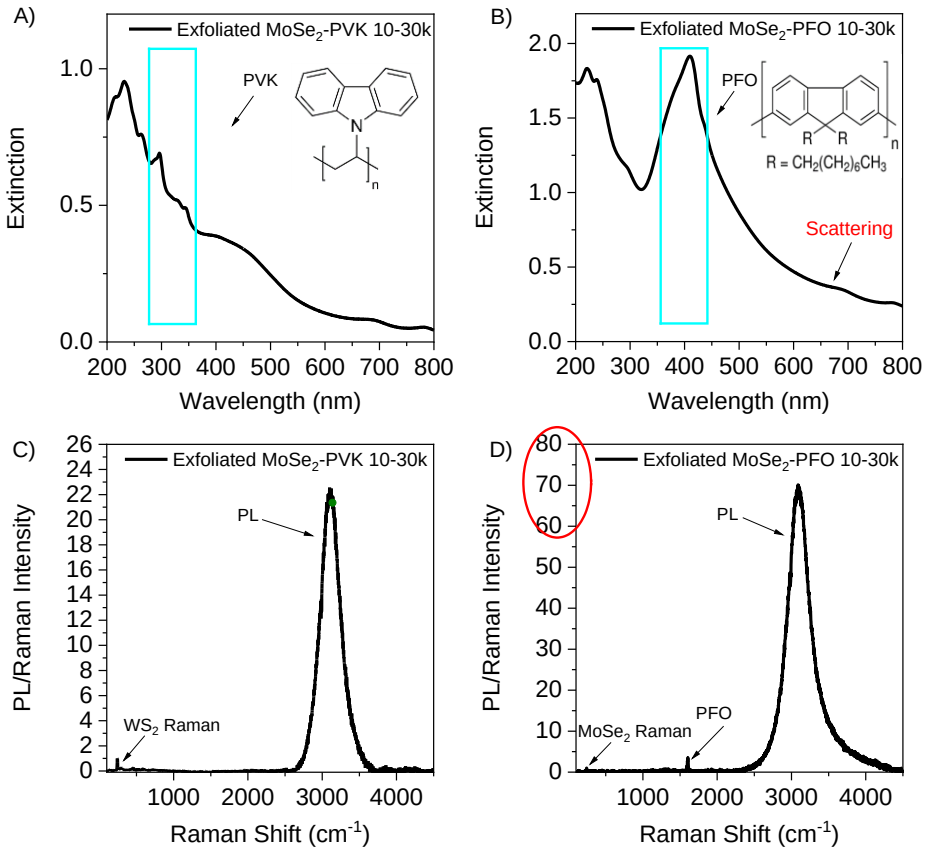

Figure 3.4-7: A, B) optical extinction spectra of $MoSe_2$-PVK and $MoSe_2$-PFO produced by the micelle swelling type technique in aqueous sodium cholate. In both samples, the nanosheets are trapped in a range of 10-30k *g*. The signatures from both polymers are observed as indicated by the blue rectangle frames in the extinction spectra. C, D) Raman/PL spectra of the dispersions. The PL linewidth is narrow in both samples and for exfoliated $MoSe_2$-PFO, the PL intensity is improved by a factor of 3.

Since this effect of improved PL in PFO was not seen for WS_2 before, it is very hard to rationalize. Therefore, it directed us to test the reproducibility in a co-exfoliation experiment with WS_2. For this experiment, two different TMD powders (WS_2 and $MoSe_2$) are mixed and then exfoliated in the presence of the polymer PFO in aqueous sodium cholate (notice: different concentration of TMDs are used as following 30 gL^{-1} and 20 gL^{-1} for WS_2 and $MoSe_2$ respectively). Figure 3.4-8A,B shows the selection of extinction spectra and relevant second derivatives of the A-exciton for three different sizes of nanosheets in the co-exfoliated samples. These spectra are a mixture of WS_2 and $MoSe_2$ as expected. It is clear that the scattering background in $MoSe_2$-WS_2-PFO is lower than the $MoSe_2$-PFO sample which was shown in Figure 3.4-7. Even though the concentration of the two TMD powder are different, the WS_2 signature is more intense than expected. For example, the $MoSe_2$ A-exciton is ~ five times lower in intensity than the WS_2 A-exciton, while the initial

concentration is only 1.5 times higher. The extinction coefficients of WS_2 and $MoSe_2$ at the A-exciton differ by a factor of 2.[68] Based on this, it can be concluded that WS_2 is exfoliated with a ~1.6 times higher yield than MoSe2 in this system.

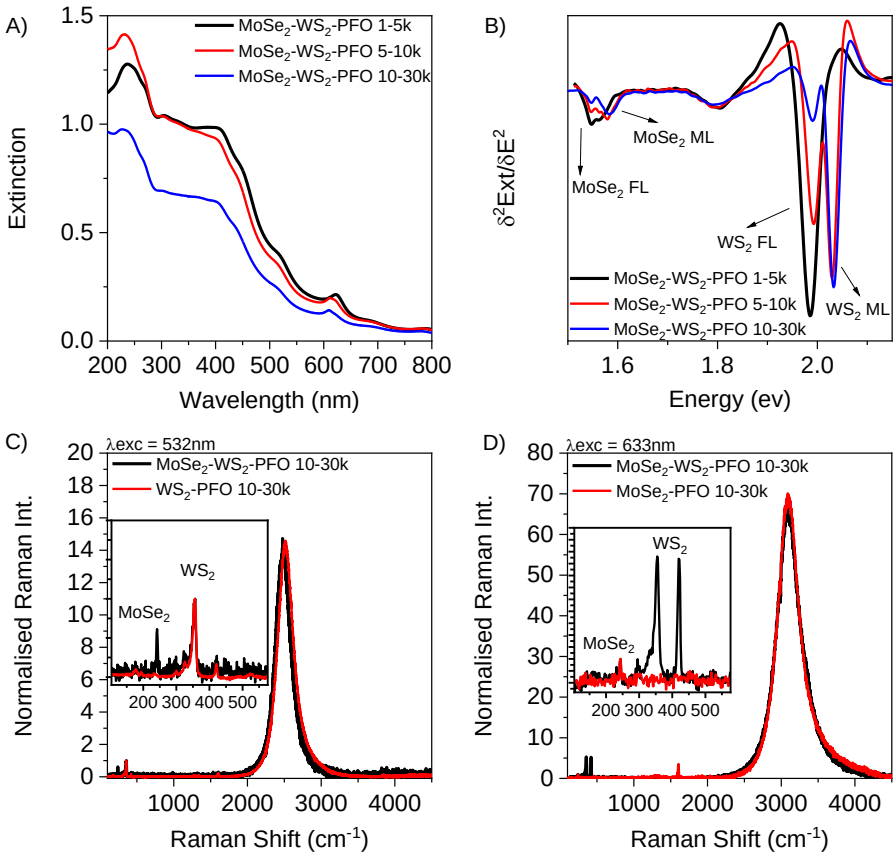

Figure 3.4-8: A) Selection of extinction spectra of co-exfoliated $MoSe_2$-WS_2 in presence of PFO. Three sizes of nanosheets are trapped in the range of 1-5 k*g*, 5-10 k*g* and 10-30 k*g* respectively. B) second derivative of A-exciton extracted from optical extinction spectra. The concentration of WS_2 and $MoSe_2$ are different. C) Raman/PL spectra of co-exfoliated $MoSe_2$-WS_2-PFO and WS_2-PFO samples are observed and compared. The excitation wavelength is considered at 532nm to detect WS_2 PL. Inset: Raman modes of $MoSe_2$ and WS_2. D) Raman/PL spectra of co-exfoliated $MoSe_2$-WS_2-PFO and $MoSe_2$-PFO samples are observed and compared. The excitation wavelength is considered at 633nm to detect $MoSe_2$ PL. Inset: Raman modes of $MoSe_2$ and WS_2. In comparison with the $MoSe_2$-PVK sample, the $MoSe_2$ PL is hugely enhanced (3.5x compared to the PVK sample).

The optical properties of the monolayers were investigated by performing Raman/PL spectroscopy. Two different excitation wavelengths were used due to the two different TMDs: The PL of WS_2 can be observed with 532nm and the PL of $MoSe_2$ with 633nm as excitation wavelength. Figures 3.4-7C,D show the spectra of the co-exfoliated WS_2/$MoSe_2$ 10-30k *g* dispersion (black traces) in comparison to the samples, where WS_2 and $MoSe_2$ were exfoliated separately and processed under otherwise identical conditions (red traces). The PL/Raman ratios

obtained from the co-exfoliated mixture are perfectly comparable with the ratios of WS_2-PFO and $MoSe_2$-PFO samples. Thus, the reproducibility of the exfoliation route is evidenced and the enhancement of $MoSe_2$ PL using PFO (3.5 times compared to PVK) is confirmed. While future work will be required to understand details, it is clear that the new route to make TMD-polymer hybrids is applicable to a range of TMDs and organic polymers and promising to produce LPE TMDs with superior optical properties.

3.**4**.5 Conclusion

In this section a new route to make TMD-polymer hybrids was presented. While previous work (Chapter 3.3) showed that the addition of polymers during transfer of WS_2 from aqueous surfactant to organic solvent could not prevent nanosheet aggregation, this issue was successfully tackled here. The principle is similar to the micelle swelling technique and relies on adding non-water soluble polymers to the aqueous TMD surfactant mixture prior to sonication. The sonication will also partly solubilize/disperse the polymer and in the dynamic scenario of sonication, it can rearrange to find the most hydrophobic area which is the interface between surfactant and 2D material. Thus, the polymer will be forced on the 2D material surface.

The route was shown to be applicable to different TMDs and polymer systems. Importantly, it was demonstrated that nanosheet aggregation can be successfully prevented when transferring to organic solvents (IPA/THF) which resulted in the demonstration of thin films with superior optical properties using WS_2-PVK as model system. The presence of the polymer in the thin film was confirmed by extinction spectroscopy which showed a similar signature as the dispersion unlike the films produced from WS_2 that was transferred to a mixture of PVK/IPA/THF. This clearly shows that polymer is associated with the nanosheet surface. The adsorbed polymer successfully shielded the nanosheets in the thin film resulting in narrow linewidth PL with a PL/Raman ratio of 23 in the thin film. The preliminary investigations on other polymers and TMDs revealed that PL can be further enhanced in some systems. While this can currently not be rationalized, the route is certainly promising.

4 General Conclusion and Outlook

In In the past years, liquid phase exfoliation has become well-known as a versatile top-down technique to produce 2D nanosheets. A whole host of layered structures can be exfoliated *via* this method and subsequently size-selected. Typically intrinsic properties are retained, for example, in the case of TMDs, the semiconducting 2H-polytype is obtained with characteristic narrow linewidth A-exciton fluorescence for monolayers originating from the direct transition at the K-point in the Brillouin zone. Due to the 2D nature, excitonic transitions are extremely sensitive to the environment and this is potentially useful to track surrounding solvents, molecules, chemical doping etc.

This thesis significantly added to the understanding in which way the A-exciton in absorbance and fluorescence responds to the environment using WS_2 as model substance. To achieve this, it was key to produce samples of high optical quality, for example with significant monolayer contents and narrow linewidth PL. While established LPE and size selection were used, minor modifications in the protocol (described in Chapter 5) and careful decanting in the cascade centrifugation resulted in a sequential improvement in sample quality from batch to batch, as illustrated by the PL/Raman spectra in Figure 4.1.

Note that the general exfoliation and size selection of the first batches was similar, but the maximum PL/Raman ratio was below 3. It is likely that sample heating during sonication and poor decanting in the size selection procedure were responsible for this. To first identify in which way the A-exciton responds to the environment, size-selected WS_2 dispersions were fabricated and a protocol elaborated to transfer the same dispersion into a range of solvent/additive system, most of them being aqueous surfactant or polymer systems (Chapter 4.1).

Since the optical response is well known to be sensitive to the size/thickness of the sheets, this transfer protocol was crucial to retain the same dimensions in each sample and only vary the environment. It was found that the A-exciton in absorbance shows characteristic shifts and broadening of the monolayer component in different environments.

Thinner nanosheets were more affected than thicker nanosheets which resulted not only in different A-exciton monolayer energies, but also different exponents relating the A-exciton energy to the layer number. Empirically, it was found that these two quantities scale linearly with each other across all systems investigated. This was an important finding which allowed to derive an

empirical expression for generalized thickness metrics for LPE WS_2 irrespective of the environment.

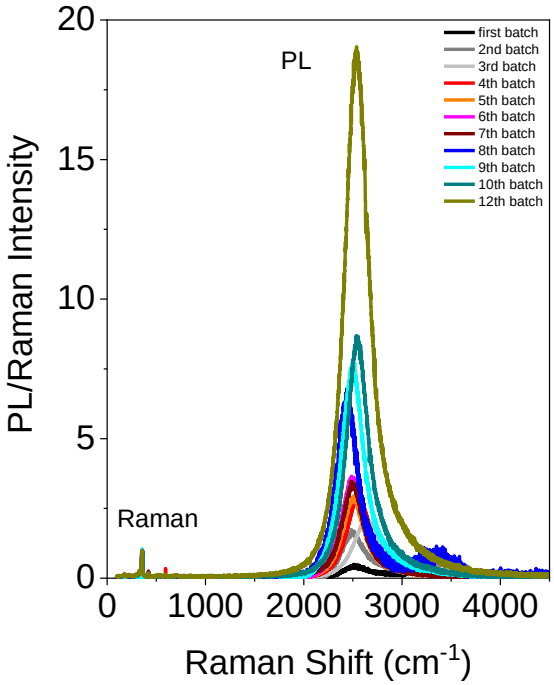

Figure 4-1: Schematic of progression in improving optical quality of WS_2 dispersion fabricated by LPE protocol and optimized LPE protocol. Sample number 1 to 10 are fabricated with the general LPE method and sample number 12 is fabricated after optimization of this method. It is clear the optical quality of the sample is perfectly improved and increased. Reproducibility of this optimized method is examined/proved and all samples in this thesis are prepared by this protocol.

Differences in the chemical environment were also reflected in the A-exciton PL. In this case, it could be observed that some stabilizers chemically dope the nanosheets resulting in enhanced trion and reduced exciton emission. Thus, it was not clear whether the changes in the A-exciton absorbance were related to chemical doping or dielectric screening effects.

This question was addressed in the second section (Chapter 4.2), where transfer to pure solvents was investigated for two reasons: i) only non-specific interactions are expected with little chemical doping; ii) the physical parameters of the environment (refractive index, dielectric constant) are known. Transfer to solvents is more challenging due to issues with aggregation, but can in principle be achieved in a similar way.

The linear scaling of monolayer A-exciton with the exponent relating exciton energy to layer number was confirmed and quantitatively agreed with the additive systems. Since PL indeed confirmed that, with few exceptions, only little chemical doping occurs in the solvents, this finding can thus be attributed to dielectric screening of the excitons irrespective of doping. In addition, it was found that the shift in monolayer A-exciton energy linearly scales with the Onsager polarity function of the solvent (related to the refractive index), while the changes in width linearly scale with the dielectric constant of the solvent.

It is thus clear, that the frequency dependence of the dielectric environment plays an important role and cannot be neglected- a scenario referred to as dynamic screening of exciton. Overall, the A-exciton response in absorbance is governed by dielectric screening, while the PL response is governed by chemical doping. With the fundamentals understood, it will be interesting to study more exotic molecules, e.g. strong acceptors or donors, dyes etc. to produce inorganic/organic hybrids where different physical phenomena can potentially occur (e.g. collective states).

A side-product of the solvent study was that it became clear that more solvents are accessible when transferring high quality samples into them than when using them as medium for the exfoliation. While aggregation was observed, monolayer PL was still detected in most cases. This was the foundation for the controlled deposition of LPE WS_2 with the aim to produce thin films with dense coverage, but minimal overlap between the sheets and thus monolayer properties retained. To this end, a spin coating protocol was established and optimized (Chapter 4.3).

Aggregation of nanosheets occurring after transfer to solvents was identified as major bottleneck. This could be tracked by repeated centrifugation at relatively low centrifugal accelerations. It was found that centrifugation can remove the aggregates, but that aggregation occurs over relatively short time periods (< 2h) and that the aggregation rate scales with the WS_2 concentration.

When immediately processing the dispersion after centrifugation, it was possible to produce high quality thin films with tunable coverage. At optimized coverage, the A-exciton monolayer photoluminescence was widely retained and it was shown that this can be used to study chemical doping with the substrate, or polymers deposited on the same substrate. At higher coverages, random restacking resulted in the loss of the PL.

While such films are in principle interesting for applications in light emitting devices, the overall procedure by spin coating is tedious and not very well reproducible greatly limiting the applicability. Nonetheless, such films can be of interest for fundamental studies, e.g. the fabrication of LPE-based heterostacks with other 2D materials. Further, the insights into aggregation are useful for other film fabrication strategies, for example the assembly at the liquid-liquid interface and subsequent transfer to substrates which was recently described in literature as interesting alternative.

In Chapter 4.3, it was found that nanosheet restacking in thin films could be prevented by introducing a polymer to shield the nanosheets from interacting in the film. However, the addition of the polymer during transfer could not improve the colloidal stability in dispersion. This prompted to develop a new strategy to force the polymer on the nanosheet surface already during exfoliation. As described in Chapter 4.4, this can be achieved by adding in hydrophobic polymers to the mixture of TMDs in aqueous surfactant solution prior to sonication.

In analogy to the micelle swelling technique, the polymer is dispersed temporarily and will be trapped at the most hydrophobic space which is the interface between nanosheet and surfactant resulting in a dense coating. Using WS_2-PVK as model system, it was found that aggregation after transfer to organic solvent is prevented greatly improving the optical quality in WS_2-polymer hybrid thin films.

The procedure was successfully applied to different polymers and TMDs. In some cases, an increased PL/Raman ratio in the dispersion was achieved. Reasons for this are currently unclear and will require further experiments including microscopic characterization such as AFM statistics to quantify monolayer contents and lateral sizes of monolayers. In this regard, low temperature photoluminescence will also be useful, since it would give insights whether this enhanced PL is due to sample morphology or a homogeneous environment through the polymer coating.

PL and vibrational spectroscopy focusing on the polymer might give further insights to understand how the polymer is arranged, while time of flight secondary ion mass spectrometry (TOF-SIMS) can potentially be useful to determine the thickness of the polymer layer.

In future work, it will be of interest to extent this method to other polymer systems, e.g. ones that are expected to induce chemical doping. Further, the dense polymer coating can potentially shield nanosheets from environmental impact, which might be of interest for 2D materials that are prone to oxidation (*e.g.* black phosphorus).

5 Experimental Methods

5.1 Sample Preparation

5.1.1 Liquid Phase Exfoliation (LPE) of TMDs Nanosheets

WS_2 dispersions were prepared by probe sonicating of WS_2 powder (Sigma Aldrich: C1254-100G) with an initial concentration of 30 gL^{-1} in an aqueous sodium cholate (SC) solution. In this study, sodium cholate was chosen as a surfactant to stabilize nanosheets against reaggregation. WS_2 powder was immersed in 80 mL of aqueous surfactant solution (C_{SC}= 8 gL^{-1}). The mixture was sonicated in a 100 mL metal beaker by probe sonication using a solid flathead tip (Sonics VXC-500, i.e. 500 W) for 1 h at 60 % amplitude with a pulse of 8 s (on) and 2 s (off). The overheating was avoided by a chiller system to preserve the external temperature at 5°C. The sonic probe was manually adjusted 1.5 cm from the bottom of the beaker. The dispersion was centrifuged in 20 mL aliquots using 50 mL vials in a Beckman Coulter AvantiXP centrifuge equipped with a JA25.50 fixed-angle rotor at 3,000 *g* for 1.5 h. After discarding the supernatant, the sediment was collected in 80 mL fresh surfactant (C_{SC}= 2 gL^{-1}) and subjected to a second sonication using a solid flathead tip (Sonics VX-500) for 5 h at 60 % amplitude with a pulse of 6 s (on) and 2 s (off). From our experience, the two step sonication procedure yields a higher concentration of exfoliated WS_2 and some water soluble impurities are removed. This prepared initial dispersion is called stock dispersion which is polydisperse in nanosheet size and thickness and will be further size-selected.

It should be noted, that during the course of the thesis, one modification was made to optimize the functionality of this protocol to increase/improve the optical quality of the sample. In the general LPE protocol, after the first (short) sonication, the entire sample is mixed again, centrifuged and subjected to the second sonication. For samples prepared in the second half of the thesis, the sample is allowed to settle after the first sonication resulting in a sediment which was discarded before performing the second step (Figure 5.1-1, top). After the second, longer sonication typically performed overnight, also some material sediments and is found as slush in the beaker (Figure 5.1-1, bottom). This was discarded prior to performing the size selection

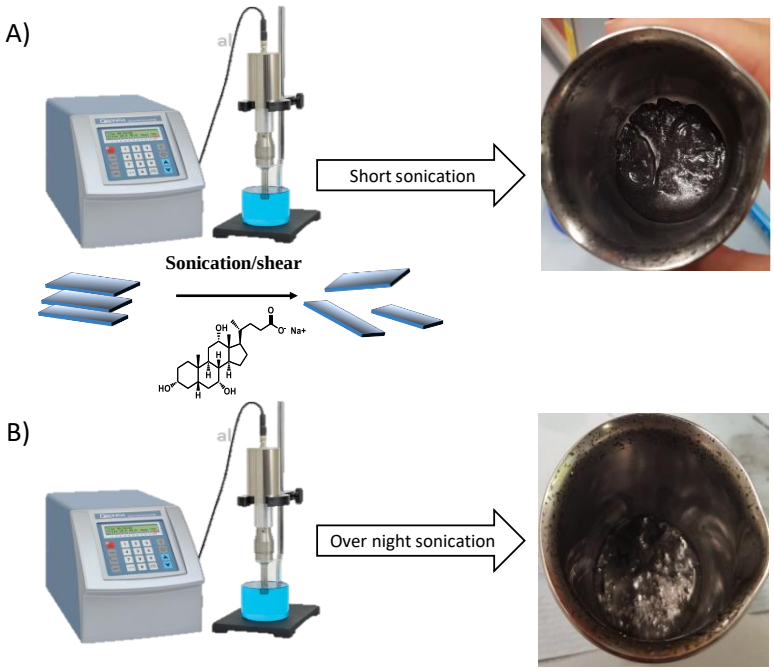

Figure 5.1-1: Schematic illustration of the LPE protocol. The sediment/slush after the first (A), as well as the second (B) sonication step was discarded.

5.1.2 Sedimentation Process and Size-Selection

Liquid cascade centrifugation (LCC) with sequentially increasing rotation speeds (2 h per run, 10 °C) was used to select nanosheets by size. This is a multi-step procedure that is extremely versatile allowing various cascades to be designed according to the desired outcome. Centrifugation conditions are expressed as a relative centrifugal field (RCF) in units of 10^3 x *g* (or k *g*) with *g* being the gravitational force. Two different rotors were used. For centrifugation at < 15000 *g*, the JA25.50 fixed angle rotor and 50 mL centrifuge tubes (VWR, order number 525-0402) were used filled with 20 mL of dispersion each. For centrifugation at > 15000 *g*, the JA25.15 rotor was used with 14 mL vials (Beckman Coulter, order number 331374), each is filled with 10 mL dispersion. The following procedure was applied:

After removing unexfoliated WS_2 by centrifugation at a low speed of 400 *g*, the supernatant was subjected to further centrifugation at 1000 *g* and further iterative steps at 5000 *g*, 10000 *g* and 22000 *g* (or 30000 *g*). After each step the sediment was collected in water at reduced volume (total 3-8 mL) and the supernatant subjected to the next run. It should be noted that the quality of the size-selected WS_2 dispersion strongly depends on carefully decanting of the supernatant in each step. Since in each step, the nanosheets were trapped between two boundaries of centrifugation

speed (between two fixed *g*-forces), these boundaries are used as sample nomenclature (e.g. 5-10k *g*). This sediment contains smaller and thinner nanosheets the higher the centrifugal accelerations.

5.1.3 Transfer to Other Liquid Environments

After exfoliation in aqueous sodium cholate and size selection by liquid cascade centrifugation, the nanosheets in the sediment were redispersed in water, the resultant dispersion centrifuged again at centrifugal accelerations above the initial higher centrifugation boundary. This was performed in 1.5 mL aliquots (Eppendorf centrifuge tubes) for 2h in each run. Specifically, the following centrifugal acceleration were used: 35k *g* for the 5-30k *g*, 30k *g* for the 5-22k *g* sample (produced only in the work on additive systems), 15k *g* for the 5-10k *g* sample. 7k *g* for the 1-5k *g* sample and 2k *g* for the 0.4-1k *g* sample. After this step, the supernatant was discarded and the WS_2 nanosheets in the sediment redispersed. Depending on whether the material was transferred to an aqueous or organic solution, water or THF is used, respectively. For the transfer to additive systems, the mixtures were sonicated ~ 3 min in a sonic bath for reagitation. For the transfer to pure solvents, the first washing step was performed in water (to remove surfactant), while the second one was done with IPA. The sonication time for reagitation was increased to 5 min. The samples were centrifuged again at high centrifugal acceleration (values as in the first step of the transfer see above). This washed WS_2 nanosheet sediment, was then redispersed in the desired solvent/additive mixture by bath sonication (~ 3-5 min). In a last step, aggregates were removed by centrifugation at 100 *g* for 30 min in the case of additive systems and 60 min in the case of pure solvents. For the preparation of high quality thin films, this centrifugation removal step was performed for 30 min at 1000 *g*.

5.1.4 Production of Thin Films Using Spin Coating

Prior to spin coating, glass substrates are cleaned in three steps. First, the substrate is embedded in a substrate holder in a beaker then immersed in acetone. The beaker containing substrates and solvent is placed in the bath sonicator for 15 minutes. Secondly, samples were taken out from acetone and washed one by one with IPA to remove the residual stain or dust. In the final step, both sides of substrates were dried and cleaned again by compressed air and kept in a glovebox.

All thin films were fabricated by a spin coater which is embedded in a glovebox to prevent sample oxidation. In this study, the spin coating technique is used because of some advantages of simplicity and relative ease. Due to the ability of having high spin speeds, the high airflow leads

to fast drying times, which in turn results in high consistency at both macroscopic and nano length scales.

To prevent loss of material as much as possible, 20 μL of optimized WS_2 dispersion was deposited as close to the centre of the substrate as possible and the substrate is rotated first at a speed of 500 rpm then followed by a higher speed of 8000 rpm. In general, sample fabrication took 60 s per round (totally 20 rounds per sample). The airflow dries the majority of the solvent, leaving a plasticized WS_2 film, before the film fully dries to just leave the nanosheets on the surface. The rotation of the substrate at 8000 rpm means that the centripetal force combined with the surface tension of the solution pulls the liquid coating into an even covering. This statistical spin coating protocol is applied for fabricating all liquid phase exfoliated WS_2 nanosheets thin films.

5.2 Characterization Methods

5.2.1 Extinction Spectroscopy

A standard UV-Vis spectrophotometer (Agilent Cary-6000i) was used to measure optical extinction spectra in transmission mode. It should be noted that extinction is the sum of absorption and scattering. To perform this experiment a quartz cuvette with a pathlength of 0.4 cm was used and spectra were measured in 0.5 nm increments. The optical density was kept below 1 over the entire spectral region if possible. The baseline of the respective solvent was subtracted from each spectrum. After the measurement, the cuvettes were cleaned and dried prior to the next measurement. Second derivatives of the A-exciton region were obtained after smoothing the spectrum with Lowess (12 points per window) and then differentiating twice.

5.2.2 Raman Spectroscopy

Liquid phase exfoliated WS_2 nanosheets based- dispersion and thin films were characterized by Raman/PL spectroscopy which was carried out in a Renishaw in-Via reflex confocal microscope-based Raman spectrometer equipped with 532 nm (for WS_2) and 633 nm (for $MoSe_2$) laser excitation. The Raman/PL emissions was collected by a 50x long working distance objective lens (in streamline mode and 2400 l/mm grating for 532 nm excitation and 1200 l/mm for 633 nm excitation) typically using 1% of the laser power (1.24 μW) to prevent heating and sample damage. All these measurements are taken at room temperature and under ambient conditions. A reference sample (silicon) was used to calibrate the spectrometer before carrying out the measurements.

It should be considered that an error in the PL/Raman ratio could happen due to the changes of the focal plane during the acquisition. This is often mirrored in a tilted baseline or an asymmetric PL line shape due to inner filter and re-absorption effects. It can also be visually realized when the size of the laser spot in the optical image has changed during the measurement. Therefore, great care has been taken during these measurements. 25 μL of WS_2 dispersion with a high concentration were drop-casted on a glass slide. Since there is a dependency between WS_2 dispersion concentration and acquisition time, it is kept as short as possible between 2 to 10s. To adjust the focus exactly above the WS_2 dispersion drop, initially the 10x objective was used to focus on the edge of the droplet and then refocused at the same spot with 50x objective and readjusted. Also to keep the focus (the lower curvature) fixed, the measurement has to be taken close to the edge instead of centre of this droplet. 10 measurements were carried out on different spots of the droplet and averaged. Baseline correction was done for each spectrum prior to averaging.

In addition, Raman mapping was used to characterize WS_2 thin films. The laser is focused to a spot of the WS_2 thin film and a point by point mapping is applied where the sample moves by a motorized stage under the laser. In this way ~ 1000 spectra were measured from a sample and all spectra were averaged and then baseline corrected.

5.2.3 Photoluminescence Spectroscopy

Photoluminescence was measured using a Horiba Scientific Fluorlog-3 spectrometer equipped with a Xe arc lamp (450 W) and a Sincerity CCD camera as detector using double monochromators for excitation and emission with a 1200l/mm grating with 330 nm blaze in excitation. For the PLE contour plots, a 1200 l/mm grating with 500 nm blaze was used in emission. The quartz cuvettes with 0.4 x 1 cm dimensions were placed inside the sample chamber so that the excitation light passed through the 0.4 cm side of the cuvette. A piezo-cooled temperature controller (TLC50/Horiba4) was used to adjust the external temperature to 20°C. Emission after 425 nm excitationwas collected in 90° angle a, i.e. after having passed through the 1 cm side. Excitation and emission bandwidths were typically 10 nm, increments 1 nm and acquisition times 0.5-1 s/nm. To avoid artefacts from scattering of the nanomaterial dispersion, a 550 nm cut-off filter was placed on the emission side. The excitation was corrected for the light intensity. All samples were diluted to optical densities < 0.4 before performing the measurements to avoid innerfilter and reasbsorption effects.

5.2.4 Atomic Force Microscopy

AFM measurements of thin films were carried out on a Bruker Icon Dimension ICON3 scanning probe microscope equipped with Bruker OLTESPA-R3 cantilevers (aluminium coated silicon) in air and under ambient conditions. Images with the size of 6x6 and 4x4 μm^2 were acquired in ScanAssyst mode with a resolution of 1024 lines per images and scan rate of 0.4 Hz. Images were further post-processed with the use of Gwyddion software in order to remove artificial lines, enhance the contrast and crop to allow direct comparison between the samples.

5.2.5 Optical Microscopy

Optical images of spin-coated WS_2 thin films were taken using a BX51 Olympus system microscope (U-TV0.5XC-3/ SN: 9F02983) with different objectives (20x and 50x) associated with an Infinity2-2 (CCD camera- charge-coupled device), in the bright field mode and analysed with

Streamline Software. To increase the contrast level, images were taken with a band pass filter (490 ± 5 nm).

6 Appendix

A)

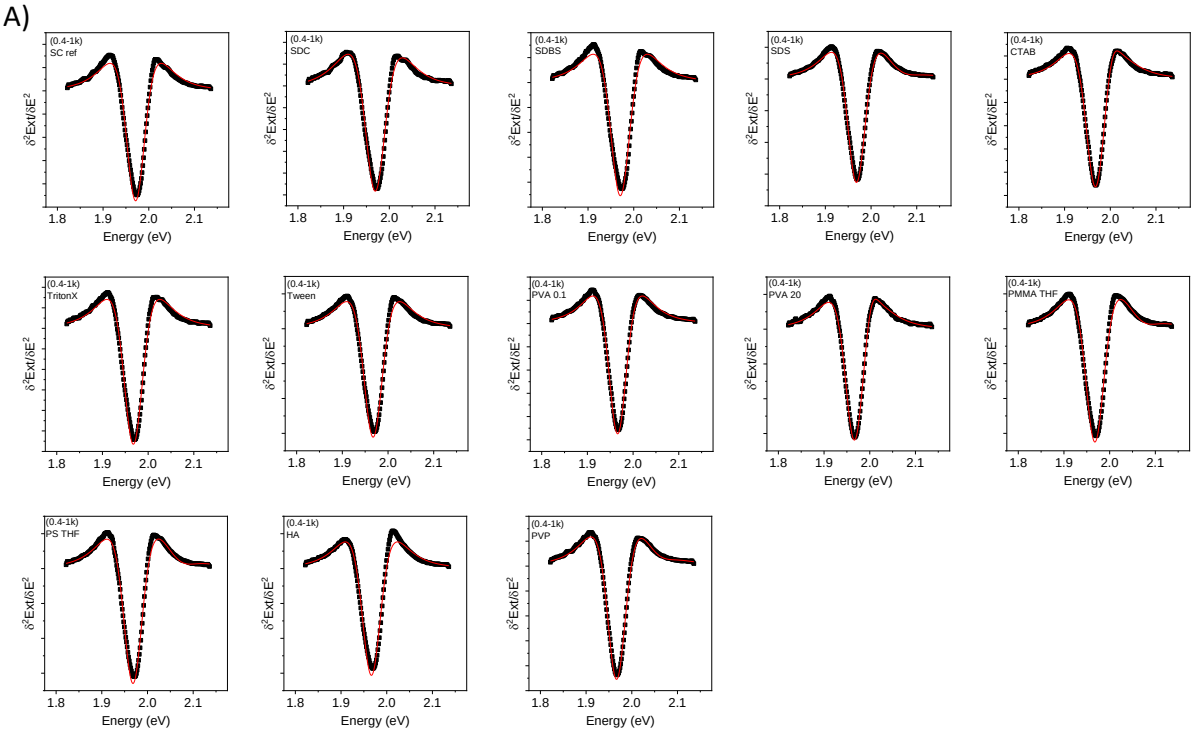

B)

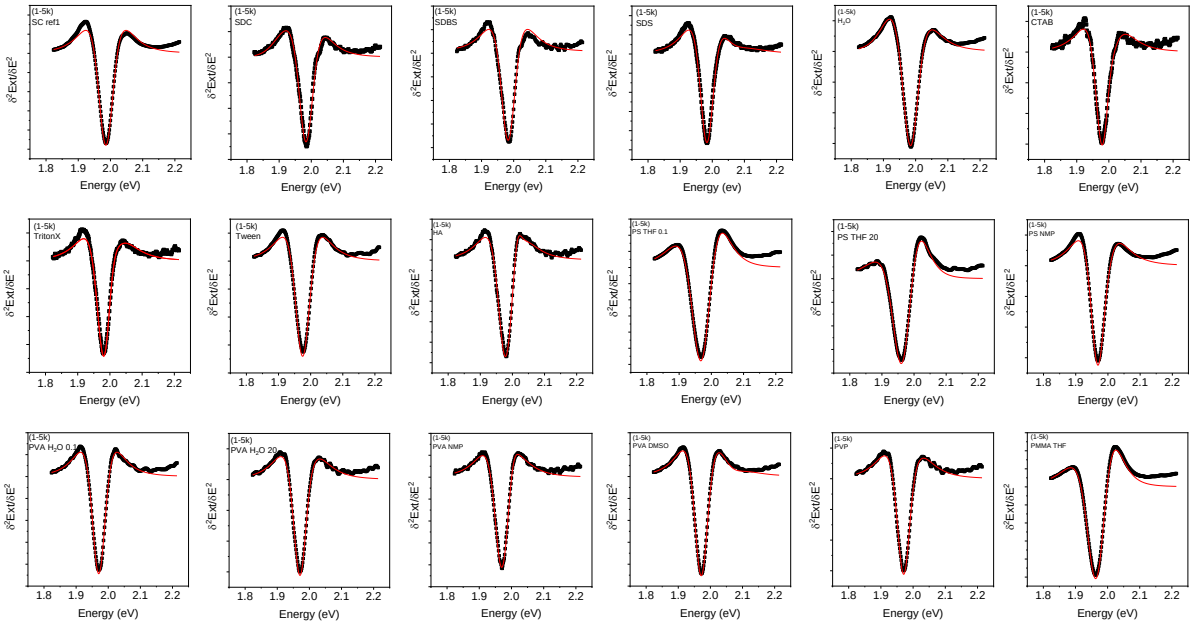

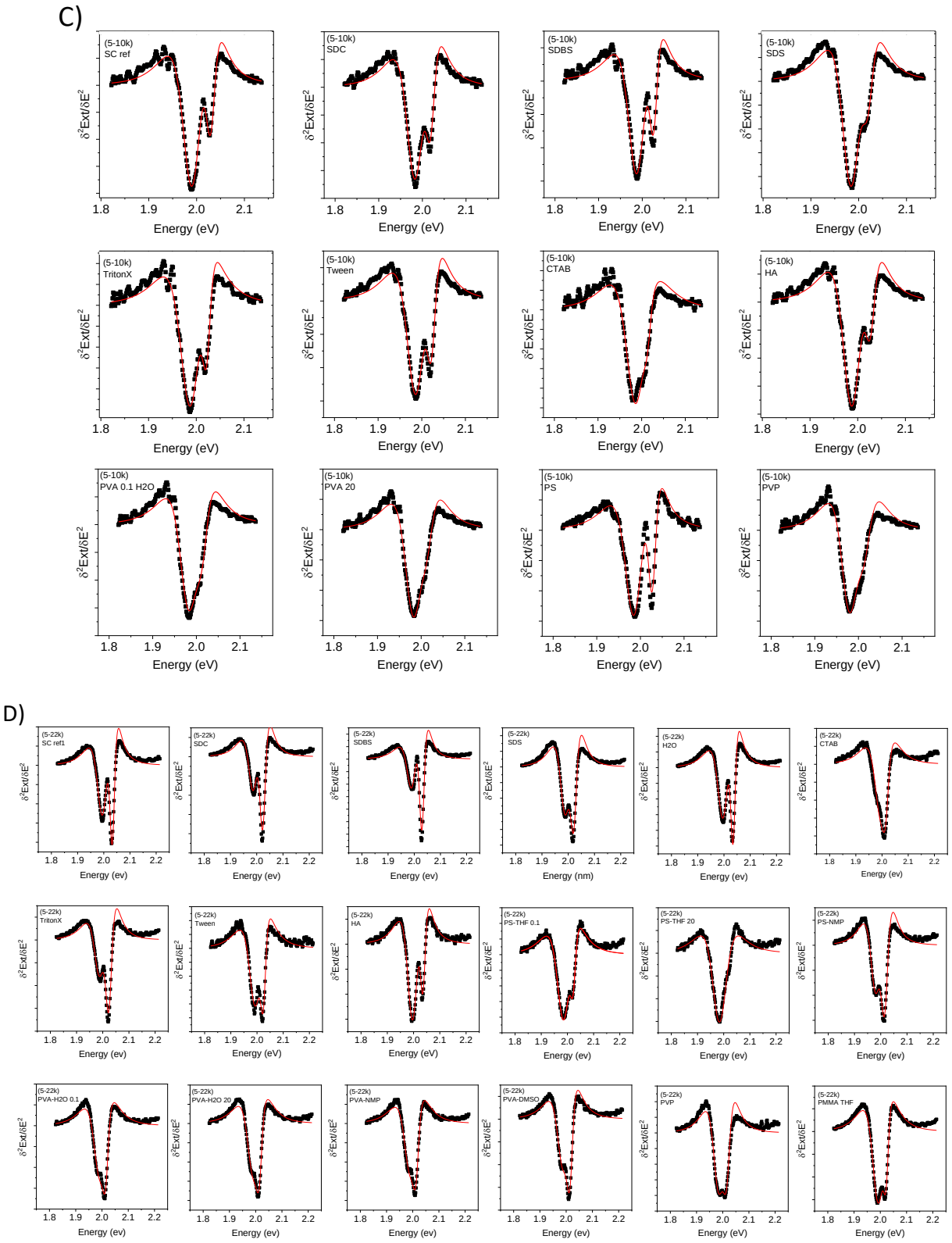

Figure A6-1: A-D) Second derivative of the A-exciton region of all size selected WS_2 fractions transferred to a range of additive solvent/systems: A) 0.4-1k *g*, B) 1-5 k*g*, C) 5-10k *g*, D) 5-22 k*g* after smoothing the spectrum with Lowess. For fractions isolated at high *g*-forces, two components are identified assigned to monolayers (ML) and few-layers (FL). The data is fit to the sum of the second derivative of two Lorentzians (solid lines) to extract peak position and energy.

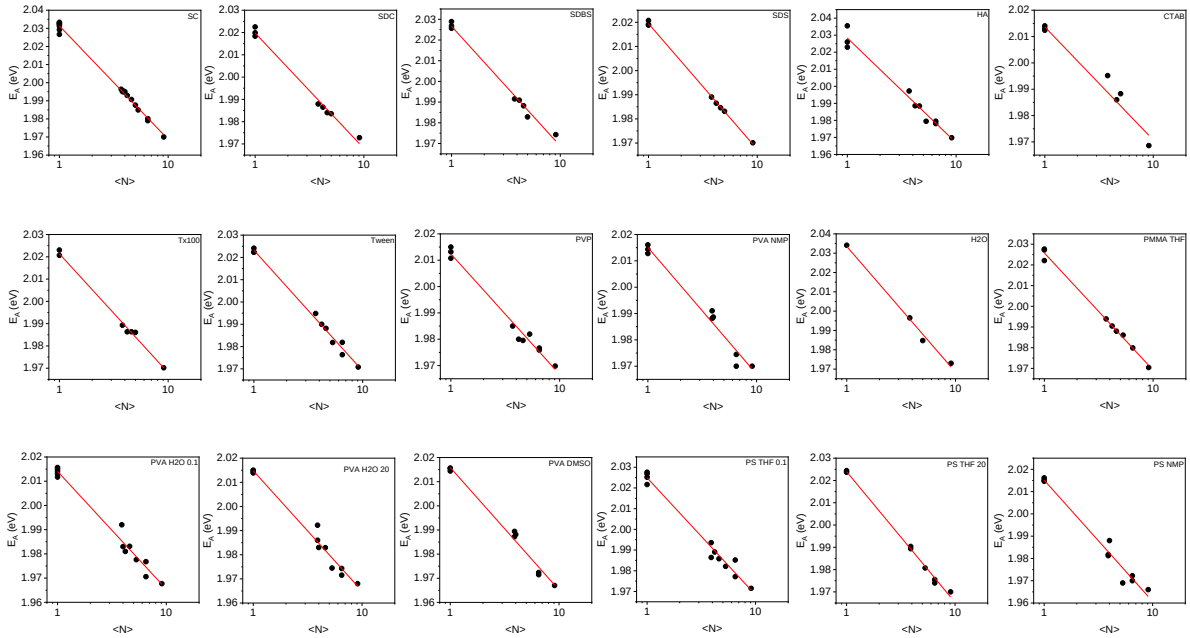

Figure A6-2: Plot of exciton energy as function of layer number of WS_2 transferred to a range of additive solvent/systems. By using a logarithmic scale, a linear relationship can be shown. While technically, an exponential relation is expected, this power law fitting is more robust and used to track solvatochromic effects.

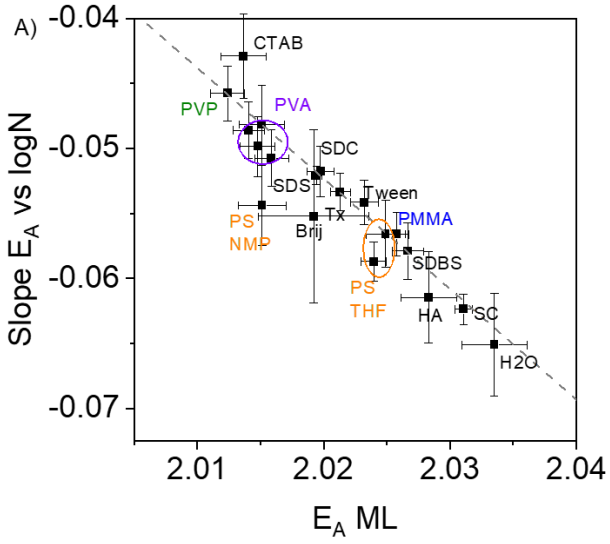

Figure A6-3: Plot of the exponent from the fits in figure A6-2 as function of monolayer exciton energy also obtained from the fits. A linear correlation is empirically found. The additive systems are labelled. Error bars are errors of the fit.

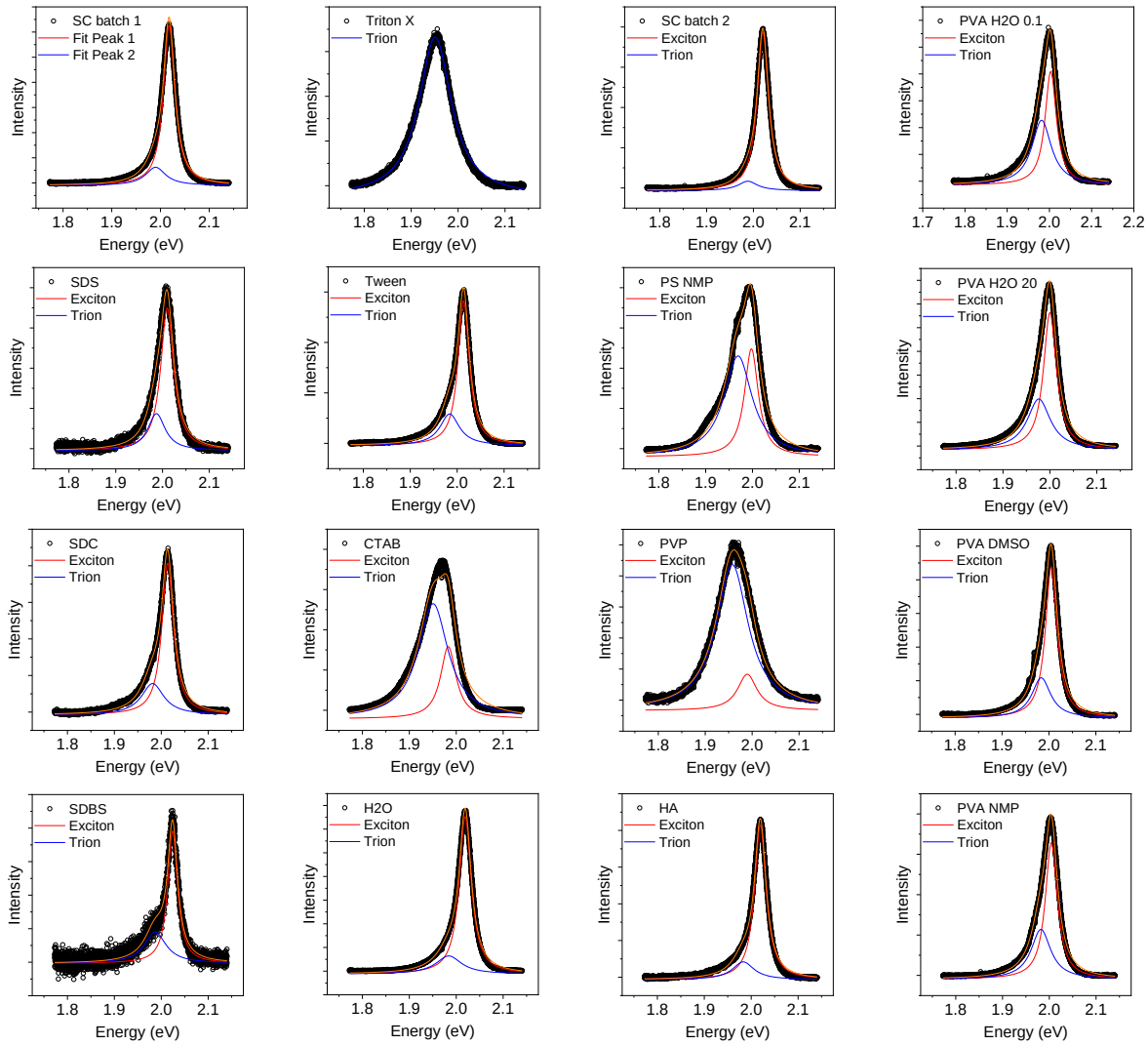

Figure A6-4: PL spectra of size-selected WS_2 nanosheets (5-22k *g*) transferred to a range of additives/solvent systems measured in the Raman spectrometer (532 nm excitation). Black dots are experimental data, and the blue, red, and orange lines are the fitting curves of the peaks of the A^- trion, A exciton, and the summation of the three fitting curves respectively. B-exciton feature is not observed in all PL spectra.

A)

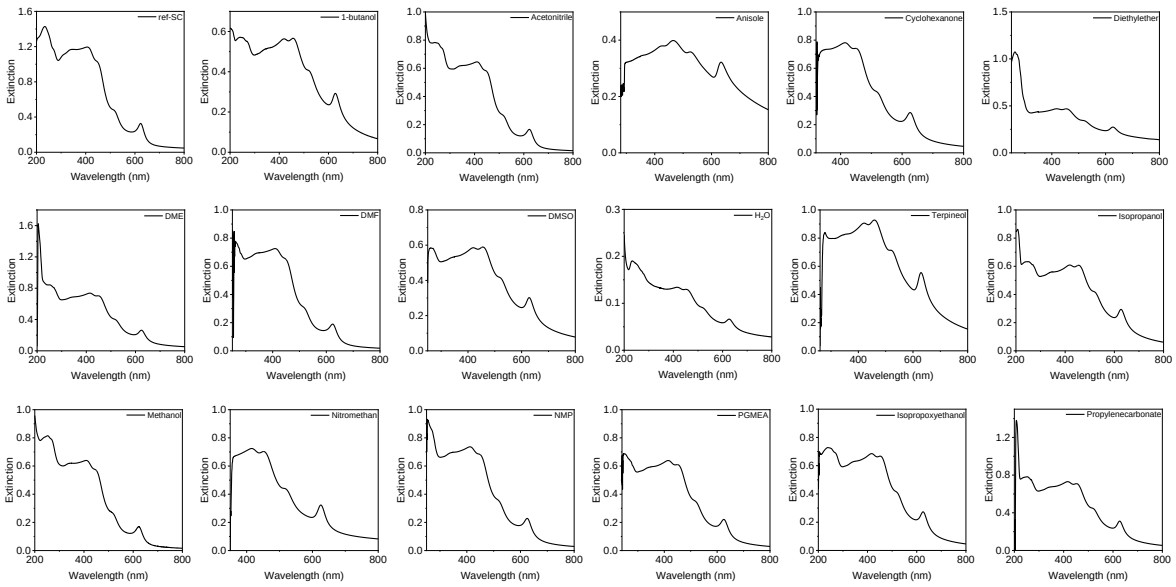
ref-SC
1-butanol
Acetonitrile
Anisole
Cyclohexanone
Diethylether
DME
DMF
DMSO
H2O
Terpineol
Isopropanol
Methanol
Nitromethan
NMP
PGMEA
Isopropoxyethanol
Propylenecarbonate
Extinction
Wavelength (nm)

B)

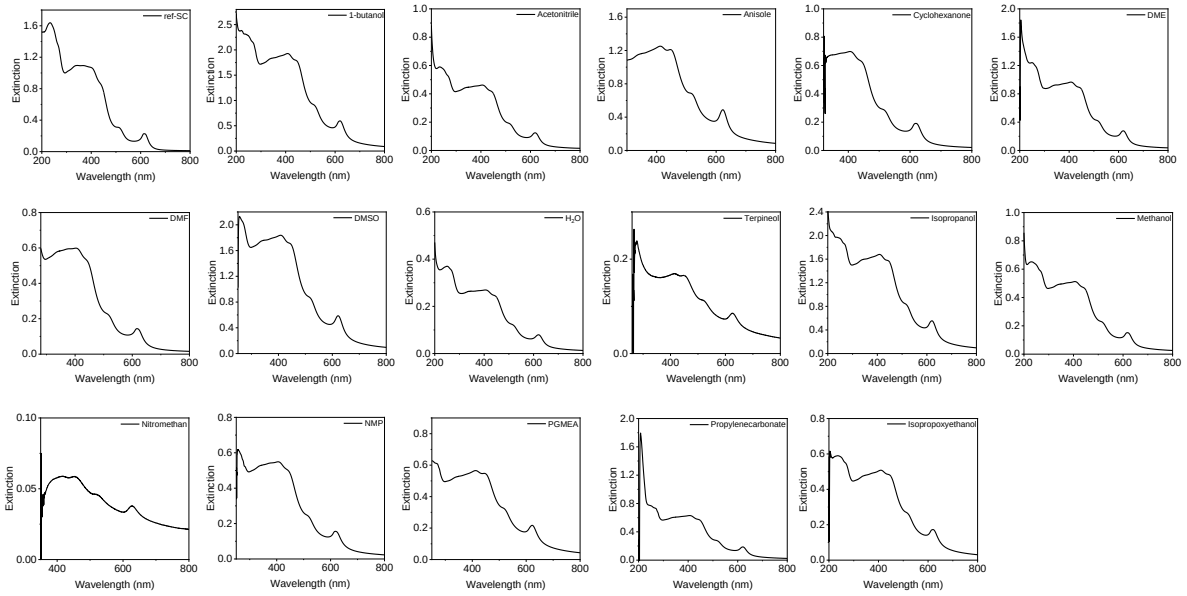
ref-SC
1-butanol
Acetonitrile
Anisole
Cyclohexanone
DME
DMF
DMSO
H2O
Terpineol
Isopropanol
Methanol
Nitromethan
NMP
PGMEA
Propylenecarbonate
Isopropoxyethanol
Extinction
Wavelength (nm)

C)

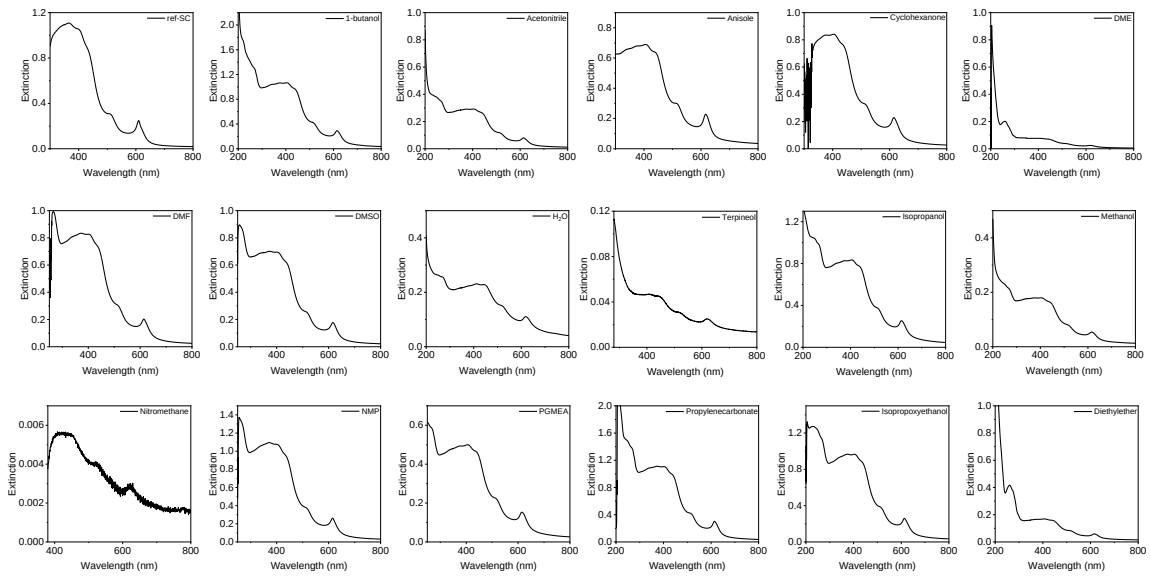

Figure A6-5: Extinction spectra of size-selected WS2 nanosheets transferred from sodium cholate to a range of pure solvents. A) 1-5k *g*, B) 5-10k *g*, C) 10-30k *g*.

A)

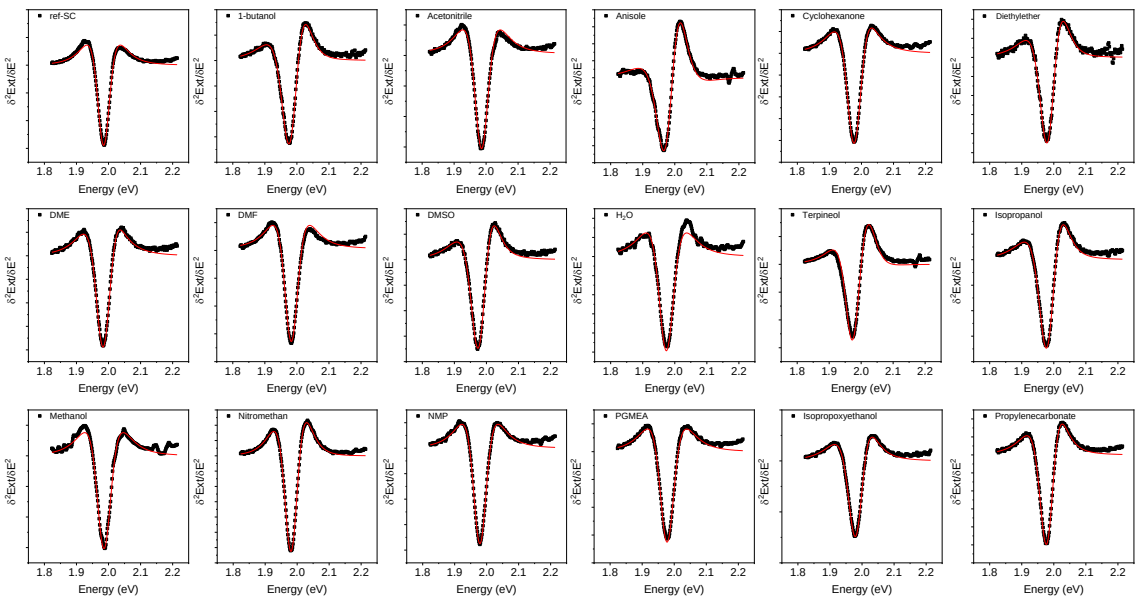

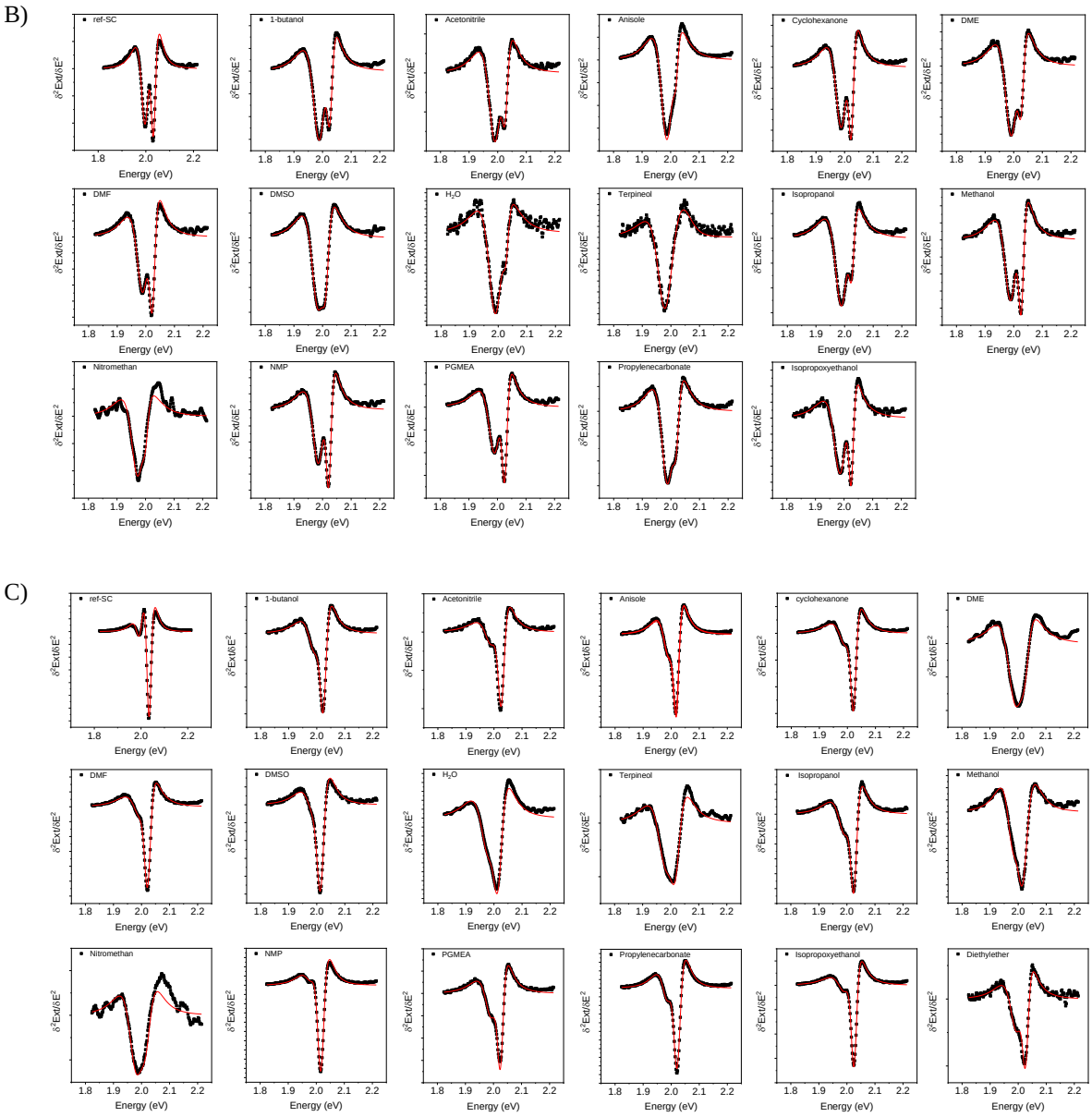

Figure A6-6: A-C) Second derivative of the A-exciton region of size-selected WS_2 fractions transferred to a range of organic solvents: A) 1-5 k*g*, B) 5-10k *g*, C) 5-22 k*g* after smoothing the spectrum with Lowess. For fractions isolated at high *g*-forces, two components are identified assigned to monolayers (ML) and few-layers (FL). The data is fit to the sum of the second derivative of two Lorentzians (solid lines) to extract peak position and energy.

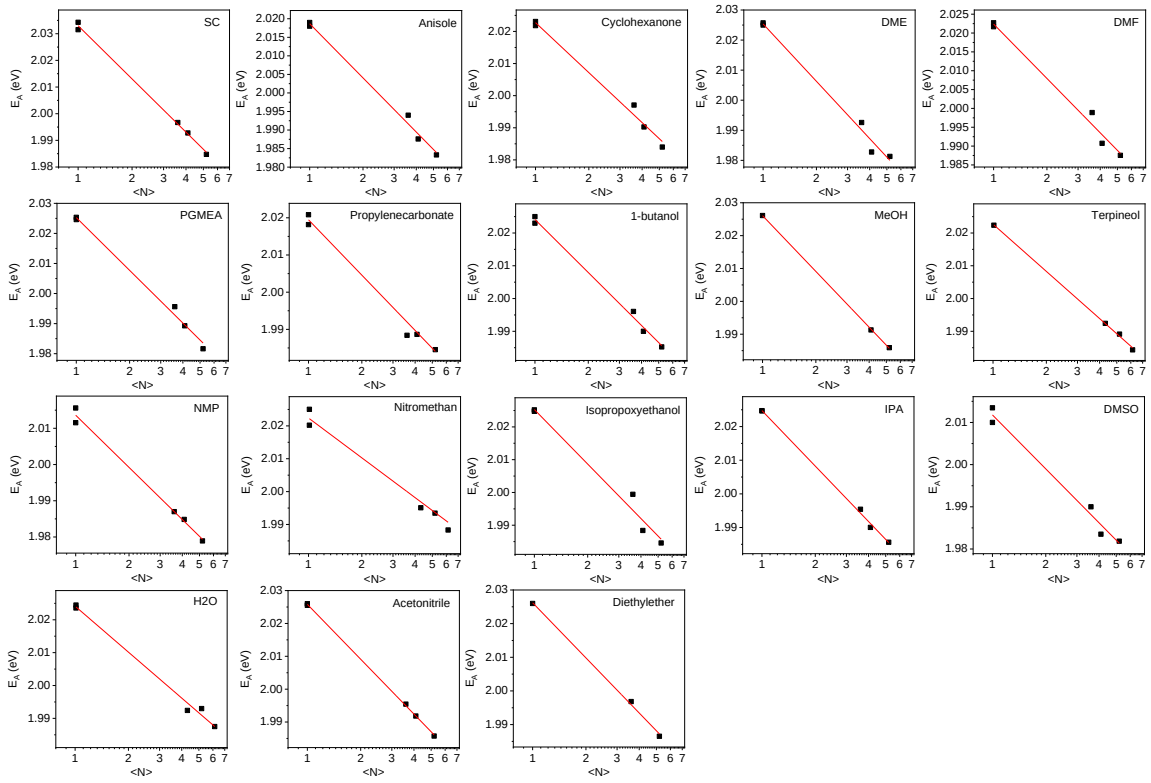

Figure A6-7: Plot of exciton energy as function of layer number of WS_2 transferred to a range of organic solvents. By using a logarithmic scale, a linear relationship can be shown. While technically, an exponential relation is expected, this power law fitting is more robust and used to track solvatochromic effects.

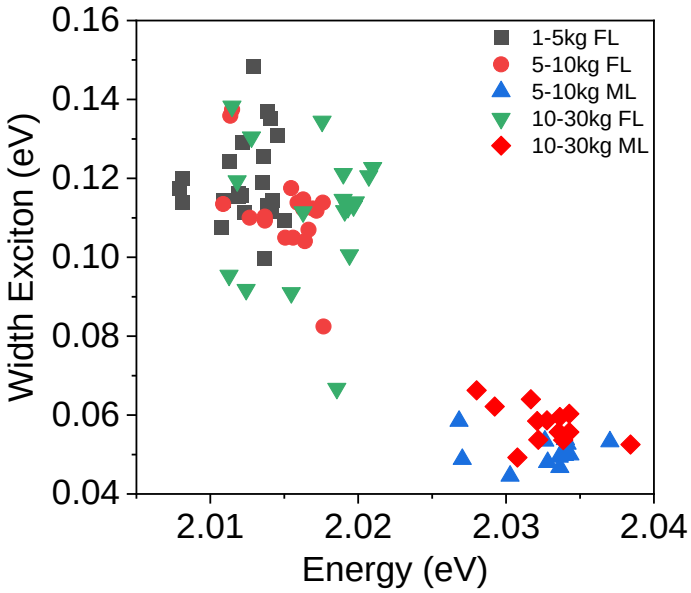

Figure A6-8: Energy and width of few layer and monolayer WS_2 transferred to a range of organic solvents extracted from fitting the second derivative of the A-exciton region in the extinction spectra for three different nanosheet fractions. Only a weak correlation between width and energy is observed in the case of the monolayers.

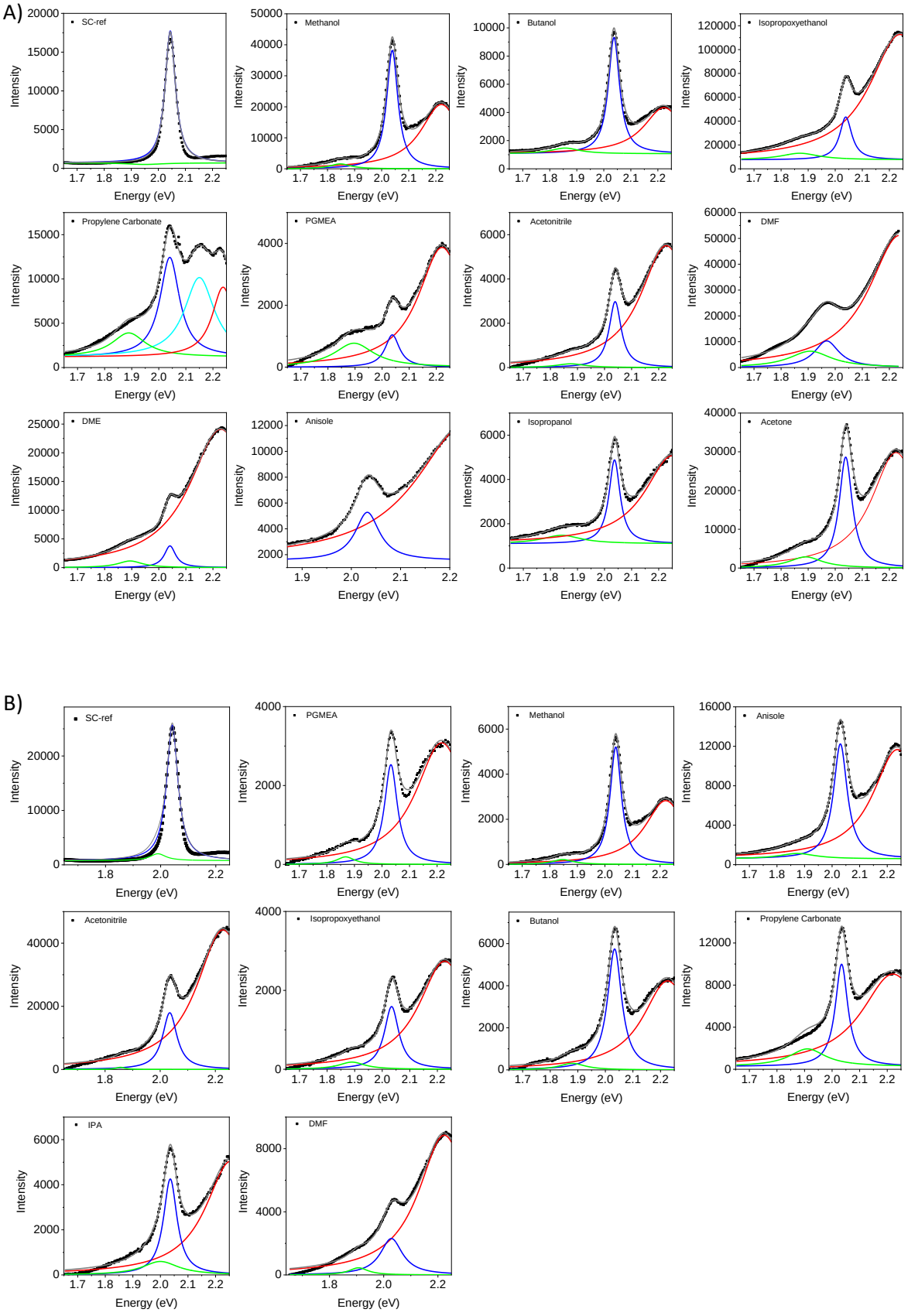

Figure A6-9: Fitted PL spectra ($\lambda_{excitation}$ = 425 nm, 20˚C) measured in the fluorescence spectrometer of two size-selected WS_2 fractions, A) 5-10k *g* and B) 10-30k *g* transferred to a range of solvents.

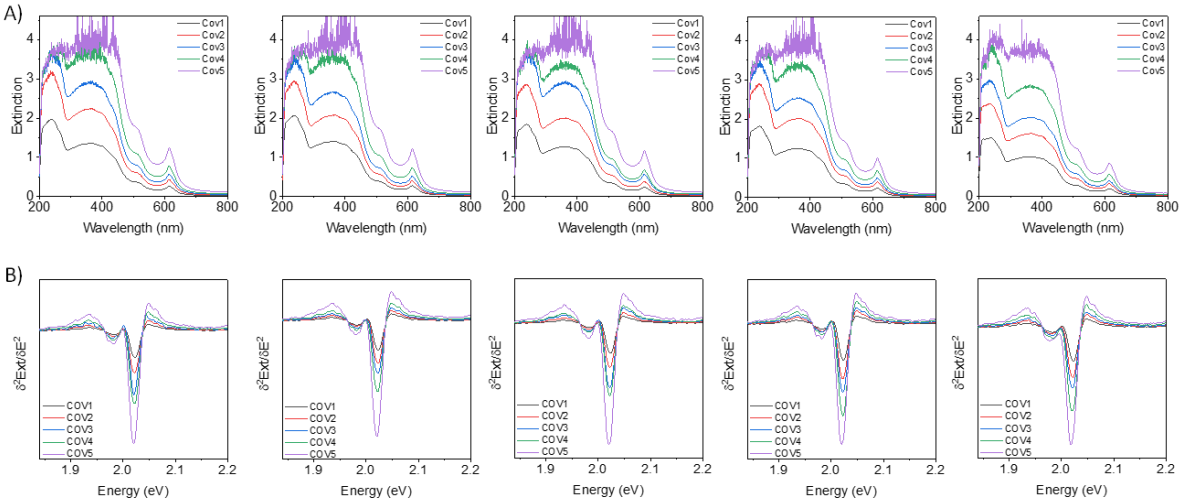

Figure A6-10: Impact of repeated centrifugation (1000 *g*, 30 min) on WS_2 (5-10k *g*) transferred to IPA/THF at different nanosheet concentration (denoted as COV1-COV5). From left to right: first to firth subsequent centrifugation. A) Optical extinction spectra. The noise in the spectra at extinction >3 is due to saturation of the detector. B) Second derivative of the A-exciton region which is extracted from the respective optical extinction spectra after smoothing.

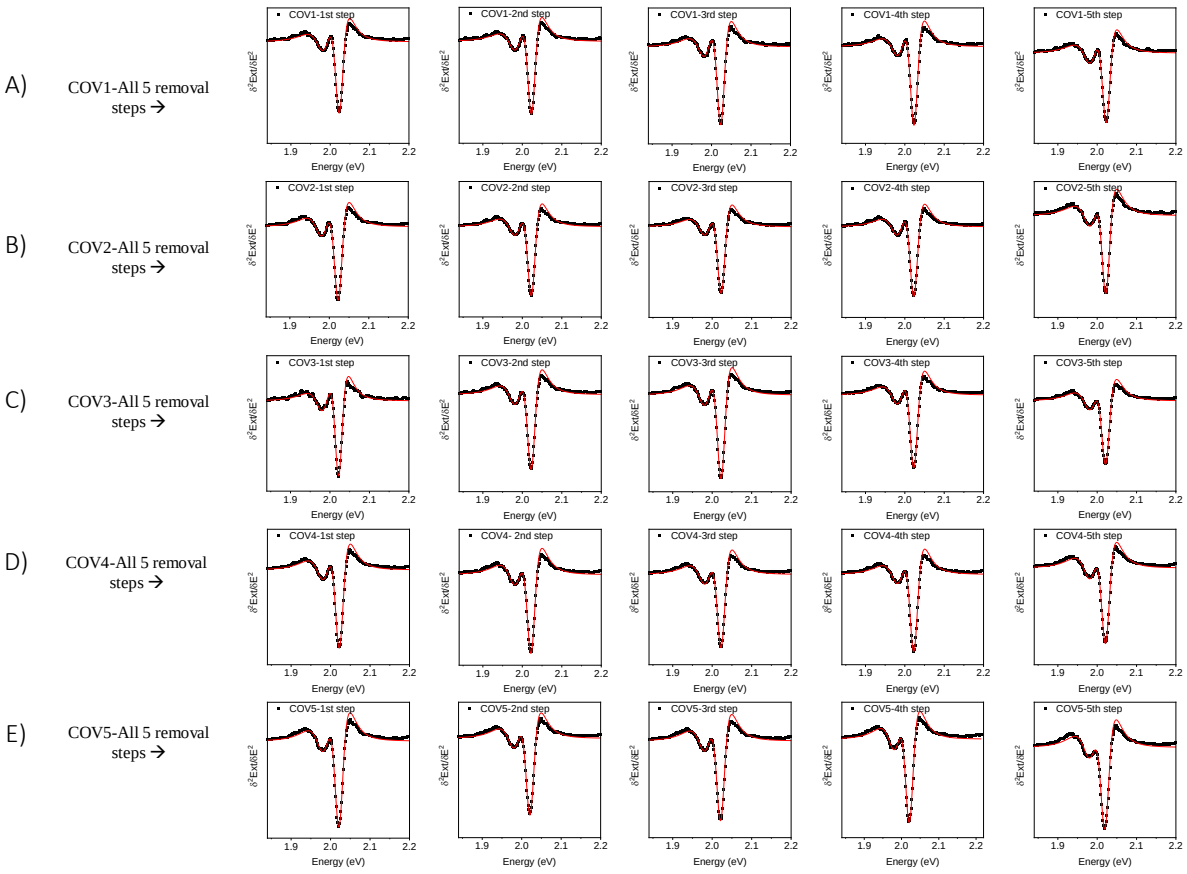

Figure A6-11: Second derivative of the A-exciton spectra in figure A6-10 fitted to the sum of the second derivative of two Lorentzians. A-E) from the lowest to highest WS_2 concentration. Each raw contains five different second derivative spectra corresponding to centrifugation run 1-5.

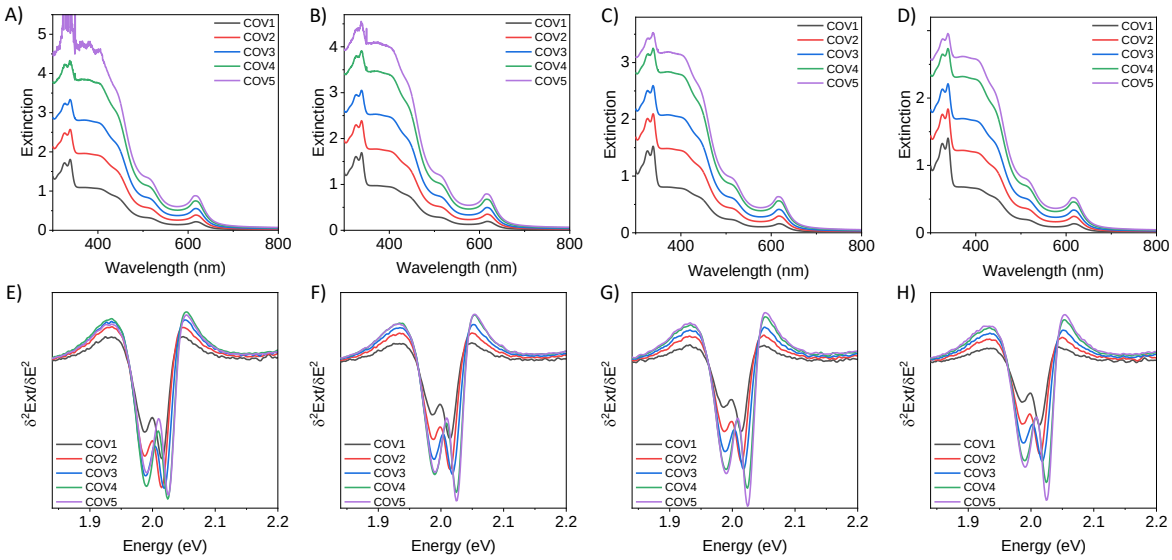

Figure A6-12: Impact of repeated centrifugation (1000 *g*, 30 min) on WS_2 (5-10k *g*) transferred to PVK/IPA/THF at different nanosheet concentration (denoted as COV1-COV5). From left to right: first to firth subsequent centrifugation. A) Optical extinction spectra. The noise in the spectra at extinction >3 is due to saturation of the detector. B) Second derivative of the A-exciton region which is extracted from the respective optical extinction spectra after smoothing.

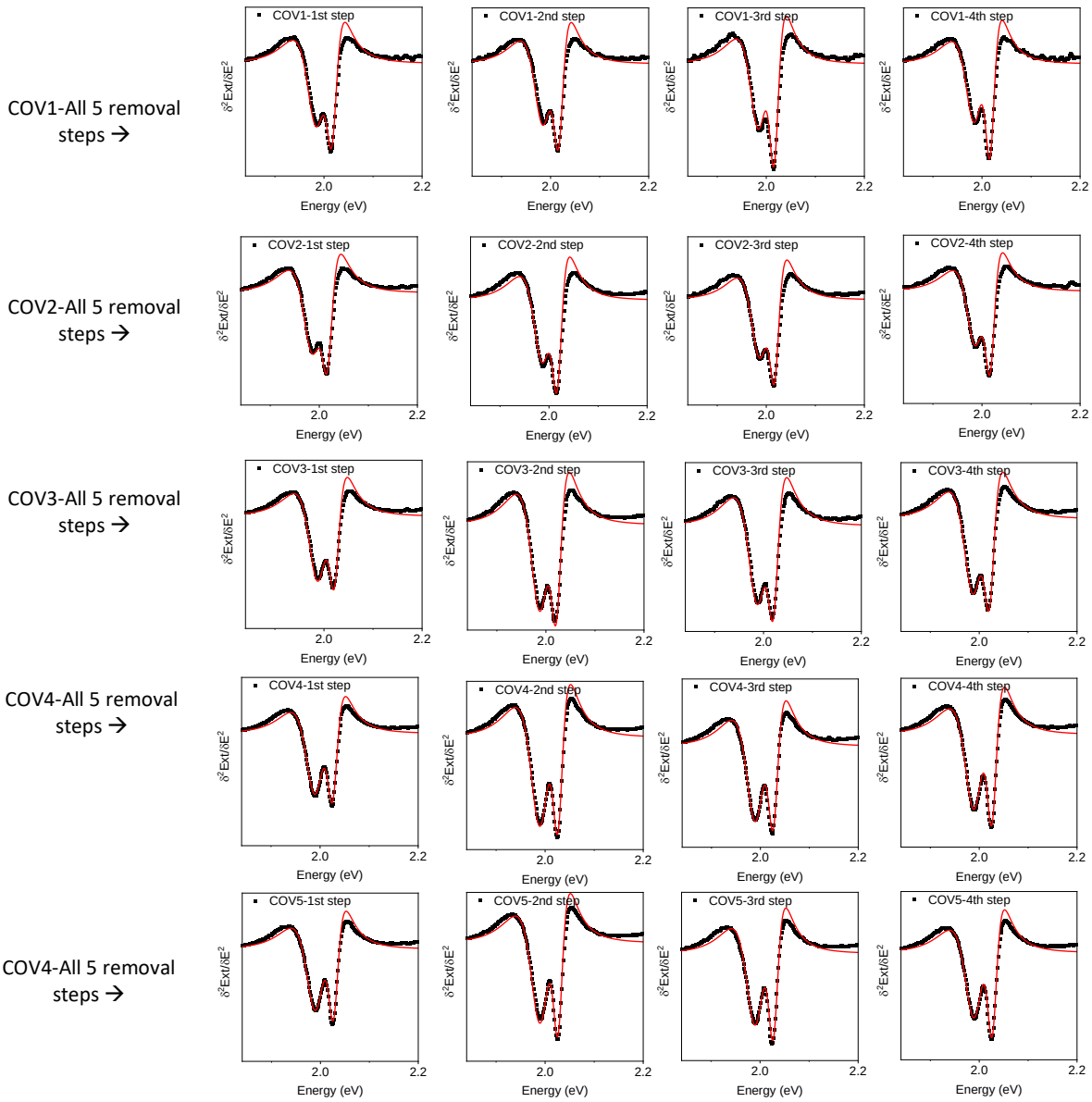

Figure A6-13: Second derivative of the A-exciton spectra in figure A6-12 fitted to the sum of the second derivative of two Lorentzians. A-E) from the lowest to highest WS_2 concentration. Each raw contains five different second derivative spectra corresponding to centrifugation run 1-5.

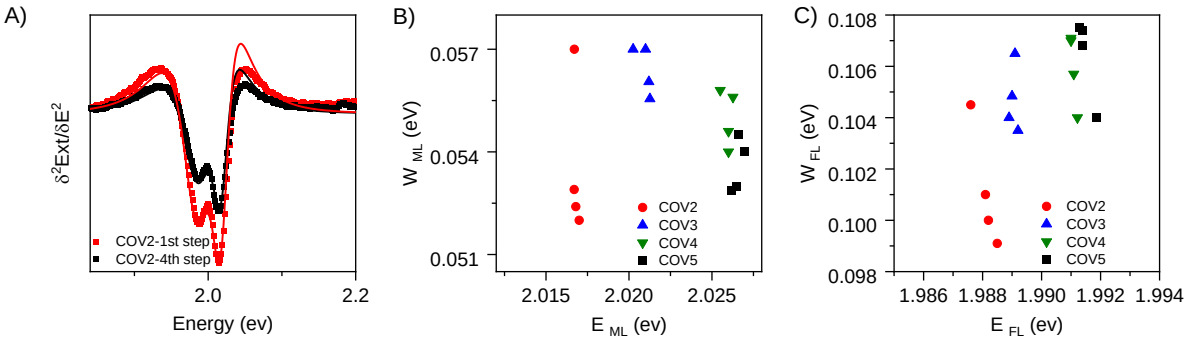

Figure A6-14: Analysis of the A-exciton of WS_2 transferred to PVK-IPA-THF after repeated centrifugation. A) Comparison of the second derivative of the A-exciton region at the highest WS_2 concentration (COV5) after smoothing the extinction spectra after the first and last iterative centrifugation step. The A-exciton splits into two components assigned to monolayers (ML) and few-layers (FL). B) ML and C) FL width as function of energy for all samples. The different initial WS_2 concentrations are color-coded.

7 Bibliography

1. Geim, A. K., Graphene: status and prospects. *science* **2009,** *324* (5934), 1530-1534.
2. Brusatin, G.; Signorini, R., Linear and nonlinear optical properties of fullerenes in solid state materials. *Journal of Materials Chemistry* **2002,** *12* (7), 1964-1977.
3. Bae, S.; Kim, H.; Lee, Y.; Xu, X.; Park, J.-S.; Zheng, Y.; Balakrishnan, J.; Lei, T.; Kim, H. R.; Song, Y. I., Roll-to-roll production of 30-inch graphene films for transparent electrodes. *Nature nanotechnology* **2010,** *5* (8), 574-578.
4. Blake, P.; Brimicombe, P. D.; Nair, R. R.; Booth, T. J.; Jiang, D.; Schedin, F.; Ponomarenko, L. A.; Morozov, S. V.; Gleeson, H. F.; Hill, E. W., Graphene-based liquid crystal device. *Nano letters* **2008,** *8* (6), 1704-1708.
5. Chieng, B. W.; Ibrahim, N. A.; Wan Yunus, W. M. Z.; Hussein, M. Z.; Silverajah, V., Graphene nanoplatelets as novel reinforcement filler in poly (lactic acid)/epoxidized palm oil green nanocomposites: Mechanical properties. *International journal of molecular sciences* **2012,** *13* (9), 10920-10934.
6. Arul, N. S.; Nithya, V. D., Two dimensional transition metal dichalcogenides: synthesis, properties, and applications. *Springer*: **2019**.
7. Banks, C. E.; Brownson, D. A., 2D materials: characterization, production and applications. *CRC Press*: **2018**.
8. Khan, U.; May, P.; O'Neill, A.; Bell, A. P.; Boussac, E.; Martin, A.; Semple, J.; Coleman, J. N., Polymer reinforcement using liquid-exfoliated boron nitride nanosheets. *Nanoscale* **2013,** *5* (2), 581-587.
9. Xia, F.; Wang, H.; Jia, Y., Rediscovering black phosphorus as an anisotropic layered material for optoelectronics and electronics. *Nature communications* **2014,** *5* (1), 1-6.
10. Susantyoko, R. A.; Wang, X.; Sun, L.; Sasangka, W.; Fitzgerald, E.; Zhang, Q., Influences of annealing on lithium-ion storage performance of thick germanium film anodes. *Nano Energy* **2015,** *12*, 521-527.
11. Choi, E.-Y.; San Choi, W.; Lee, Y. B.; Noh, Y.-Y., Production of graphene by exfoliation of graphite in a volatile organic solvent. *Nanotechnology* **2011,** *22* (36), 365601.
12. Rao, C. N. R., Transition metal oxides. *Annual Review of Physical Chemistry* **1989,** *40* (1), 291-326.
13. Radisavljevic, B.; Radenovic, A.; Brivio, J.; Giacometti, V.; Kis, A., Single-layer MoS 2 transistors. *Nature nanotechnology* **2011,** *6* (3), 147-150.

14. Cunningham, G.; Hanlon, D.; McEvoy, N.; Duesberg, G. S.; Coleman, J. N., Large variations in both dark-and photoconductivity in nanosheet networks as nanomaterial is varied from MoS 2 to WTe 2. *Nanoscale* **2015,** *7* (1), 198-208.

15. Chhowalla, M.; Shin, H. S., Goki Eda, Lain-Jong Li, Kian Ping Loh, and Hua Zhang. *The* chemistry of two-dimensional layered transition metal dichalcogenide nanosheets. *Nature Chemistry* **2013,** *5*, 263.

16. Backes, C., Ten Years of Liquid-phase Exfoliation of Layered Crystals–A Bright Future ahead? *CHIMIA International Journal for Chemistry* **2019,** *73* (6), 498-502.

17. Castellanos-Gomez, A.; Poot, M.; Steele, G. A.; Van Der Zant, H. S.; Agraït, N.; Rubio-Bollinger, G., Elastic properties of freely suspended MoS2 nanosheets. *Advanced materials* **2012,** *24* (6), 772-775.

18. Coleman, J. N., Liquid-phase exfoliation of nanotubes and graphene. *Advanced Functional Materials* **2009,** *19* (23), 3680-3695.

19. Zuckerkandl, E.; Pauling, L., Evolutionary divergence and convergence in proteins. In *Evolving genes and proteins*, Elsevier: 1965; pp 97-166.

20. Pauling, L.; Corey, R., Proc. nat. *Acad. Sei. US A* **1930,** *16*, 578.

21. Chen, Z.; Cummins, D.; Reinecke, B. N.; Clark, E.; Sunkara, M. K.; Jaramillo, T. F., Core–shell MoO3–MoS2 nanowires for hydrogen evolution: a functional design for electrocatalytic materials. *Nano letters* **2011,** *11* (10), 4168-4175.

22. Berkdemir, A.; Gutiérrez, H. R.; Botello-Méndez, A. R.; Perea-López, N.; Elías, A. L.; Chia, C.-I.; Wang, B.; Crespi, V. H.; López-Urías, F.; Charlier, J.-C., Identification of individual and few layers of WS 2 using Raman spectroscopy. *Scientific reports* **2013,** *3* (1), 1-8.

23. Böker, T.; Severin, R.; Müller, A.; Janowitz, C.; Manzke, R.; Voß, D.; Krüger, P.; Mazur, A.; Pollmann, J., Band structure of MoS 2, MoSe 2, and α− MoTe 2: Angle-resolved photoelectron spectroscopy and ab initio calculations. *Physical Review B* **2001,** *64* (23), 235305.

24. Detriche, S.; Zorzini, G.; Colomer, J.-F.; Fonseca, A.; Nagy, J. B., Application of the Hansen solubility parameters theory to carbon nanotubes. *Journal of nanoscience and nanotechnology* **2008,** *8* (11), 6082-6092.

25. Mak, K. F.; He, K.; Lee, C.; Lee, G. H.; Hone, J.; Heinz, T. F.; Shan, J., Tightly bound trions in monolayer MoS 2. *Nature materials* **2013,** *12* (3), 207-211.

26. Fang, H.; Tosun, M.; Seol, G.; Chang, T. C.; Takei, K.; Guo, J.; Javey, A., Degenerate n-doping of few-layer transition metal dichalcogenides by potassium. *Nano letters* **2013,** *13* (5), 1991-1995.

27. Li, Y.; Chernikov, A.; Zhang, X.; Rigosi, A.; Hill, H. M.; Van Der Zande, A. M.; Chenet, D. A.; Shih, E.-M.; Hone, J.; Heinz, T. F., Measurement of the optical dielectric function of monolayer transition-metal dichalcogenides: MoS 2, Mo S e 2, WS 2, and WS e 2. *Physical Review B* **2014,** *90* (20), 205422.

28. Raja, A.; Chaves, A.; Yu, J.; Arefe, G.; Hill, H. M.; Rigosi, A. F.; Berkelbach, T. C.; Nagler, P.; Schüller, C.; Korn, T., Coulomb engineering of the bandgap and excitons in two-dimensional materials. *Nature communications* **2017,** *8* (1), 1-7.

29. Wang, G.; Chernikov, A.; Glazov, M. M.; Heinz, T. F.; Marie, X.; Amand, T.; Urbaszek, B., Colloquium: Excitons in atomically thin transition metal dichalcogenides. *Reviews of Modern Physics* **2018,** *90* (2), 021001.

30. Splendiani, A.; Sun, L.; Zhang, Y.; Li, T.; Kim, J.; Chim, C.-Y.; Galli, G.; Wang, F., Emerging photoluminescence in monolayer MoS2. *Nano letters* **2010,** *10* (4), 1271-1275.

31. Latzke, D. W.; Zhang, W.; Suslu, A.; Chang, T.-R.; Lin, H.; Jeng, H.-T.; Tongay, S.; Wu, J.; Bansil, A.; Lanzara, A., Electronic structure, spin-orbit coupling, and interlayer interaction in bulk MoS 2 and WS 2. *Physical Review B* **2015,** *91* (23), 235202.

32. Lepeshkin, N. N.; Schweinsberg, A.; Piredda, G.; Bennink, R. S.; Boyd, R. W., Enhanced nonlinear optical response of one-dimensional metal-dielectric photonic crystals. *Physical review letters* **2004,** *93* (12), 123902.

33. Lépine, F.; Ivanov, M.; Vrakking, M., Attosecond molecular dynamics: fact or fiction? *Nat. Photonics*, **2014**, 8, 195-204.

34. Lee, G.; Yu, Y.; Cui, X.; Petrone, N.; Lee, C.; Choi, M.; Lee, D.; Lee, C.; Yoo, W.; Watanabe, K., *ACS Nano* **2013**, 7, 7931–7936. DOI.

35. Vasyukov, D.; Anahory, Y.; Embon, L.; Halbertal, D.; Cuppens, J.; Neeman, L.; Finkler, A.; Segev, Y.; Myasoedov, Y.; Rappaport, M. L., A scanning superconducting quantum interference device with single electron spin sensitivity. *Nature nanotechnology* **2013,** *8* (9), 639-644.

36. Mattevi, C.; Kim, H.; Chhowalla, M., A review of chemical vapour deposition of graphene on copper. *Journal of Materials Chemistry* **2011,** *21* (10), 3324-3334.

37. Li, H.; Yin, Z.; He, Q.; Li, H.; Huang, X.; Lu, G.; Fam, D. W. H.; Tok, A. I. Y.; Zhang, Q.; Zhang, H., Fabrication of single-and multilayer MoS2 film-based field-effect transistors for sensing NO at room temperature. *small* **2012,** *8* (1), 63-67.

38. Li, Y.; Dong, N.; Zhang, S.; Wang, K.; Zhang, L.; Wang, J., Optical identification of layered MoS 2 via the characteristic matrix method. *Nanoscale* **2016,** *8* (2), 1210-1215.

39. Eda, G.; Yamaguchi, H.; Voiry, D.; Fujita, T.; Chen, M.; Chhowalla, M., Photoluminescence from Chemically Exfoliated MoS2. *Nano Lett.* **2011,** *11* (12), 5111-5116.

40. Hernandez, Y.; Nicolosi, V.; Lotya, M.; Blighe, F. M.; Sun, Z.; De, S.; McGovern, I.; Holland, B.; Byrne, M.; Gun'Ko, Y. K., High-yield production of graphene by liquid-phase exfoliation of graphite. *Nature nanotechnology* **2008,** *3* (9), 563-568.

41. Coleman, J. N.; Lotya, M.; O'Neill, A.; Bergin, S. D.; King, P. J.; Khan, U.; Young, K.; Gaucher, A.; De, S.; Smith, R. J., Two-dimensional nanosheets produced by liquid exfoliation of layered materials. *Science* **2011,** *331* (6017), 568-571.

42. Backes, C.; Campi, D.; Szydlowska, B. M.; Synnatschke, K.; Ojala, E.; Rashvand, F.; Harvey, A.; Griffin, A.; Sofer, Z.; Marzari, N., Equipartition of energy defines the size–thickness relationship in liquid-exfoliated nanosheets. *ACS nano* **2019,** *13* (6), 7050-7061.

43. Khan, U.; O'Neill, A.; Lotya, M.; De, S.; Coleman, J. N., High-concentration solvent exfoliation of graphene. *small* **2010,** *6* (7), 864-871.

44. Paton, K. R.; Varrla, E.; Backes, C.; Smith, R. J.; Khan, U.; O'Neill, A.; Boland, C.; Lotya, M.; Istrate, O. M.; King, P., Scalable production of large quantities of defect-free few-layer graphene by shear exfoliation in liquids. *Nature materials* **2014,** *13* (6), 624-630.

45. Vega-Mayoral, V.; Backes, C.; Hanlon, D.; Khan, U.; Gholamvand, Z.; O'Brien, M.; Duesberg, G. S.; Gadermaier, C.; Coleman, J. N., Photoluminescence from liquid-exfoliated WS2 monomers in poly (vinyl alcohol) polymer composites. *Advanced Functional Materials* **2016,** *26* (7), 1028-1039.

46. Kang, J.; Sangwan, V. K.; Wood, J. D.; Hersam, M. C., Solution-based processing of monodisperse two-dimensional nanomaterials. *Accounts of chemical research* **2017,** *50* (4), 943-951.

47. Giordani, S.; Bergin, S. D.; Nicolosi, V.; Lebedkin, S.; Kappes, M. M.; Blau, W. J.; Coleman, J. N., Debundling of single-walled nanotubes by dilution: observation of large populations of individual nanotubes in amide solvent dispersions. *The journal of physical chemistry B* **2006,** *110* (32), 15708-15718.

48. Hansen, C. M., *Hansen solubility parameters: a user's handbook*. CRC press: 2007.

49. Hughes, J. M.; Aherne, D.; Coleman, J. N., Generalizing solubility parameter theory to apply to one-and two-dimensional solutes and to incorporate dipolar interactions. *Journal of Applied Polymer Science* **2013,** *127* (6), 4483-4491.

50. Hernandez, Y.; Lotya, M.; Rickard, D.; Bergin, S. D.; Coleman, J. N., Measurement of multicomponent solubility parameters for graphene facilitates solvent discovery. *Langmuir* **2010,** *26* (5), 3208-3213.

51. Cunningham, G.; Lotya, M.; Cucinotta, C. S.; Sanvito, S.; Bergin, S. D.; Menzel, R.; Shaffer, M. S.; Coleman, J. N., Solvent exfoliation of transition metal dichalcogenides: dispersibility of exfoliated nanosheets varies only weakly between compounds. *ACS nano* **2012,** *6* (4), 3468-3480.

52. Smith, R. J.; King, P. J.; Lotya, M.; Wirtz, C.; Khan, U.; De, S.; O'Neill, A.; Duesberg, G. S.; Grunlan, J. C.; Moriarty, G., Large-scale exfoliation of inorganic layered compounds in aqueous surfactant solutions. *Advanced materials* **2011,** *23* (34), 3944-3948.

53. Rosen, M. J.; Kunjappu, J. T., *Surfactants and interfacial phenomena*. John Wiley & Sons: 2012.

54. Mak, K.; Lee, C.; Hone, J., j. Shan and TF Heinz. *Phys. Rev. Lett* **2010,** *105*, 036805.

55. Griffin, A.; Nisi, K.; Pepper, J.; Harvey, A.; Szydłowska, B. M.; Coleman, J. N.; Backes, C., Effect of surfactant choice and concentration on the dimensions and yield of liquid-phase-exfoliated Nanosheets. *Chemistry of Materials* **2020,** *32* (7), 2852-2862.

56. Smith, R. J.; Lotya, M.; Coleman, J. N., The importance of repulsive potential barriers for the dispersion of graphene using surfactants. *New Journal of Physics* **2010,** *12* (12), 125008.

57. May, P.; Khan, U.; Hughes, J. M.; Coleman, J. N., Role of solubility parameters in understanding the steric stabilization of exfoliated two-dimensional nanosheets by adsorbed polymers. *The Journal of Physical Chemistry C* **2012,** *116* (20), 11393-11400.

58. Guan, G.; Zhang, S.; Liu, S.; Cai, Y.; Low, M.; Teng, C. P.; Phang, I. Y.; Cheng, Y.; Duei, K. L.; Srinivasan, B. M.; Zheng, Y.; Zhang, Y.-W.; Han, M.-Y., Protein Induces Layer-by-Layer Exfoliation of Transition Metal Dichalcogenides. *J. Am. Chem. Soc.* **2015,** *137* (19), 6152-6155.

59. Szydłowska, B. M.; Graf, A.; Kelly, A.; Blau, W. J.; Gather, M. C.; Zaumseil, J.; Backes, C., Preparation of WS 2–PMMA composite films for optical applications. *Journal of Materials Chemistry C* **2020,** *8* (31), 10805-10815.

60. Backes, C.; Smith, R. J.; McEvoy, N.; Berner, N. C.; McCloskey, D.; Nerl, H. C.; O'Neill, A.; King, P. J.; Higgins, T.; Hanlon, D., Edge and confinement effects allow in situ measurement of size and thickness of liquid-exfoliated nanosheets. *Nature communications* **2014,** *5* (1), 1-10.

61. Chenot, C. c.; Robiette, R. l.; Collin, S., First evidence of the cysteine and glutathione conjugates of 3-sulfanylpentan-1-ol in hop (Humulus lupulus L.). *Journal of agricultural and food chemistry* **2019,** *67* (14), 4002-4010.

62. Williams, J.; Van Holde, K. E.; Baldwin, R. L.; Fujita, H., The theory of sedimentation analysis. *Chemical Reviews* **1958,** *58* (4), 715-744.

63. Bildirici, L.; Rickwood, D., Fractionation of differentiating cells using density perturbation. *Journal of immunological methods* **2000,** *240* (1-2), 93-99.

64. Patel, D.; Rickwood, D., Optimization of conditions for specific binding of antibody-coated beads to cells. *Journal of immunological methods* **1995,** *184* (1), 71-80.

65. Backes, C.; Szydłowska, B. M.; Harvey, A.; Yuan, S.; Vega-Mayoral, V.; Davies, B. R.; Zhao, P.-l.; Hanlon, D.; Santos, E. J.; Katsnelson, M. I., Production of highly monolayer enriched dispersions of liquid-exfoliated nanosheets by liquid cascade centrifugation. *ACS nano* **2016,** *10* (1), 1589-1601.

66. Mie, G., Beiträge zur Optik trüber Medien, speziell kolloidaler Metallösungen. *Annalen der Physik* **1908,** *330* (3), 377-445.

67. Harvey, A.; Backes, C.; Boland, J. B.; He, X.; Griffin, A.; Szydlowska, B.; Gabbett, C.; Donegan, J. F.; Coleman, J. N., Non-resonant light scattering in dispersions of 2D nanosheets. *Nature communications* **2018,** *9* (1), 1-11.

68. Synnatschke, K.; Cieslik, P. A.; Harvey, A.; Castellanos-Gomez, A.; Tian, T.; Shih, C.-J.; Chernikov, A.; Santos, E. J.; Coleman, J. N.; Backes, C., Length-and thickness-dependent optical response of liquid-exfoliated transition metal dichalcogenides. *Chemistry of Materials* **2019,** *31* (24), 10049-10062.

69. Backes, C.; Hanlon, D.; Szydlowska, B. M.; Harvey, A.; Smith, R. J.; Higgins, T. M.; Coleman, J. N., Preparation of liquid-exfoliated transition metal dichalcogenide nanosheets with controlled size and thickness: a state of the art protocol. *JoVE (Journal of Visualized Experiments)* **2016,** (118), e54806.

70. Zhou, M.; Wang, W.; Lu, J.; Ni, Z., How defects influence the photoluminescence of TMDCs. *Nano Research* **2021,** *14* (1), 29-39.

71. Chernikov, A.; Berkelbach, T. C.; Hill, H. M.; Rigosi, A.; Li, Y.; Aslan, O. B.; Reichman, D. R.; Hybertsen, M. S.; Heinz, T. F., Exciton binding energy and nonhydrogenic Rydberg series in monolayer WS 2. *Physical review letters* **2014,** *113* (7), 076802.

72. Backes, C.; Higgins, T. M.; Kelly, A.; Boland, C.; Harvey, A.; Hanlon, D.; Coleman, J. N., Guidelines for exfoliation, characterization and processing of layered materials produced by liquid exfoliation. *Chemistry of materials* **2017,** *29* (1), 243-255.

73. Lin, Y.; Ling, X.; Yu, L.; Huang, S.; Hsu, A. L.; Lee, Y.-H.; Kong, J.; Dresselhaus, M. S.; Palacios, T., Dielectric screening of excitons and trions in single-layer MoS2. *Nano letters* **2014,** *14* (10), 5569-5576.

74. Amani, M.; Lien, D.-H.; Kiriya, D.; Xiao, J.; Azcatl, A.; Noh, J.; Madhvapathy, S. R.; Addou, R.; Santosh, K.; Dubey, M., Near-unity photoluminescence quantum yield in MoS2. *Science* **2015,** *350* (6264), 1065-1068.

75. Hanbicki, A. T.; Kioseoglou, G.; Currie, M.; Hellberg, C. S.; McCreary, K. M.; Friedman, A. L.; Jonker, B. T., Anomalous temperature-dependent spin-valley polarization in monolayer WS 2. *Scientific reports* **2016,** *6* (1), 1-9.

76. Currie, M.; Hanbicki, A.; Kioseoglou, G.; Jonker, B., Optical control of charged exciton states in tungsten disulfide. *Applied Physics Letters* **2015,** *106* (20), 201907.

77. Kotsakidis, J. C.; Zhang, Q.; Vazquez de Parga, A. L.; Currie, M.; Helmerson, K.; Gaskill, D. K.; Fuhrer, M. S., Oxidation of monolayer WS2 in ambient is a photoinduced process. *Nano letters* **2019,** *19* (8), 5205-5215.

78. McCreary, K. M.; Hanbicki, A. T.; Singh, S.; Kawakami, R. K.; Jernigan, G. G.; Ishigami, M.; Ng, A.; Brintlinger, T. H.; Stroud, R. M.; Jonker, B. T., The effect of preparation conditions on Raman and photoluminescence of monolayer WS 2. *Scientific reports* **2016,** *6* (1), 1-10.

79. Palummo, M.; Bernardi, M.; Grossman, J. C., Exciton radiative lifetimes in two-dimensional transition metal dichalcogenides. *Nano letters* **2015,** *15* (5), 2794-2800.

80. Raja, A.; Waldecker, L.; Zipfel, J.; Cho, Y.; Brem, S.; Ziegler, J. D.; Kulig, M.; Taniguchi, T.; Watanabe, K.; Malic, E., Dielectric disorder in two-dimensional materials. *Nature nanotechnology* **2019,** *14* (9), 832-837.

81. Coleman, J. N., Liquid Exfoliation of Defect-Free Graphene. *Acc. Chem. Res.* **2013,** *46* (1), 14-22.

82. Luo, J.; Xu, W.; Zhai, Y.; Zhang, Q., Experimental study on the mesoscale causes of the influence of viscosity on material erosion in a cavitation field. *Ultrasonics sonochemistry* **2019,** *59*, 104699.

83. Velický, M.; Toth, P. S., From two-dimensional materials to their heterostructures: An electrochemist's perspective. *Applied Materials Today* **2017,** *8*, 68-103.

84. Silvera-Batista, C. A.; Wang, R. K.; Weinberg, P.; Ziegler, K. J., Solvatochromic shifts of single-walled carbon nanotubes in nonpolar microenvironments. *Physical Chemistry Chemical Physics* **2010,** *12* (26), 6990-6998.

85. Suppan, P., Invited review solvatochromic shifts: The influence of the medium on the energy of electronic states. *Journal of Photochemistry and Photobiology A: Chemistry* **1990,** *50* (3), 293-330.

86. Suppan, P.; Ghoneim, N., *Solvatochromism*. Royal Society of Chemistry: 1997.

87. Dalgleish, S.; Reissig, L.; Shuku, Y.; Ligorio, G.; Awaga, K.; List-Kratochvil, E. J., Potential modulations in flatland: near-infrared sensitization of MoS 2 phototransistors by a solvatochromic dye directly tethered to sulfur vacancies. *Scientific reports* **2019,** *9* (1), 1-8.

88. Ugeda, M. M.; Bradley, A. J.; Shi, S.-F.; Felipe, H.; Zhang, Y.; Qiu, D. Y.; Ruan, W.; Mo, S.-K.; Hussain, Z.; Shen, Z.-X., Giant bandgap renormalization and excitonic effects in a monolayer transition metal dichalcogenide semiconductor. *Nature materials* **2014,** *13* (12), 1091-1095.

89. Gupta, A.; Arunachalam, V.; Vasudevan, S., Liquid-phase exfoliation of MoS2 nanosheets: the critical role of trace water. *The journal of physical chemistry letters* **2016,** *7* (23), 4884-4890.

90. Klots, A. R.; Weintrub, B.; Prasai, D.; Kidd, D.; Varga, K.; Velizhanin, K. A.; Bolotin, K. I., Controlled dynamic screening of excitonic complexes in 2D semiconductors. *Scientific reports* **2018,** *8* (1), 1-8.

91. Karmakar, M.; Bhattacharya, S.; Mukherjee, S.; Ghosh, B.; Chowdhury, R. K.; Agarwal, A.; Ray, S. K.; Chanda, D.; Datta, P. K., Observation of dynamic screening in the excited exciton states in multilayered MoS 2. *Physical Review B* **2021,** *103* (7), 075437.

92. Krane, N.; Lotze, C.; Reecht, G.; Zhang, L.; Briseno, A. L.; Franke, K. J., High-Resolution Vibronic Spectra of Molecules on Molybdenum Disulfide Allow for Rotamer Identification. *ACS nano* **2018,** *12* (11), 11698-11703.

93. Franck, J.; Dymond, E., Elementary processes of photochemical reactions. *Transactions of the Faraday Society* **1926,** *21* (February), 536-542.

94. Condon, E., A theory of intensity distribution in band systems. *Physical Review* **1926,** *28* (6), 1182.

95. Pradhan, N. A.; Liu, N.; Ho, W., Vibronic spectroscopy of single C60 molecules and monolayers with the STM. *The Journal of Physical Chemistry B* **2005,** *109* (17), 8513-8518.

96. Kistler, S. F.; Schweizer, P. M., *Liquid film coating: scientific principles and their technological implications*. Springer: 1997.

97. Pichumani, M.; Bagheri, P.; Poduska, K. M.; González-Viñas, W.; Yethiraj, A., Dynamics, crystallization and structures in colloid spin coating. *Soft Matter* **2013,** *9* (12), 3220-3229.

98. Bonaccorso, F.; Bartolotta, A.; Coleman, J. N.; Backes, C., 2D-crystal-based functional inks. *Advanced Materials* **2016,** *28* (29), 6136-6166.

99. Voiry, D.; Mohite, A.; Chhowalla, M., Phase engineering of transition metal dichalcogenides. *Chemical Society Reviews* **2015,** *44* (9), 2702-2712.

100. Yun, W. S.; Han, S.; Hong, S. C.; Kim, I. G.; Lee, J., Thickness and strain effects on electronic structures of transition metal dichalcogenides: 2H-M X 2 semiconductors (M= Mo, W; X= S, Se, Te). *Physical Review B* **2012,** *85* (3), 033305.

101. Usui, H.; Shimizu, Y.; Sasaki, T.; Koshizaki, N., Photoluminescence of ZnO nanoparticles prepared by laser ablation in different surfactant solutions. *The Journal of Physical Chemistry B* **2005,** *109* (1), 120-124.

102. Mitterreiter, E.; Schuler, B.; Micevic, A.; Hernangómez-Pérez, D.; Barthelmi, K.; Cochrane, K. A.; Kiemle, J.; Sigger, F.; Klein, J.; Wong, E., The role of chalcogen vacancies for atomic defect emission in MoS2. *Nature Communications* **2021,** *12* (1), 1-8.

103. Yuan, S.; Han, B.; Fang, T.; Shan, Q.; Song, J., Flat, Luminescent, and Defect-Less Perovskite Films on PVK for Light-Emitting Diodes with Enhanced Efficiency and Stability. *ACS Applied Electronic Materials* **2020,** *2* (11), 3530-3537.

104. Kumar, S.; Borriello, C.; Nenna, G.; Rosentsveig, R.; Di Luccio, T., Dispersion of WS2 nanotubes and nanoparticles into conducting polymer matrices for application as LED materials. *The European Physical Journal B* **2012,** *85* (5), 1-7.

105. Wang, Y.; Li, N.; Cui, M.; Li, Y.; Tian, X.; Xu, X.; Rong, Q.; Yuan, D.; Zhou, G.; Nian, L., High-performance hole transport layer based on WS2 doped PEDOT: PSS for organic solar cells. *Organic Electronics* **2021,** *99*, 106305.

106. Kuilla, T.; Bhadra, S.; Yao, D.; Kim, N. H.; Bose, S.; Lee, J. H., Recent advances in graphene based polymer composites. *Progress in polymer science* **2010,** *35* (11), 1350-1375.

107. Sreenivasulu, B.; Ramji, B.; Nagaral, M., A review on graphene reinforced polymer matrix composites. *Materials Today: Proceedings* **2018,** *5* (1), 2419-2428.

108. Mak, K. F.; Shan, J., Nature Photonics 10, 216 (2016). *URL https://doi. org/10.1038/nphoton* **2015**.

109. Szydlowska, B. M.; Blau, W. J. In Highly Monolayer Enriched WS2 Dispersions Produced by Liquid Phase Exfoliation in Liquid Cascade as Nonlinear Optical Materials, *Novel Optical Materials and Applications, Optical Society of America*: **2016**; p NoTu3D. 5.

110. Park, S.-H.; King, P. J.; Tian, R.; Boland, C. S.; Coelho, J.; Zhang, C. J.; McBean, P.; McEvoy, N.; Kremer, M. P.; Daly, D., High areal capacity battery electrodes enabled by segregated nanotube networks. *Nature Energy* **2019,** *4* (7), 560-567.

111. Liu, Y.; He, X.; Hanlon, D.; Harvey, A.; Khan, U.; Li, Y.; Coleman, J. N., Electrical, mechanical, and capacity percolation leads to high-performance MoS2/nanotube composite lithium ion battery electrodes. *ACS nano* **2016,** *10* (6), 5980-5990.

112. Mansukhani, N. D.; Guiney, L. M.; Kim, P. J.; Zhao, Y.; Alducin, D.; Ponce, A.; Larios, E.; Yacaman, M. J.; Hersam, M. C., High-Concentration Aqueous Dispersions of Nanoscale 2D Materials Using Nonionic, Biocompatible Block Copolymers. *Small* **2016,** *12* (3), 294-300.

113. Lin, S.; Shih, C.-J.; Strano, M. S.; Blankschtein, D., Molecular insights into the surface morphology, layering structure, and aggregation kinetics of surfactant-stabilized graphene dispersions. *Journal of the American Chemical Society* **2011,** *133* (32), 12810-12823.

114. Liscio, A.; Kouroupis-Agalou, K.; Kovtun, A.; Gebremedhn, E.; El Garah, M.; Rekab, W.; Orgiu, E.; Giorgini, L.; Samorì, P.; Beljonne, D., Exfoliation of few-layer graphene in volatile solvents using aromatic perylene diimide derivatives as surfactants. *ChemPlusChem* **2016,** *82* (3), 358-367.

115. Langevin, D., Micelles and microemulsions. *Annual Review of Physical Chemistry* **1992,** *43* (1), 341-369.

116. O'Callaghan, J. M.; McNamara, H.; Copley, M. P.; Hanrahan, J. P.; Morris, M. A.; Steytler, D. C.; Heenan, R. K.; Holmes, J. D., Swelling of Ionic and Nonionic Surfactant Micelles by High Pressure Gases. *Langmuir* **2010,** *26* (11), 7725-7731.

NATURWISSENSCHAFTLICH-MATHEMATISCHE GESAMTFAKULTÄT

COMBINED FACULTY OF NATURAL SCIENCES AND MATHEMATICS

RUPRECHT-KARLS-
UNIVERSITÄT
HEIDELBERG

Eidesstattliche Versicherung gemäß § 8 der Promotionsordnung für die Naturwissenschaftlich-Mathematische Gesamtfakultät der Universität Heidelberg /
Sworn Affidavit according to § 8 of the doctoral degree regulations of the Combined Faculty of Natural Sciences and Mathematics

1. Bei der eingereichten Dissertation zu dem Thema / The thesis I have submitted entitled
   Chemical Doping Of Liquid Exfoliated 2D-Materials
   handelt es sich um meine eigenständig erbrachte Leistung / is my own work.

2. Ich habe nur die angegebenen Quellen und Hilfsmittel benutzt und mich keiner unzulässigen Hilfe Dritter bedient. Insbesondere habe ich wörtlich oder sinngemäß aus anderen Werken übernommene Inhalte als solche kenntlich gemacht. / I have only used the sources indicated and have not made unauthorised use of services of a third party. Where the work of others has been quoted or reproduced, the source is always given.

3. Die Arbeit oder Teile davon habe ich wie folgt/bislang nicht[1)] an einer Hochschule des In- oder Auslands als Bestandteil einer Prüfungs- oder Qualifikationsleistung vorgelegt. / I have not yet/have already[1)] presented this thesis or parts thereof to a university as part of an examination or degree.

   Titel der Arbeit / Title of the thesis: Chemical Doping Of Liquid Exfoliated 2D-Materials

   Hochschule und Jahr / University and year: Heidelberg University, 2021

   Art der Prüfungs- oder Qualifikationsleistung / Type of examination or degree: Dissertation

4. Die Richtigkeit der vorstehenden Erklärungen bestätige ich. / I confirm that the declarations made above are correct.

5. Die Bedeutung der eidesstattlichen Versicherung und die strafrechtlichen Folgen einer unrichtigen oder unvollständigen eidesstattlichen Versicherung sind mir bekannt. / I am aware of the importance of a sworn affidavit and the criminal prosecution in case of a false or incomplete affidavit.

   Ich versichere an Eides statt, dass ich nach bestem Wissen die reine Wahrheit erklärt und nichts verschwiegen habe. / I affirm that the above is the absolute truth to the best of my knowledge and that I have not concealed anything.

Ort und Datum / Place and date

Unterschrift / Signature

[1)] Nicht Zutreffendes streichen. Bei Bejahung sind anzugeben: der Titel der andernorts vorgelegten Arbeit, die Hochschule, das Jahr der Vorlage und die Art der Prüfungs- oder Qualifikationsleistung. / Please cross out what is not applicable. If applicable, please provide: the title of the thesis that was presented elsewhere, the name of the university, the year of presentation and the type of examination or degree.

The German text is legally binding.